1987

Anodic oxygen-transfer electrocatalysis at pure and modified lead dioxide electrodes in acidic media

In-Hyeong Yeo
Iowa State University

INFORMATION TO USERS

While the most advanced technology has been used to photograph and reproduce this manuscript, the quality of the reproduction is heavily dependent upon the quality of the material submitted. For example:

- Manuscript pages may have indistinct print. In such cases, the best available copy has been filmed.

- Manuscripts may not always be complete. In such cases, a note will indicate that it is not possible to obtain missing pages.

- Copyrighted material may have been removed from the manuscript. In such cases, a note will indicate the deletion.

Oversize materials (e.g., maps, drawings, and charts) are photographed by sectioning the original, beginning at the upper left-hand corner and continuing from left to right in equal sections with small overlaps. Each oversize page is also filmed as one exposure and is available, for an additional charge, as a standard 35mm slide or as a 17"x 23" black and white photographic print.

Most photographs reproduce acceptably on positive microfilm or microfiche but lack the clarity on xerographic copies made from the microfilm. For an additional charge, 35mm slides of 6"x 9" black and white photographic prints are available for any photographs or illustrations that cannot be reproduced satisfactorily by xerography.

Yeo, In-Hyeong

ANODIC OXYGEN-TRANSFER ELECTROCATALYSIS AT PURE AND MODIFIED LEAD-DIOXIDE ELECTRODES IN ACIDIC MEDIA

Iowa State University PH.D. 1987

PLEASE NOTE:

In all cases this material has been filmed in the best possible way from the available copy. Problems encountered with this document have been identified here with a check mark __✓__.

1. Glossy photographs or pages __✓__
2. Colored illustrations, paper or print __✓__
3. Photographs with dark background __✓__
4. Illustrations are poor copy _____
5. Pages with black marks, not original copy _____
6. Print shows through as there is text on both sides of page _____
7. Indistinct, broken or small print on several pages __✓__
8. Print exceeds margin requirements _____
9. Tightly bound copy with print lost in spine _____
10. Computer printout pages with indistinct print _____
11. Page(s) _____ lacking when material received, and not available from school or author.
12. Page(s) _____ seem to be missing in numbering only as text follows.
13. Two pages numbered _____. Text follows.
14. Curling and wrinkled pages _____
15. Dissertation contains pages with print at a slant, filmed as received _____
16. Other _____

_____

_____

University
Microfilms
International

Anodic oxygen-transfer electrocatalysis at pure and modified lead dioxide electrodes in acidic media

by

In-Hyeong Yeo

A Dissertation Submitted to the
Graduate Faculty in Partial Fulfillment of the
Requirements for the Degree of
DOCTOR OF PHILOSOPHY

Department: Chemistry
Major: Analytical Chemistry

Approved:

Signature was redacted for privacy.

In Charge of Major Work

Signature was redacted for privacy.

For the Major Department

Signature was redacted for privacy.

For the Graduate College

Iowa State University
Ames, Iowa

1987

TABLE OF CONTENTS

LIST OF FIGURES

LIST OF TABLES

DEDICATION

To my parents

Chang-Koo Yeo and Myung-Soon Kim

I. INTRODUCTION

Historically, the search for new electrode materials has been motivated primarily by interest in the development of new electrochemical energy storage cells, fuel cells, and electrosynthetic routes in organic chemistry. To a much lesser extent, development of new electrode materials has been inspired by the need for improved transducers in electrochemical analysis.

Lead dioxide, as an electrode material, has been used primarily for so-called "lead-acid batteries" and for electrosynthesis. Application of lead dioxide electrodes in voltammetric analysis has been restricted because of the very narrow range of useful applied potential. Anodic, amperometric applications (i.e., constant applied potential) for lead dioxide electrodes deposited on inert substrates (e.g., noble metals or carbon) are restricted somewhat because of the low reactivity observed for many analytes whose thermodynamically allowed oxidation reactions are accompanied by oxygen transfer. Anodic oxygen-transfer rates are larger at lead electrodes which have been anodized in acidic sulfate media; however, their use requires the presence of sulfate and a large baseline current persists because of the continuing, although slow, conversion of lead to lead dioxide at the metal-metal oxide interface.

This research was motivated by the goal of increasing the electrocatalytic reactivity of electrodeposited lead dioxide for anodic oxygen-transfer reactions. It was the premise of the research that oxygen transfer mechanisms involve exchange of labile surface oxygen as represented schematically by the reaction sequence below where [O] represents the labile surface oxygen, [ ] represents a surface site devoid of labile oxygen, R is the reactant and RO is the anodic reaction product.

$$PbO_2[\ ] + H_2O \longrightarrow PbO_2[O] + 2H^+ + 2e$$
$$PbO_2[O] + R \longrightarrow PbO_2[\ ] + RO$$

$$\text{net: } R + H_2O \longrightarrow RO + 2H^+ + 2e$$

Hence, it was proposed that the electrocatalytic reactivity of PbO_2 could be altered by small changes made to the crystalline structure of the oxide. The experimental approach was to attempt to incorporate various foreign metal oxides as doping agents into the electrodeposited lead dioxide matrix. Doping agents selected were metals which form oxides having stoichiometry different from PbO_2.

II. LITERATURE REVIEW

A. Electrocatalysis and Metal Oxides

"Electrocatalysis" is defined as the acceleration of a heterogeneous electron-transfer process which results from the beneficial physico-chemical interaction of the electrode surface in the electrochemical mechanism. Since the word "electrocatalysis" was introduced by Grubb in 1963 [1], many researchers have been active in the development and characterization of numerous electrocatalysts. The research described here was concerned with the possible electrocatalysis of anodic reactions involving transfer of oxygen from the water solvent to the oxidation product. Specifically, it was proposed that O-transfer reactions could be electrocatalyzed by modification of the composition of lead dioxide anodes.

Historically, the study of electrocatalysis at conductive metal-oxide electrodes started with the pioneering work of Beer [2] in 1967 which he prepared noble metal oxides by thermal methods. The study of electrocatalysis at oxide electrodes has experienecd a renaissance in the last two decades and much research has been done on a large number of electrodes fabricated from pure and mixed oxides [3-5]. Even so, the theoretical basis of electrocatalysis is not clearly understood. Pletcher [6] has summarized the gulf that exists

between theory and practice in electrocatalysis: "It must be recognized that the development of electrocatalysts has been essentially empirical and there remains a gulf between those who develope electrode materials and these who seek to understand the physical chemistry of electrocatalysis."

For the purpose of discussion, the numerous metal oxide electrodes used in electrocatalysis can be divided into four structural groups: rutiles, spinels, perovskites, and others. Table II-1 summarizes the literature of the many oxide electrode systems according to their structure type, methods of preparation, and applications. Many references are to patent literature in which the details of preparation of pure and mixed-metal oxides are frequently hidden because of proprietory considerations. Review articles have appeared on spinel-type oxides [7], perovskite-type oxides [8], and rutile-type oxide electrodes [9]. These reviews have covered thoroughly both experimental techniques and theoretical considerations.

Table II-1. Summary of literature citations for various metal oxide electrodes in electrochemical systems

(i) Rutile-type oxides

Oxide (rutile)[b]	Refs.	Preparation[a]	Applications & Systems
RuO_2	10-13,14, 15	T.D.(14,15)	Cl_2 & O_2 evol.(15), O_2 evol.(14,15)
IrO_2	15,16,17, 18,19,20 21	T.D.(15,20, 21), T.D. & E.D (17)	Cl_2 evol.(16),ESCA(17) O_2 evol.(15), Anodic formation of $S_2O_8^-$ in H_2SO_4(20), Cl_2 evol. in 5M NaCl(21)
MnO_2	21,22,23, 24,25,26, 27	T.D.(21,22, 23), E.D.(24,25)	O_2 red. in 1M NaOH(22), O_2 evol. in 1N H_2SO_4 and 1N KOH(23), O_2 & Cl_2 evol.(24), SEM studies(25), theoretical treatment (26,27), Cl_2 evol. in 5M NaCl(21)

[a]Methods of preparation of oxides: T. D., thermal decomposition; E. D., electrochemical deposition; C. V. D., chemical vapor decomposition; S. C., single crystal; P. B., painting and baking method; S. A., sputtering and anodizing method; T. O., thermal oxidation; F. D., freeze-drying method.

[b]Structure of oxides.

Table II-1. (continued)

Oxide (rutile)[b]	Refs.	Preparation[a]	Applications & Systems
PbO_2	28,29,30, 31,32,	E.D.(28) Anodizing of Pb(30,32)	O_2 evol. in 1M H_2SO_4(28), Oxd. of aromatic organic compounds(29), Deposition on Pt & C(30), Electrochemical nucleation and growth on C(31), Oxd. of benzene(32)
PtO_2	33,21,	T.D.(21,33)	O_2 evol. in 1N KOH(33), Cl_2 evol. in 5M NaCl(21)
Fe_2O_3	34	T.D.(34)	Photoelectrochemical behaviors(35)
TiO_2	36,37,38	CVD.(36) SC.(37,38)	Photochemical behavior (36), O_2 red.(37), $Fe(CN)_6^{4-}$(38)
Ru-doped SnO_2	39	T.D.	Cl_2 evol. in 1M HCl (39)
Fe,Sb doped SnO_2	40	T.D.	Cl_2 evol. in HCl(40)
RuO_2 contained TiO_2	14	T.D.	Chlor-alkali electrolysis(14), O_2 evol.(14)

Table II-1. (continued)

Oxide (rutile)[b]	Refs.	Preparation[a]	Applications & Systems
Nb-doped TiO_2	41	S.C.	Impedance measurements(41)
Pd-doped MnO_2	42	T.D.	Cl_2 evol. in 1M $HClO_4$ (42)
Ti/RuO_2	43	T.D.	Br^- oxd.(43)
Cr_2O_3/TiO_2	44	T.D.	oxd. of aliphatic alcohols & ethers in 1M H_2SO_4(44)
RuO_2/TiO_2	45,46,47, 48	P.B.(45), T.D.(46,47, 48)	Cl_2 evol.(45,47,48), O_2 evol.(46), Cl_2 red.(48)
RuO_2/ZrO_2	49	P.B.	O_2 evol. in 6M NaOH(49)
Ta_2O_5/Al_2O_3	50	S.A.	Auger electron spec. anlysis(50)
RuO_2/Ta_2O_5	51	T.D.	O_2 evol. & XPS, AES, XRD(51)
RuO_2/IrO_2	52	T.D.	point of zero charge(52)
ZrO_2	53	E.D	electrical characteristics(53)

Table II-1. (continued)

Oxide (rutile)[b]	Refs.	Preparation[a]	Applications & Systems
10% Sb-SnO_2 & 10% Ru-SnO_2	54	T.D.	Fe^{2+}/Fe^{3+}, Ce^{3+}/Ce^{4+} kinetics(54)
$RuO_x/SbO_x/SnO_2$	55	T.D.	Cl_2 & O_2 evol. in 1M KOH(55)

(ii) Spinel-type oxides

Oxide (spinel)[b]	Refs.	Preparation[a]	Applications & Systems
Co_3O_4	15,56,57 58	T.D.(15,57)	O_2 evol.(15,56,57), Cl_2 evol.(15,58)
Li-doped Co_3O_4	59,60	T.O. of Co/Li alloy (60)	O_2 evol. in KOH(59), O_2 red. in alkali(60)
$NiCo_2O_4$	61,62,63 64,65,66 67,68	T.D.(64,66 69) F.D.(61,65)	O_2 evol.(61,63,64,65, 69),$Fe(CN)_6^{3-}/Fe(CN)_6^{4}$ (66), optimization of preparation(67), Cl_2 evol. in NaCl(69)
$NiFe_2O_4$	70	F.D.	O_2 evol.(70)
$CdCo_2O_4$	68,69	T.D.(69)	Cl_2 & O_2 evol. in NaCl & NaOH soln(69)

Table II-1. (continued)

(iii) Perovskite-type oxides

Oxide (perovskite)[b]	Refs.	Preparation[a]	Applications & Systems
$NiLaO_4$	71		O_2 evol.(71)
$LaMnO_3$	72	T.D.	O_2 red.(72)
$LaCoO_3$	73,74	T.D.(73)	O_2 evol. in 6M KOH(73)
$LaNiO_3$	75,76,77 78	T.D.(75,78)	O_2 red. in basic soln(75,78) O_2 evol.(76)
$SrFeO_3$	72,79,80 81	T.D.(72,81)	O_2 red.(72), O_2 evol. in KOH & H_2SO_4(81)
$LaTiO_3$	71	T.D.	O_2 red.(71)
Cr,Co,Pt,Rh-doped $SrTiO_3$	82	T.D.	photoelectrolysis of H_2O(82)
$La_{1-x}Sr_xMnO_3$	72,75,83	T.D.(72,75, 83)	O_2 red.(72,75) O_2 evol. in 1M KOH(83)
$La_{1-x}Sr_xCoO_3$	75,84-90	T.D.(75,84-90,91)	O_2 red. in 6M KOH(75 84-90), electrochemical properties(91)
$La_{0.5}Sr_{0.5}CoO_3$	92	T.D.	impedance measurements (92)

Table II-1. (continued)

Oxide (perovskite)[b]	Refs.	Preparation[a]	Applications & Systems
$LaNi_{1-x}Fe_xO_3$	93	T.D.	O_2 red. in 1M NaOH(93)
$Ni_2Re_2O_{7-x}$	69	T.D.	Cl_2 evol. in NaCl(69)
$La_{0.5}Ba_{0.5}CoO_3$	94,95	T.D.(94,95)	O_2 evol. in KOH, XRD, & TEM studies(94), O_2 evol.(95)

(iv) Metal-oxide electrodes

Oxide (others)[b]	Refs.	Preparation[a]	Applications & Systems
Li doped NiO	96,97	T.D.(96)	O_2 red. in KOH(96)
PdO	98	T.D.	pH sensing electrode(98)
Na_xWO_3	99,100	T.D.(99)	O_2 red. in 10% H_3PO_4(99)
$Eu_{0.1}WO_3$	20	T.D.	Cl_2 evol. in 5M NaCl (20)
NiO_x	101	F.D.	O_2 evol.(101)

Table II-1. (continued)

Oxide (others)[b]	Refs.	Preparation[a]	Applications & Systems
$NiMoO_4$	66	T.D. & rf magnetron sputt.	$Fe(CN)_6^{3-}/Fe(CN)_6^{4-}$ in 0.1M NaOH (66)
NiOOH	102,103 104	anodizing Ni(102,103) E.D.(104)	oxd. of alcohols & amines in KOH(102), kinetics of the oxd. of org. compounds in NaOH(103), deposition of NiOOH on Au(104)

B. Lead Dioxide and Modified Lead Dioxide

Lead dioxide has been widely and favorably used as an inert anode material in electrochemical processes because of several desirable properties including (i) a large oxygen overpotential, (ii) high electrical conductivity, and (iii) chemical inertness during use for supporting electrochemical reactions.

The major application of lead dioxide is as the positive electrode in the lead-acid storage battery [105]. A secondary use is in the commercial electrolysis of aqueous solutions containing Cl^-, Br^-, and IO_3^- to produce Cl_2, Br_2, and IO_4^-, respectively [106]. Because of the commercial importance, lead dioxide has been the subject of theoretical considerations [106].

There are several reviews in the literature [107-112] which have dealt with the use of lead dioxide in lead-acid batteries. Also, numerous works have been performed to investigate properties of lead dioxide from the point of view of nonstoichiometry [113-118], electronic conductivity [116-117,119], and structure [120-124]. Other more general reviews have appeared [125-128], including a review of the preparation of lead dioxide anodes by electrodeposition [129].

Lead dioxide is known to exist in two crystalline modifications. Orthohombic α-PbO_2 and tetragonal β-PbO_2 can

be obtained by anodic deposition from aqueous solutions of high pH and low pH, respectively [130]. It has been determined that the extent of oxygen deficiency is different for the two crystalline modifications [130-131]. The existence of hydrogen in the lead dioxide has been claimed by several authors [124,132-135]. Lead dioxide is known as a highly conducting metal oxide which shows high electron mobility [119,125]. It has been suggested by a number of workers that the conductivity of lead dioxide is associated with the presence of excess lead, i.e., a deficiency of oxygen [114,136]. In many cases, the oxygen content of α-PbO_2 is less than that of β-PbO_2: therefore, if oxygen deficiency is the cause of the conductivity of lead dioxide, the α form should be a slightly better electronic conductor than the β form. This conclusion is supported by Frey and Weaver [137]. It is well known that lead dioxide is not a true stoichiometric oxide with exactly two oxygen atoms per every lead atom [115,138-139]. The nonstoichiometry of this oxide is represented empirically by the formula PbO_{2-x}, where the value of x ranges between 0.02 and 0.34. This may be explained as a vacancies of oxygen in a lead(IV) dioxide [131] or excess of lead [135]. The fact that oxygen appears to have a high mobility in PbO_2 [140] supports the conclusion of oxygen vacancies.

Although the potential use of lead dioxide for the oxidation of organic compounds in industry has been

demonstrated [141], the analytical usage of lead dioxide as an electrode materials for amperometric detection in HPLC or FIA is fairly new [142]. There are two problems with the use of lead dioxide in commercial electrosynthesis and as an analytical transducer: (i) insufficient stability and (ii) low reactivity. Beneficial changes of these characteristics of the lead dioxide have been observed as a result of the presence of other metal oxides in the lead dioxide matrix [143-144]. Specifically, this has been observed as the result of metal impurities contained in the sulfuric acid electrolyte in lead acid batteries, and as a result of impurities in the lead metal used for making the positive plates of lead batteries.

It was proposed for the research described here that incorporation of foreign metal oxides in lead dioxide used for analytical transducers could have a beneficial effect on reactivity and stability. Modifications of the oxide surface resulting from the presence of other metal oxides could possibly change the adsorption kinetics of analyte, the strength of reactant adsorption, the surface coverage, oxygen bond strength, and the surface concentration of active oxygen available to support anodic oxygen-transfer reactions [145]. The improvement of cycle life, hardness, strength, and castability of the battery grid by preparation of the anodes from lead alloys and doped lead dioxide has been of great interest. Especially, antimony has been the center of

attention [146-152] because mechanical properties of the positive plate are improved and cycle life is increased.

The study of antimony effects also has emphasized the factors of self discharge and morphology. Caldara et al. [131] studied the effect of antimony on the properties and electrocrystallization of lead dioxide by scanning electron microscopy, X-ray diffraction, and chemical analysis. They concluded that antimony enters the lattice of lead dioxide changing the morphology and electrochemical behavior of the anode. The physical size of crystallites of α-PbO_2 decreases as the amount of antimony is increased, whereas the size of crystallites of β-PbO_2 apparently is not modified. They also found that antimony fills the lattice vacancies of α-PbO_2 up to a concentration of 0.2 %, changes the O:Pb atomic ratio, and substitutes for Pb(IV) in the β-PbO_2 matrix.

More extended studies of the doping effects of various elements (Ag, As, Co, Ge, Mn, Ni, Sb, Se, Sn, Te, and Zn) on the O:Pb ratio, on morphology, and on self-discharge of α-PbO_2 and β-PbO_2, have appeared in the literature [153]. Some general conclusions were drawn. The greatest effect of the presence of doping elements on the self-discharge current occurs for Sn in the case of β-PbO_2 and for Ge in the case of α-PbO_2. For crystal morphology, the effect of dopants on β-PbO_2 is practically negligible, whereas the dopants in α-PbO_2 cause a small reduction of crystal size. The doping of α-PbO_2 produces an increase in the O:Pb ratio which always corresponds to the decrease in the oxygen evolution rate.

The effects of trace As, Co, Ni, Sb, and Te ions on the current-potential curves obtained by linear potential at lead-acid battery electrodes also were investigated by Mahato and Tiedemann [154]. They showed that current-potential curves obtained by the linear potential sweep (LPS) technique were sensitive to the presence of impurities which alter the hydrogen evolution rate at a lead electrode (cathode) and oxygen evolution rate at a lead dioxide electrode (anode). Some elements, such as Sb and As, increase the rate of hydrogen evolution by reducing the hydrogen overpotential on lead electrode. Other elements, such as Co and Ni, increase the rate of oxygen evolution by reducing oxygen overpotential of the lead dioxide electrode.

There is no single report of the study of doped lead dioxide and mixed lead oxides as electrode materials for electrocatalytic oxidation of organic and inorganic compounds.

C. Theoretical Consideration of Anodic Oxygen-transfer Reactions

The electrochemical kinetics of redox reactions can be described by rate constants, k_f and k_b, for the forward and back reactions, respectively, as

$$k_f = k^{\circ}\exp[-\alpha nF(E-E^{\circ})/RT] \qquad (1)$$

$$k_b = k^\circ \exp[(1-\alpha)nF(E-E^\circ)/RT] \quad (2)$$

In equations (1) and (2), E is the electrode potential, α is the transfer coefficient, E° is the standard potential for a given reaction process, k° is the heterogeneous rate constant, and n, F, R, and T have their usual meanings. The rate constants are related to an easily measurable quantity, the electrode current, i, which corresponds to the net rate of the electrochemical reactions,

$$i = nFA[k_f C_{ox}^{\,s} - k_b C_{red}^{\,s}] \quad (3)$$

Here, $C_{ox}^{\,s}$ and $C_{red}^{\,s}$ are the concentration of the oxidized and reduced species at the electrode surface, respectively. Combination of equation (1), (2), and (3) yields the general equation for heterogeneous electrochemical kinetics,

$$i = nFAk^\circ[C_{ox}^{\,s}\exp\{-\alpha nF(E-E^\circ)/RT\} - C_{red}^{\,s}\exp\{(1-\alpha)nF(E-E^\circ)/RT\}] \quad (4)$$

At equilibrium, the forward and back reaction rates are equal so the net current is zero and all surface concentrations equal the bulk values. Then, we have,

$$k^\circ C_{ox}^{\,b}\exp\{-\alpha nF(E-E^\circ)/RT\} = k^\circ C_{red}^{\,b}\exp\{(1-\alpha)nF(E-E^\circ)/RT\} \quad (5)$$

By rearranging of the equation above, the Nernst form can be written as

$$E = E^{\circ} + (RT/nF)\ln\{C_{ox}{}^{b}/C_{r}{}^{b}\} \qquad (6)$$

Although the net current is zero at equilibrium, there still remains faradaic activity that can be expressed as the exchange current, i_o.

$$\begin{aligned} i_o &= nFAk^{\circ}C_{ox}{}^{b}\exp\{-\alpha nF(E-E^{\circ})/RT\} \\ &= nFAk^{\circ}C_{red}{}^{b}\exp\{(1-\alpha)nF(E-E^{\circ})/RT\} \end{aligned} \qquad (7)$$

The mathematics of heterogeneous electrochemistry can be simplified greatly if the reaction is irreversible so that the back reaction can be ignored. For example, if the cathodic reaction can be neglected, then the net rate becomes equal to the rate of the anodic half reaction. Consequently, the current-potential relationship can be written as

$$i = i_a = nFAk^{\circ}C_{red}{}^{s}\exp\{-\alpha nF(E-E^{\circ})/RT\} \qquad (8)$$

By rearranging equation (8), we obtain

$$E - E^{\circ} = (RT/\alpha nF)\ln\{nFk^{\circ}AC_{red}{}^{s}\} - (RT/\alpha nF)\ln\{i\} \qquad (9)$$

Substitution of E° obtained from equation (6) into equation (9) yields

$$E - E_{eq} = (RT/\alpha nF)\ln\{nFk^{\circ}AC_{ox}^{b}\} - (RT/\alpha nF)\ln\{i\} \qquad (10)$$

which has the same form of the empirical Tafel equation,

$$\eta = E - E_{eq} = a + b \log\{i\} \qquad (11)$$

In the Tafel equation above, η is the overpotential, a is the intercept and b is the slope of the so-called "Tafel plot", i.e., the plot of η vs. log{i}. The parameter α and i_o obtained from the slope and intercept, respectively, are used for the diagnostic study of electrochemical mechanisms and comparison of electrocatalysts [155]. From equations (10) and (11), we have the Tafel slope,

$$b = 2.3RT/\alpha nF \qquad (12)$$

and the Tafel intercept,

$$a = (RT/\alpha nF)\ln\{nFk^{\circ}AC_{ox}^{b}\} \qquad (13)$$

As an example, it is often found that for a mechanism in which an electron-transfer step is rate determining, b will have a value close to 0.12 and α is concluded to be 0.5.

For the oxygen evolution reaction at β-PbO_2, the normal Tafel slope of 0.12 was obtained in acidic solution; but at α-PbO_2, a slope of 0.05 was observed in alkaline solution

[114]. Different slopes indicate that the mechanism of oxygen evolution is different on the two forms of PbO_2 in the solutions of different pH. The Tafel slope for α-PbO_2 corresponds to a process where two electrons are involved when the rate determining reaction occurs once [114], whereas the Tafel slope for β-PbO_2 indicates that only one electron is involved in the rate determining step. The Tafel slope deviates sharply from linear behavior as η approaches zero because the back reaction, which can be assumed to be negligible for large η, is no longer negligible. The exchange current, i_o, can be obtained when the Tafel slope is extrapolated to a point on the log{i} axis where η equals to zero. When η is zero, an electrode reaction is truly reversible and the activation energy barrier is very small. The procedure for evaluating i_o assumes that the electrode reaction at very low current densities is the same as that at high current densities. When this assumption is wrong, the value of i_o obtained may no longer have significance. The observation of a larger value of i_o at β-PbO_2 than at α-PbO_2 [155] can have two interpretations: (i) β-PbO_2 has a better catalytic surface for the oxygen evolution process or (ii) there is a large increase in the roughness factor for the β-PbO_2.

Concentration polarization occurs when the concentration of the reactive species at the surface of electrode is no longer equal to that in bulk. In this case, C_{red}^{s} in the equation (8) is changed to,

$$C_{red}^{s} = \frac{i_{l,c} - i}{nFAD/\delta} \tag{14}$$

Substitution of equation (14) for equation (8) yields,

$$i = \frac{nFAk^{\circ}C_{red}^{b}\exp[-\alpha nF(E-E^{\circ})/RT]}{1 + (k^{\circ}\delta/D)\cdot\exp[-\alpha nF(E-E^{\circ})/RT]} \tag{15}$$

In equation (15), δ is the thickness of the diffusion layer at the electrode surface and is defined for a rotating disc electrode (RDE) as

$$\delta = 1.61\ D^{1/3}\omega^{-1/2}\upsilon^{1/6} \tag{16}$$

In equation (16), υ represents the kinematic viscosity of the solution ($cm^2\ sec^{-1}$), ω is the rotation velocity of the electrode (rad sec^{-1}), and D is the diffusion coefficient ($cm^2\ sec^{-1}$). Equation (12) can be reduced to a relationship valid for electrode reactions controlled exclusively by either mass-transport or electron-transfer rate depending on the relative values of δ and D/k°.

The electrocatalytic participation of "surface oxygen" at an oxide electrode is assumed to be a necessary step for anodic oxygen-transfer reactions. The real state of surface oxygen is difficult to determine at an oxide electrode in

aqueous electrolyte solution because of the various states possible for surface oxygen, such as atomic oxygen bound to a metal on the surface (M-O), adsorbed hydroxyl radicals (M-$OH^{\bullet}$), adsorbed hydroxide ions (M-OH^{-}), etc. It would seem possilbe, also, that any two surface oxygens can easily combine to form the dioxygen molecule, O_2, i.e., anodic oxygen evolution. It is natural to consider that the oxygen evolution reaction may occur simultaneously and competitively with faradaic reaction of analytes present in the solution. When the analytes are adsorbed on a surface site adjacent to oxygen at the oxide electrode, oxidative desorption may proceed by combining the analytes adsorbed and surface oxygens. Uptake of surface oxygen could also occur by active analytes without prior adsorption of the analyte. The chance of the oxygen evolution reaction increases as the amount of analytes adsorbed decreases. The anodic oxygen-transfer reactions proceed more efficiently when the analytes adsorbed are closely located to the surface oxygen.

The bond energy and geometrical state of surface oxygen are considered to be important functions for either oxygen evolution or anodic oxygen-transfer reactions. If the oxygen evolution reaction proceeds by the combination of two surface oxygens produced by the discharge of H_2O molecules or OH^{-} ions [156], then it is predicted that the oxygen overpotential should decrease as the free energy of adsorption of the oxygen species increases. However, of

course, if the energy of adsorption is low such that there is no significant adsorption, oxygen evolution cannot occur by this mechanism.

A theoretical investigation was carried out by Ruetschi and Delahay [157] to test the premise that the oxygen overpotential on various metal anodes is correlated with the respective M-OH bond energies. They assumed that the initial discharge of water to form adsorbed hydroxyl radical at a metal site (M-OH) was the rate determining step at high current densities. Because of the lack of experimental data on OH adsorption, they proposed three methods to calculate the M-OH bond strengths: (i) from the heat of formation of the most stable oxide of a particular metal, (ii) the heat of formation of the metal hydroxide, and (iii) the dissociation heat of the gaseous molecules MO. The calculated M-OH bond strengths and experimental values of oxygen overpotential at the corresponding metals are listed in Table II-2 and Table II-3, respectively. The plots of the oxygen overpotential at a current density of 1 A cm^{-2} as a function of the calculated values of M-OH bond strength are shown in Figure II-1. Ruetschi and Delahay [157] concluded that variation of overpotential for oxygen evolution from one metal to another results primarily from variation in the energy of the bond strength of oxygen atoms adsorbed on the oxide surface.

Since the adsorption of oxygen on bare metals produces the corresponding bulk oxides [159] and the adsorption of

Table II-2. Values of bond energies calculated from thermodynamic data for various anode material [157]

Electrode material	Heat of formation of hydroxide (Kcal)	Heat of formation of oxide (Kcal)	Dissociation heat of gaseous molecule (Kcal)
Silver	-	-	60
Gold	43.4	35.8	-
Cadmium	76.8	69.4	53
Cobalt	69.0	64.5	-
Copper	63.2	57.5	66
Iron	75.7	71.8	65
Nickel	64.1	53.8	59
Lead	71.6	55.5	59
Palladium	52.4	49.2	-
Platinum	53.7	44.1	-

Table II-3. Values of overpotential for oxygen evolution at twelve anode materials [158]

Electrode material	Oxygen overpotential (V) at constant current density (amp cm^{-2})				
	10^{-5}	10^{-3}	10^{-2}	10^{-1}	1.0
Cadmium	-	0.80	0.96	1.21	1.21
Cobalt	0.27	0.39	0.46	0.54	0.61
Copper	-	0.58	0.66	0.73	0.77
Gold	0.73	0.96	1.05	1.53	1.63
Graphite	0.31	0.50	0.96	1.12	2.20
Iron	0.35	0.41	0.48	0.56	0.63
Lead	-	0.80	0.97	1.02	1.04
Nickel	0.32	0.60	0.75	0.91	1.04
Palladium	0.39	0.89	1.01	1.12	1.28
Platinum	0.52	1.11	1.32	1.50	1.55
Platinized	0.21	0.46	0.66	0.89	1.14
Silver	0.41	0.60	0.71	0.94	1.06

Figure II-1. Relationship between oxygen overpotential and M-OH strength [157]

$$M + OH^- \xrightarrow{\text{Slow}} M - OH + e$$

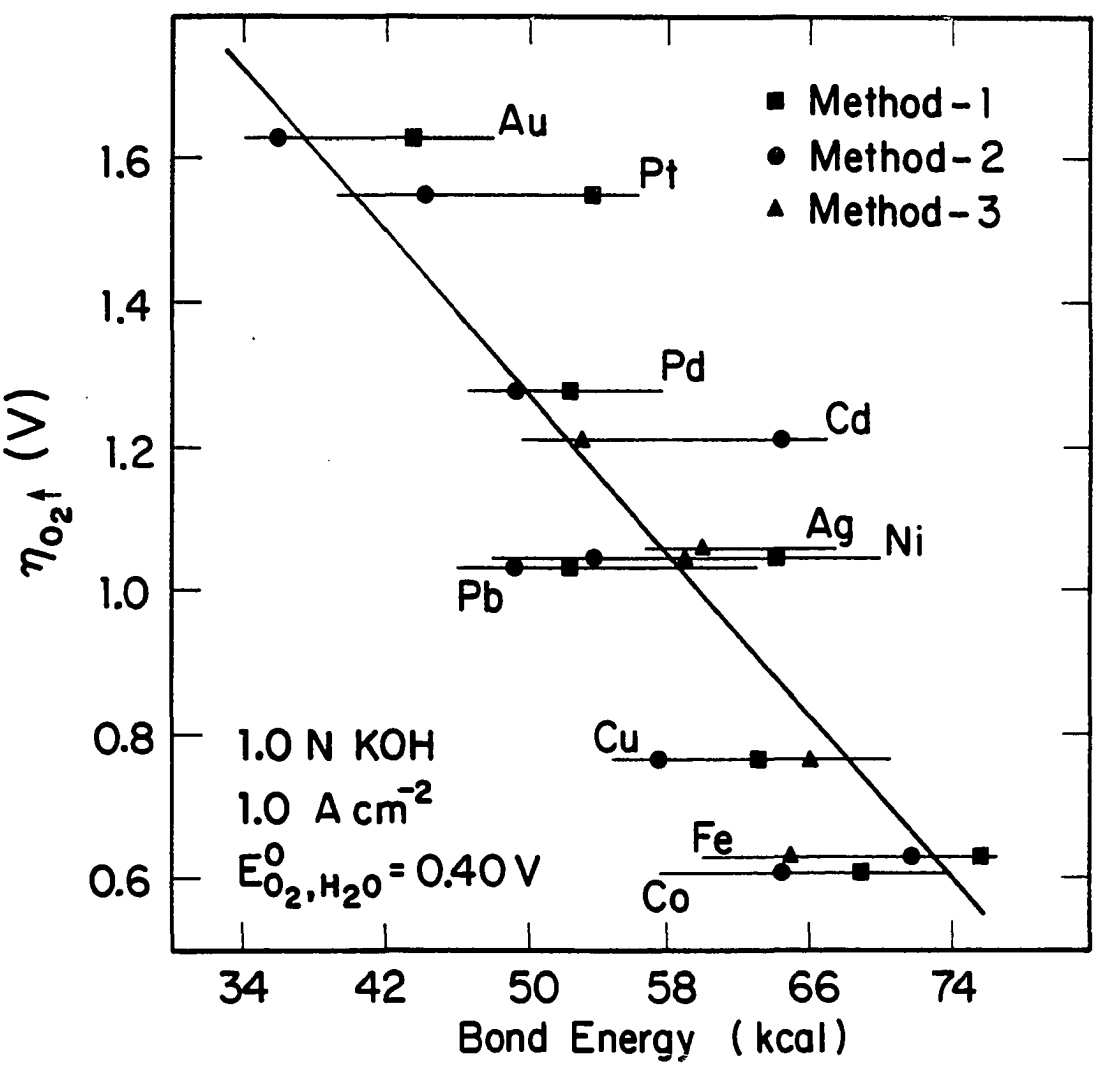

oxygen on the bulk oxides is expected to form a higher state of oxide, direct correlation between overpotentials for oxygen evolution and bond strengths for oxygen on bare metal was concluded to be unsatisfactory [160-161]. Trasatti [160] revised the theory of Ruetschi and Delahay. He considered the transition between the two oxides to be the rate determining step for oxygen evolution. The primary water discharge and subsequent decomposition of the higher state of

$$M(OH) + H_2O \xrightarrow{k_1} M(OH)_2 + H^+ + e \qquad (17)$$

$$M(OH)_2 \xrightarrow{k_2} M(OH) + 1/2\ O_2 + H^+ + e \qquad (18)$$

oxide is considered to produce molecular oxygen. In reaction (17), the energy change occurring during the electrochemical reaction corresponds to the enthalphy of transition of the oxide from a lower to a higher oxidation state [162]. The overpotential for oxygen evolution is plotted against the enthalpy of transition of oxides in Figure II-2. As the enthalpy of transition of oxides increases, the overpotential for oxygen evolution decreases, with a minimum for RuO_2, and then starts to increase. It is interesting that the oxides (Fe_3O_4 and Co_3O_4) on the descending branch of the plot in Figure II-2 (dashed line) are more easily oxidized than the oxides on the ascending branch (e.g., PbO_2, PtO_2, RuO_2, etc.)

Figure II-2. Oxygen overpotential at different oxides as a function of enthalpy of oxide transition [160]

(1) PbO_2, (2) Ni_2O_3, (3) PtO_2, (4) MnO_2, (5) RuO_2, (6) IrO_2, (7) and (8) Co_3O_4, (9) and (10) Fe_3O_4
(●) in acidic solution, (o) in basic solution

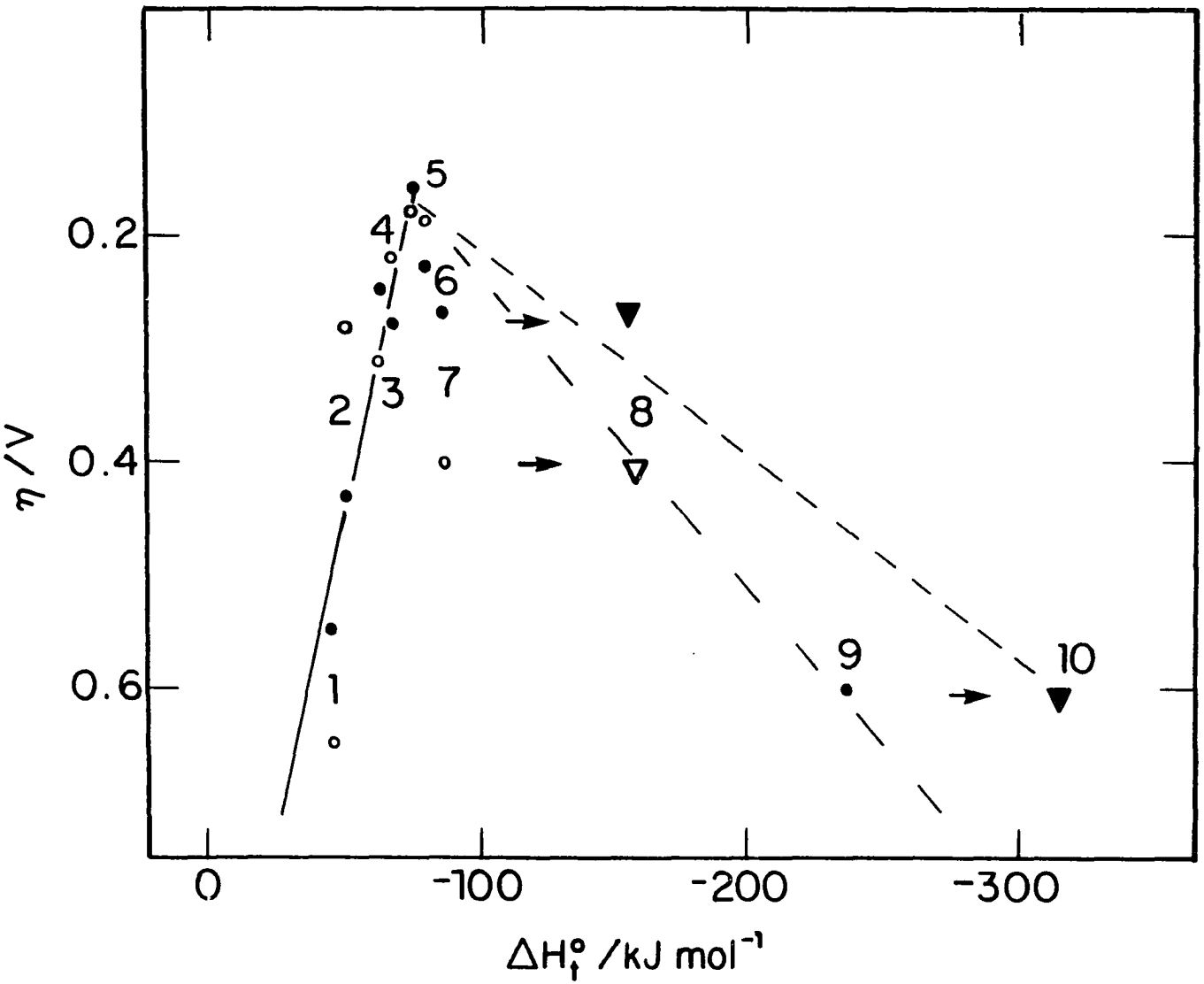
0.2
0.4
0.6
η /V
0
-100
-200
-300
ΔH°f /kJ mol⁻¹
1
2
3
4
5
6
7
8
9
10

and yet exhibit a high oxygen evolution overpotential.

The overpotential for oxygen evolution at the oxides located on the ascending branch in Figure II-2 decreases as the enthalpy of transition of the corresponding oxides increases. This indicates that the rate of oxygen evolution depends on the formation of the $M(OH)_2$ species (equation 17). Hence, the rate of decomposition of $M(OH)_2$ to produce molecular oxygen is relatively fast in comparison to that of the discharge of water ($k_2 >> k_1$). It follows that the rate law can be expressed as follows:

$$R(O_2\uparrow) = \text{rate of } O_2 \text{ evolution}$$

$$= k_1\Theta_{M(OH)} \tag{19}$$

$$= A \exp\{-\Delta G^*_t/RT\}\Theta_{M(OH)} \tag{20}$$

$$= A' \exp\{-\Delta G_t/RT\}\Theta_{M(OH)} \tag{21}$$

In equation (20), $-\Delta G^*_t$ can be replaced by $-\Delta G_t$ because $-\Delta G^*_t$ is a function of the free energy ($-\Delta G_t$) when the contribution of back reaction for oxygen evolution is negligible. Since the free energy of a transition depends linearly on heat of transition [163] and the coverage of M(OH) is almost equal to unity in this case, the rate of oxygen evolution can be written as

$$R(O_2\uparrow) = A'' \exp\{-\Delta H_t/RT\} \quad (22)$$

The overpotential for oxygen evolution at the oxides located in the descending branch increase as the enthalpy of transition increases. This supports the conclusion that the rate of oxygen evolution depends on the decomposition of $M(OH)_2$ species, i.e., equation (18). Hence, the rate of formation of $M(OH)_2$ is faster than that of the decomposition ($k_1 >> k_2$). Therefore, the rate of oxygen evolution is expressed as follows:

$$R(O_2\uparrow) = k_2\Theta_{M(OH)_2} \quad (23)$$

$$= A' \exp\{\Delta G_t/RT\}\Theta_{M(OH)_2} \quad (24)$$

Continuing, the rate of oxygen evolution is

$$R(O_2\uparrow) = A'' \exp\{\Delta H_t/RT\} \quad (25)$$

It is shown that the rate of oxygen evolution is a function of the transition enthalpy of the oxides for the two cases described above.

Although this approach with the "volcano-shaped" curve is approximate and conceptual, it has some useful predictive value and perhaps can enable us to understand some of the features of the oxygen evolution reaction on metal oxides.

The approach also does not conflict with other views that the potential of transition from a lower to a higher oxide is considered as a parameter to select a prospective catalyst [164].

D. References

1. Grubb, W. T. Nature, London 1963, 198, 883.
2. Beer, H. B. Chem. Abstr. 1967, 67, 17397m.
3. Trasatti, S., Ed. "Electrodes of Conductive Metallic Oxides", part A & B; Elsevier: Amsterdam, 1980.
4. Trasatti, S. Electrochim. Acta 1984, 29, 1503.
5. Novak, D. M.; Tilak, B. V.; Conway, B. E. In "Modern Aspects of Electrochemistry"; Bockris, J. O'M.; Conway, B. E.; White, R. E., Eds.; Plenum: New York, 1982; Vol 14, Page 195.
6. Pletcher, D. J. Appl. Electrochem. 1984, 14, 403.
7. Tarasevich, M. R.; Efremov, B. N. In "Electrodes of Conductive Metallic Oxides"; Trasatti, S., Ed.; Elsevier: Amsterdam, 1980; Chapter 5.
8. Tamura, H.; Yoneyama, H.; Matsumoto, Y. In "Electrodes of Conductive Metallic Oxides"; Trasatti, S., Ed.; Elsevier: Amsterdam, 1980; Chapter 6.
9. Trasatti, S.; Lodi, G. In "Electrodes of Conductive metallic Oxides"; Trasatti, S., Ed.; Elsevier: Amsterdam, 1980; Chapter 7.
10. Kuhn, A. T.; Mortimer, C. J. J. Electrochem. Soc. 1973, 120, 231.
11. Dukes, R. R.; Milner, R. G. J. Electrochem. Soc. 1970, 117, 9C.
12. O'Grady, W.; Iwakura, C.; Huang, J.; Yeager, E. In "Proc. Symp. Electrocatalysis"; Breiter, M. W., Ed.; The Electrochemistry: Princeton, 1974; Page 286.

13. Burke, L. D.; Murphy, O. J.; O'Neill, J. F.; Venkatesan, S. J. Chem. Soc. Faraday Trans. 1, 1977, 73, 1659.

14. Kokoulina, D. V.; Bunakova, L. V. J. Electroanal. Chem. 1984, 164, 377.

15. Trasatti, S. Electrochim. Acta 1984, 29, 1503.

16. Mozota, J.; Conway, B. E. J. Electrochem. Soc. 1981, 128, 2142.

17. Augustynski, J.; Koudelka, M.; Sanchez, J. J. Electroanal. Chem. 1984, 160, 233.

18. Kuhn, A. T.; Mortimer, C. J. J. Electrochem. Soc. 1973, 120, 231.

19. Horkans, J.; Shafer, W. W. J. Electrochem. Soc. 1977, 124, 1202.

20. Fukuda, K.; Iwakura, C.; Tamura, H. Electrochim. Acta 1979, 24, 363.

21. Arikado, T.; Iwakura, C.; Tamura, H. Electrochim. Acta 1978, 23, 9.

22. Matsuki, M.; Kamada, H. Electrochim. Acta 1986, 31, 13.

23. Morita, M.; Iwakura, C.; Tamura, H. Electrochim. Acta 1977, 22, 325.

24. Mraz, R.; Srb, V.; Tichy, S. Electrochim. Acta 1973, 18, 551.

25. Matsuki, K.; Endo, T.; Kamada, H. Electrochim. Acta 1984, 29, 983.

26. Maskell, W. C.; Shaw, J. E. A.; Tye, F. L. Electrochim. Acta 1983, 28, 225.

27. Maskell, W. C.; Shaw, J. E. A.; Tye, F. L. Electrochim. Acta 1983, 28, 231.

28. Hine, F.; Yasuda, M.; Iidam T.; Ogata, Y.; Hara, K. Electrochim. Acta 1984, 29, 1447.

29. Harrison, J. A.; Mayne, J. M. Electrochim. Acta 1983, 28, 1223.

30. Barradas, R. G.; Contractor, A. Q. J. Electroanal. Chem. 1982, 138, 425.

31. Ramamurthy, A. C.; Kuwann, T. J. Electroanal. Chem. 1982, 135, 243.

32. Wendt, H. Electrochim. Acta 1984, 29, 1513.

33. Iwakura, C.; Fududa, K.; Tamura, H. Electrochim. Acta 1976, 21, 501.

34. Candea, R. M. Electrochim. Acta 1981, 26, 1803.

35. Kennedy, J. H.; Anderman, M. J. Electrochem. Soc. 1983, 130, 849.

36. Minoura, H.; Nasu, M.; Takahashi, Y. Ber. Bunsenges. Phys. Chem. 1985, 89, 1064.

37. Dutoit, E. C.; Cardon, F.; Gomes, W. P. Bur. Bunsenges. Phys. Chem. 1976, 80, 475.

38. Parkinson, B.; Decker, F.; Juliao, J. F.; Abramovich, M.; Chagas, H. C. Electrochim. Acta 1980, 25, 521.

39. Chertykovseva, T. A.; Skuridina, Z. D.; Shub, D. M.; Veselovskii, V. I. Electrokhimiya 1978, 14, 1412.

40. Chertykovseva, T. A.; Shub, D. M.; Veselovskii, V. I. Electrokhimiya 1978, 14, 1260.

41. Madou, M. J.; Kinoshita, K.; Mckubre, M. C. Electrochim. Acta 1984, 29, 1173.

42. Morita, M.; Iwakura, C.; Tamura, H. Electrochim. Acta 1980, 25, 1341.

43. Cettou, P.; Robertson, P. M.; Ibl, N. Electrochim. Acta 1984, 29, 875.

44. Beck, F.; Schulz, H. Electrochim. Acta 1984, 29, 1569.

45. Harrison, J. A.; Caldwell, D. L.; White, R. E. Electrochim. Acta 1984, 29, 203.

46. Denton, D. A.; Harrison, J. A.; Knowles, R. I. Electrochim. Acta 1981, 26, 1197.

47. Denton, D. A.; Harrison, J. A.; Knowles, R. I. Electrochim. Acta 1980, 25, 1147.

48. Denton, D. A.; Harrison, J. A.; Knowles, R. I. Electrochim. Acta 1979, 24, 521.

49. Burke, L. D.; McCarthy, A. Electrochim. Acta 1984, 29, 211.

50. Labunov, V.; Sokol, V.; Vorobiova, A.; Bondarenko, V. Electrochim. Acta 1985, 30, 1079.

51. Battisti, A. D.; Brina, R.; Gavelli, G.; Benedetti, A.; Fragherazz, G. J. Electroanal. Chem. 1986, 200, 93.

52. Vigaho, R.; Taraszewska, J.; Daghetti, A.; Trasatti, S. J. Electroanal. Chem. 1985, 182, 203.

53. Llewelynleach, J. S.; Pearson, B. R. Electrochim. Acta 1984, 29, 1271.

54. Badawy, W.; Doblhofer, K.; Eiselt, I.; Gerischer, H.; Krause, S.; Melsheimer, J. Electrochim. Acta 1984, 29, 1617.

55. Iwakura, C.; Inai, M.; Uemura, T.; Tamura, H. Electrochim. Acta 1981, 26, 579.

56. Trasatti, S. In "The International Society of Electrochemistry, 31st Meeting Proceedings"; Vecchi, E., Ed.; The Electrochemistry: Princeton, 1980; Page 115.

57. Iwakura, C.; Honji, A.; Tamura, H. Electrochim. Acta 1981, 26, 1319.

58. Boggio, R.; Caragati, A.; Lodi, G.; Trasatti, S. J. Appl. Electrochem. 1985, 15, 335.

59. Rasiyah, P.; Tseung, A. C. C. J. Electrochem. Soc. 1983, 130, 365.

60. Savy, M. Electrochim. Acta 1968, 13, 1359.

61. Tseung, A. C. C.; Jasem, S. M. Electrochim. Acta 1977, 22, 31.

62. Jasem, S. M.; Tseung, A. C. C. J. Electrochem. Soc. 1979, 126, 1353.

63. Rasiyah, P.; Tseung, A. C. C. J. Electrochem. Soc, 1983, 130, 2384.

64. Haenen, J. G. D.; Visscher, W.; Burendrecht, E. J. Appl. Electrochem. 1985, 15, 29.

65. Davidson, C. R.; Kissel, G.; Srinivasan, S. J. Electroanal. Chem. 1982, 132, 129.

66. Tanabe, H.; Fukushima, S. Electrochim. Acta 1984, 29, 1173.

67. Domnikov, A. A.; Reznikov, G. L.; Yuppets, F. R. Elektrokhimiya 1976, 12, 1868.

68. Burshtein, R.; Vilinskaya, V. S.; Tarasevich, M. R.; Bulavina, N. G. Reaction Kinet. Catal. Lett. 1976, 4, 159.

69. Krishtalik, L. I. Electrochim. Acta 1981, 26, 329.

70. Orehotsky, J.; Huang, H.; Davidson, C. R.; Srinivasan, S. J. Electroanal. Chem. 1979, 95, 233.

71. Fiori, G.; Mandelli, C.; Mari, C. M.; Scolari, P. V. In "Hydrogen Energy Systems"; Viziroglu, T. N.; Seifritz, W., Eds.; Pergamon: New York, 1978; Vol. 1, Page 193.

72. Matsumoto, H.; Yoneyama, H.; Tamura, H. J. Electroanal. Chem. 1977, 80, 237.

73. Kobussen, A. G. C.; Vanburen, F. R.; Vandenbett, T. G. M.; Vanwees, H. J. A. J. Electroanal. Chem. 1979, 96, 123.

74. Libby, W. F. Science 1971, 171, 499.

75. Manoharan, R.; Shukla, A. K. Electrochim. Acta 1985, 30, 205.

76. Otagawa, T.; Bockris, J. O'M. J. Electrochem. Soc. 1982, 129, 2391.

77. Sazonov, L. A.; Moskvina, Z. V.; Artamonov, E. V. Kinet. Katal. 1974, 15, 120.

78. Matsumoto, Y.; Yoneyama, H.; Tamura, H. J. Electroanal. Chem. 1977, 80, 115.

79. Tofield, B. C.; Greaves, C.; Fender, B. E. F. Mat. Res. Bull. 1975, 10, 737.

80. Greaves, C.; Jacobson, A. J.; Tofield, B. C.; Fender, B. E. F. Acta Crystallogr. 1975, B31, 641.

81. Matsumoto, Y.; Kurimoto, J.; Sato, E. J. Electroanal. Chem. 1979, 102, 77.

82. Watanabe, I.; Matsumoto, Y.; Sato, E. J. Electroanal. Chem. 1982, 133, 359.

83. Matsumoto, Y.; Sato, E. Electrochim. Acta 1979, 22, 421.

84. Tedmon, C. S.; Spacil, H. S.; Mitoff, S. P. J. Electrochem. Soc. 1969, 116, 1170.

85. Hibbert, D. B.; Tseung, A. C. C. J. Electrochem. Soc. 1978, 125, 74.

86. Yeung, K. L. K.; Tseung, A. C. C. J. Electrochem. Soc. 1978, 125, 878.

87. Tseung, A. C. C.; Bevan, H. L. J. Electroanal. Chem. 1973, 45, 429.

88. Van Buren, F. R.; Broers, G. H. J.; Bouman, A. J.; Boesveld, C. J. Electroanal. Chem. 1978, 87, 389.

89. Van Buren, F. R.; Broers, G. H. J.; Bouman, A. J.; Boesveld, C. J. Electroanal. Chem. 1978, 87, 381.

90. Van Buren, F. R.; Broers, G. H. J.; Bouman, A. J.; Boesveld, C. J. Electroanal. Chem. 1978, 88, 353.

91. Vondrak, J.; Delezal, L. Electrochim. Acta 1984, 29, 477.

92. Willems, H.; Moers, M.; Broers, G. H. J.; Dewit, J. H. W. J. Electroanal. Chem. 1985, 194, 305.

93. Matsumoto, Y.; Yoneyama, H.; Tamura, H. J. Electroanal. Chem. 1977, 79, 319.

94. Kobussen, A. G. C.; Willems, H.; Broers, G. H. J. J. Electroanal. Chem. 1982, 142, 85.

95. Willems, H.; Kobussen, A. G. C; Dewit, J. H. W. J. Electroanal. Chem. 1985, 194, 317.

96. Tseung, A. C. C.; Hobbs, B. S.; Tantram, A. D. S. Electrochim. Acta 1970, 15, 473.

97. Tench, D. M.; Yeager, E. J. Electrochem. Soc. 1973, 120, 164.

98. Kinoshita, E.; Ingman, F.; Edwall, G.; Glab, S. Electrochim. Acta 1986, 31, 29.

99. Fishman, J. H.; Henry, J. F.; Tessor, S. Electrochim. Acta 1969, 14, 1314.

100. Bockris, J. O'M.; McHardy, J. J. Electrochem. Soc. 1973, 120, 61.

101. Nadesam, J. C. B.; Tseung, A. C. C. J. Electrochem. Soc. 1985, 132, 2957.

102. Robertson, P. M. J. Electroanal. Chem. 1980, 111, 97.

103. Vertes, G.; Horanyi, G. J. Electroanal. Chem. 1974, 52, 47.

104. Goledzinowski, M.; Haupt, S.; Schultze, J. W. Electrochim. Acta 1984, 29, 493.

105. Ellis, S. R.; Hampson, N. A.; Ball, M. C.; Wilkinson, F. J. Appl. Electrochem. 1986, 16, 159.

106. Hampel, C. A. Ed. In "The Encyclopedia of Electrochemistry"; Reinhold: New York, 1964; Page 762.

107. Ness, P. Electrochim. Acta 1967, 12, 161.

108. Burbank, J.; Simon, A. C.; Willihanganz, E. In "Advances in Electrochemistry and Electrochemical Engineering"; Delahay, P.; Tobias, C. W., Eds.; Interscience: New York, 1971; Vol. 8, Page 157.

109. Ruetschi, P. J. Power Sources 1977, 2, 3.

110. Bode, H. "Lead-Acid Batteries"; Wiley: New York, 1977.

111. Weissman, E. Y. In "Batteries"; Kordesch, K. V., Ed.; Marcel Dekker: New York, 1977; Vol. 2.

112. Voss, E. J. Power Sources 1982, 7, 343.

113. Clarke, G. L.; Rowan, R. J. Am. Chem. Soc. 1941, 63, 1305.

114. Ruetschi, P.; Cahan, B. D. J. Electrochem. Soc. 1958, 105, 369.

115. Rao, P. V. V.; Udupa, H. V. K. Electrochim. Acta 1965, 10,651.

116. Bagshaw, N. E.; Clarke, R. L.; Halliwell, B. J. Appl. Chem. 1966, 16, 180.

117. Duisman, J. A.; Giauque, W. F. J. Phys. Chem. 1968, 72, 562.

118. Schlechtrimen, G. L. Z. Phys. Chem. 1982, 130, 193.

119. Mindt, M. J. Electrochem. Soc. 1969, 116, 1076.

120. Harada, H.; Sasa, Y.; Uda, M. J. Appl. Crystallogr. 1981, 14, 142.

121. Thanos, J. C. G.; Wabner, D. W. J. Electroanal. Chem. 1985, 182, 37.

122. Thanos, J. C. G.; Wabner, D. W. J. Electroanal. Chem. 1985, 182, 25.

123. Hill, R. J.; Madsen, I. C. J. Electrochem. Soc. 1984, 131, 1486.

124. Santoro, A.; D'Antonio, P.; Caulder, S. M. J. Electrochem. Soc. 1983, 130, 1451.

125. Carr, J. P.; Hampson, N. A. Chem. Rev. 1972, 72, 679.

126. Pohl, J. P.; Rickert, H. In "Electrodes of Conductive Metallic Oxides"; Trasatti, S., Ed.; Elsevier: Amsterdam, 1980; Chapter 4.

127. Ellis, S. R.; Hampson, N. A.; Ball, M. C.; Wilkinson, F. J. Appl. Electrochem. 1986, 16, 159.

128. Kuhn, A. T. "The Electrochemistry of Lead"; Academic: London, 1979.

129. Kelsall, G. H. "Electricity Council Research Centre"; ECRE/N-1060; Capenhurst: England, 1977.

130. Caulder, S. M.; Murday, J. S.; Simon, A. C. J. Electrochem. Soc. 1973, 120, 1515.

131. Caldara, F.; Delmastro, A.; Fracchis, G.; Maja, M. J. Electrochem. Soc. 1980, 127, 1869.

132. Pohl, J. P.; Rickert, H. In "Power Source 5"; Collins, D. H., Ed.; Academic: New York, 1974; Page 15.

133. Pohl, J. P.; Schendler, W. J. Power Sources 1985, 6, 245.

134. Pohl, J. P.; Rickert, H. Z. Phys. Chem. 1978, 112, 117.

135. Jorgensen, J. D.; Varma, R.; Rotella, F. J.; Cook, G.; Yao, N.P. J. Electrochem. Soc. 1982, 129, 1678.

136. Lappe, F. J. Phys. Chem. Solids 1962, 23, 1563.

137. Frey, D. A.; Weaver, H. E. J. Electrochem. Soc. 1960, 107, 930.

138. Buttler, G.; Lopp, J. L. J. Chem. Soc. 1956, 145, 725.

139. Gancy, A. B. J. Electrochem. Soc. 1969, 116, 1496.

140. Kabanov, B. N.; Weisberg, E. S.; Romanova, I. L.; Krivolapova, E. V. Electrochim. Acta 1964, 9, 1197.

141. Wagenknecht, J. H. J. Chem. Educ. 1983, 60, 271.

142. Tang, A. P-C.; Johnson, D. C. J. Electrochem. Soc. 1987, 00, 0000

143. Vinal, G. "Storage Batteries"; Wiley: New York, 1955; Page 138.

144. Sinfelt, J. H. Catal. Rev. 1974, 9, 147.

145. Thomas, J. M.; Thomas, W. J. In "Introduction to the Principles of Heterogeneous Catalysis"; Academic: New York, 1967; Page 270.

146. Burbank, J. J. Electrochem. Soc. 1964, 111, 1112.

147. Ritchie, E. J.; Burbank, J. J. Electrochem. Soc. 1970, 117, 299.

148. Swets, D. E. J. Electrochem. Soc. 1973, 120, 925.

149. Maskalick, N. J. J. Electrochem. Soc. 1975, 122, 19.

150. Abdularim, A. A.; Ismail, A. A. J. Appl. Electrochem. 1977, 7, 119.

151. Boggio, A.; Maja, M.; Penazzi, N. J. Power Sources 1983, 9, 221.

152. Maja, M.; Penazzi, N. Electrochim. Acta 1985, 30, 773.

153. Delmastro, A.; Maja, M. J. Electrochem. Soc. 1984, 131, 2756.

154. Mahato, B.; Tiedemann, W. J. Electrochem. Soc. 1983, 130, 2139.

155. Hoare, J. P. "The Electrochemistry of Oxygen"; Wiley: New York, 1968; Page 83.

156. Iwakura, C.; Hirao, K.; Tamura, H. Electrochim. Acta 1977, 22, 329.

157. Ruetschi, P; Delahay, P. J. Chem. Phys. 1955, 23, 556.

158. Hickling, A.; Hill, S. Discussions Faraday Soc. 1947, 1, 236.

159. Bond, G. C. R. I. C. Rev. 1970, 3, 1.

160. Trasatti, S. J. Electroanal. Chem. 1980, 111, 125.

161. Trasatti, S. In "Proceedings of the Symposium on Electrocatalysis"; O'Grady, W. E.; Ross, P. N.; Will, F. G., Eds.; Electrochem. Soc. Inc.: Pennington, New Jersey, 1982; Page 73.

162. Trasatti, S. Electrochim. Acta 1984, 29, 1503.

163. Klier, K. J. Catalysis 1967, 8, 14.

164. Tseung, A. C. C.; Jasem, S. Electrochim. Acta 1977, 22, 31.

III. SURVEY OF METAL IONS AS DOPING AGENTS IN LEAD DIOXIDE

A. Introduction

Extensive research on lead dioxide as an electrode material has been performed in the past directed toward commercial applications, especially in the field of the lead-acid battery. Other directions of research have been focused on the possible use of this electrode as an anode for electroorganic synthesis and also for fundamental studies as a typical example of an oxide electrode. The electrode is usually made on any suitable base material such as carbon, platinum, and gold. These substrates play no significant role for the electrode process other than providing an electronic contact with the lead dioxide.

Some characteristics such as high conductivity, large oxygen overpotential, i.e., a lower rate of self-discharge in batteries, are certainly advantages of PbO_2 electrodes. However, electrocatalytic activity implied by the rate of the electrodic reaction and the limited cathodic potential range (E_c < 1.40 V) are probably serious disadvantages for the use of electrodeposited PbO_2 electrodes as analytical anodes.

In general, it is recognized that electronic and surface geometric factor are the main parameters to be considered for the design and optimization of the oxide electrocatalysts

[1]. The influence of the addition of foreign atoms or ions on the conductivity (electronic properties) and surface morphology have been demonstrated [2-3]. It was the premise of this work that the incorporation of foreign metal oxides into the PbO_2 matrix could have a profound effect on the electrocatalytic activity of PbO_2, especially for anodic oxygen-transfer reactions. Furthermore, a secondary benefit might be an improved cathodic stability of the mixed oxide in comparison to pure PbO_2.

Lead dioxide electrodes can be prepared anodically by galvanostatic (constant current) or potentiostatic (constant potential) electrodeposition methods. Depending on the pH, current density, and electrolyte, two different crystal structures of PbO_2 have been obtained, i.e., α-PbO_2 and β-PbO_2. α-PbO_2 is obtained from an alkaline solution at low current density ($\leq$10 mA cm^{-2}) and β-PbO_2 is obtained from an acidic solution at high current density ($\geq$100 mA cm^{-2}) [4]. It was anticipated that the desired mixed oxides would be electrodeposited from solutions of Pb(II) containing the dopant metal ion.

Results are described here of the survey of numerous doping metal ions and the resulting changes in electrocatalytic activity for oxidation of selected organic and inorganic compounds.

B. Experimental

Reagents. All chemicals were Reagent Grade from Fisher Scientific, Baker Chemicals, or Aldrich Chemical Co. All solutions were prepared with deionized and distilled water: condensate from the university steam system was passed through a mixed-bed deionization cartridge, and subsequently redistilled for an alkaline permanganate solution (ca. 0.1M NaOH and 0.1N $KMnO_4$) and again from 1.0M H_2SO_4. All test solutions contained 1.0M $HClO_4$ as the supporting electrolyte. All experiments were performed under a N_2 atmosphere unless other conditions are specified.

Electrodes. Various inert materials such as platinum and gold can be used as substrates for the anodic electrodeposition of lead dioxide. Three kinds of gold disc electrodes (Pine Instrument Co., Grove City, PA) were used as substrates for deposition of lead dioxide. For X-ray diffraction (XRD), Auger and Raman experiments, a gold disc electrode (Pine Instrument Co., ACMDI 6070Au, 0.283 cm^2) without a Teflon shroud was used. The absence of Teflon avoided possible interference from the Teflon in the spectroscopic experiments. An electrode with a detachable gold disc (Pine Instrument Co., AFMT28Au, 0.196 cm^2) was used when lead dioxide samples were to be examined by a scanning

electron microscopy (SEM). Finally, a typical gold disc electrode with a Teflon shroud (Pine Instrument Co., AFDD20Au, 0.496 cm^2) was used for the measurement of the electrocatalytic reactivity of electrodeposited pure and mixed lead dioxide electrodes. Prior to electrodeposition, the electrodes were polished with 0.05μm Buehler alumina (Buehler Ltd., Lake Bluff, Illinois) and rinsed thoroughly with triply distilled water.

Potentiostat. Potentiostatic control for electrodeposition and testing of electrocatalytic activity of oxide electrodes was by a Model RDE3 Potentiostat/Galvanostat (Pine Instrument Co.). A miniature saturated calomel electrode (SCE; Model 13-639-79, Fisher Scientific) and a piece of Pt wire served as reference electrode and counter electrode, respectively. All potentials are reported as volts (V) vs. the SCE.

Rotator. A rotator (Model ASR-2, Pine Instrument Co.) was used to control the rotational velocity of the electrodes in the process of electrodeposition and activity measurements. This rotator could control the rotation velocity of the electrode between 0 and 10,000 rev min^{-1} by manual adjustment of a servo-controlled system.

Recorder. Current-voltage (i-E) curves were recorded on a X-Y recorder (Model 7035B, Hewlett Packard, San Diego, CA).

Current-time (i-t) curves were recorded on a stripchart recorder (Model SR-225B, Heath Schlumberger).

Coulommetry. Exhaustive electrolysis at constant potential (1.50 V vs. SCE) was applied to determine the number of electrons (n, eq mol^{-1}) for each compound used for testing of the electrocatalytic reactivity of PbO_2 and mixed Bi-Pb oxide. The coulometric cell was assembled from a cylindrical Pt gauze (ca. 30 cm^2) plated with PbO_2 or a mixed oxide as a working electrode, a reference electrode (SCE), and a Pt wire counter electrode. The counter electrode was placed within a cylindrical fritted-glass tube and was located at the center of the cylindrical working electrode. The reference electrode was placed in a glass cell with a side-arm connected to the coulometric cell through a stopcock. The net volume of the working chamber of the cell was about 40 mL. The test solutions containing usually 5-10 μmoles of each compound were stirred magnetically.

Preparation of electrodes. Pure and doped PbO_2 electrodes were prepared by electrodeposition on a gold rotating disc electrode. The electrode was scanned from -0.45 V to 1.65 V in the solution of Pb(II), or in the solution of Pb(II) containing the doping metal ion, using a rotation rate of 900 rev min^{-1}. After ca. 20 cycles, the potential was fixed at 1.60 V vs. SCE for a sufficiently long time so that the gold

electrode was covered with oxide. The thickness of oxide films, estimated from the coulombs passed for stripping the PbO_2 and the density of PbO_2, was about 6,000-10,000 Å. The thickness of oxide was not critical for the electrocatalytic reactivity so long as the substrate (Au) was totally covered.

Test of electrocatalytic reactivity. The electrocatalytic reactivity of the electrodeposited pure and doped PbO_2 was compared by measuring a current at a constant detection potential (1.60 V vs. SCE) in the presence of the various selected inorganic and organic compounds. The analytes were introduced into the cell containing 1.0M $HClO_4$ while using a rotation rate of 3600 rev min^{-1} to produce rapid mixing. Then, currents were recorded on a stripchart recorder as the rotation velocity was decreased in a stepwise fashion. The rotation velocities of the electrode were 3600, 2500, 1600, 900, 400, and 100 rev min^{-1}. At the detection potential of 1.60 V, there was no contribution to total current resulting from oxygen evolution at the pure or mixed-oxide electrodes in 1.0M $HClO_4$.

Calculation of rate constants. Heterogeneous rate constants (k, cm sec^{-1}) for all analytes at each electrode were calculated according to the following equation [5]:

$$\frac{1}{i} = \frac{1}{nFAkC^b} + \frac{1}{0.62nFAD^{2/3}\nu^{-1/6}C^b} \cdot \frac{1}{\omega^{1/2}}$$

where A is the electrode area (cm^2), n is the number of electrons involved in the oxidation step (eq mol^{-1}), F is Faraday constant (coulomb eq^{-1}), D is the diffusion coefficient (cm^2 sec^{-1}), ν is the kinematic viscosity (cm^2 sec^{-1}), C^b is the bulk concentration of analytes (mol cm^{-3}), and ω is the angular velocity of electrode rotation (radian sec^{-1}). The rate constants (k) were calculated from the intercepts in the plots of $1/i$ vs. $1/\omega^{1/2}$.

C. Results and Discussion

Some of the doping agents tested and the various analytes used for testing electrocatalytic reactivity are listed in Table III-1. Further details about the dopant and analyte concentrations, and the values of heterogeneous rate constants (k) obtained are listed in the Appendix.

After a mixed lead dioxide was prepared by electrodeposition from solutions of lead(II) containing the metal ion of interest as a doping agent, no effort was made to confirm qualitatively whether the dopant was electrodeposited with lead into a mixed oxide. Heterogeneous rate constants for oxidation of a selected compound at the

Table III-1. Survey of doping agents and analytes tested for the measurement of the electrocatalytic activity of metal-oxide doped PbO_2

Analyte	Doping Agents[a]							
	Ag^{2+}	Bi^{3+}	Co^{2+}	Cr^{3+}	Fe^{3+}	Ge^{4+}	Mn^{2+}	pure
5-sulfursacylic-acid		G						F P
phenol		G		F				P
n-propanol		F	F			F	F	P
allyl alcohol		F	F		F	F	F	P
methanol	G	F	F	F				P
chromium(III)	F	P	F				F	P
glucose	F	P					F	P
propyl glycol					F	F		P
manganize(II)	G	G			G	F	P	P

[a]G, F and P represent effects of metal ions as a doping agent for oxidation of compounds in the left column (G: good, F: fair, P: poor).

Analyte	Doping Agents							
	Mo^{6+}	Na^{+}	Ni^{2+}	Os^{2+}	Pd^{2+}	Ti^{4+}	V^{4+}	pure
methanol			F		G			P
glucose				F				P
n-propanol				F	F		F	P
allyl alcohol	G		F	F	F		F	P
manganize(II)	G	F	F		F	F	F	P

mixed oxide were measured and compared to that at pure lead dioxide. The absence of significant change in the rate constant, in comparison to electrodeposited pure PbO_2, was sufficient ground to eliminate that ion from further consideration.

Metal ions tested can be largely divided into three groups in terms of changes in electrocatalytic activity: (i) no change, (ii) decrease, (iii) increases in rate constant. This classification was based on the ratio of the value of heterogeneous rate constant of oxidation of compounds on the mixed oxide (k_m) to the value on the pure PbO_2 (k_p). If the value of the ratio, i.e., k_m/k_p, was greater than 2.0, then the dopants belonged to group (iii), i.e., As, Bi, Fe, Ir, Mo, Rh. If the value was less than 0.5, then the dopants belonged to group (ii), i.e., Ga, In, Tl. If the value was between 0.5 and 2.0, i.e., $0.5 \leq k_m/k_p \leq 2.0$, then the dopants were classified as belonging to group (i), i.e., Na, Mg, K, Ca, V, Zr, Mn, Ru, Ni, Cu, Zn. There are several ions which were observed to interfere with the electrodeposition of lead dioxide, i.e., Nb, Sn, and Se.

Most metal ions were not effective in producing electrocatalysis. However, the metal ions, As(V), Bi(III), Fe(III), Ag(II), Mo(VI), and Pd(II) showed siginificant increase among the group (iii) metal ions. Metal ions from the platinum series (Pt, Pd, Rh, Ru, and Os) also showed interesting results. The dopant concentrations of the

platinum series could not be high because they usually were available only as the chloride complexes. In the presence of Cl^-, severe attack by Cl^- was found to cause the partial corrosion or chemical stripping of the oxide. Some organic compounds were effectively oxidized, although the reactions were still kinetically controlled, on the Pd(II) doped lead dioxide. The dopant concentration was at the part-per-thousand level. The use of Bi(III) ion as a doping agent was especially effective to increase the reactivity of β-PbO_2 for oxidation of many compounds.

The promising effect of Bi(III) for numerous oxygen-transfer reactions stimulated further study of this mixed oxide. The characteristic current-potential curves (i-E) obtained by cyclic voltammetry for gold electrode in the presence of Pb(II) only (dashed line) or Pb(II) plus Bi(III) in the electrolyte of 1.0M $HClO_4$ are shown in Figure III-1 and will be described briefly. The anodic current observed in the region $1.0\ V < E < 1.5\ V$ during the positive scan of the potential is due to the formation of oxides: lead dioxide, the mixed lead dioxide, and gold oxide. Appreciable O_2 evolution occurs at $E > 1.65$ V, which serves to set an anodic limit for the positive potential scan. During the negative scan of potential, reduction of the oxides occurs yielding the two cathodic peak at $E = 1.1$ V and $E = 0.8$ V. The cathodic peak at $E = 1.1$ V is for the reductive stripping of lead dioxide. The other cathodic peak at $E = 0.8$ V is for

Figure III-1. I-E curves of Pb(II) and Pb(II) + Bi(III) in 1.0M $HClO_4$ at a Au RDE

Rotation velocity of electrode (ω): 900 rev min^{-1}
Potential scan rate (ϕ): 6 V min^{-1}
(•••): 1.0mM Pb(II)
(——): 1.0mM Pb(II) + 0.05mM Bi(III)

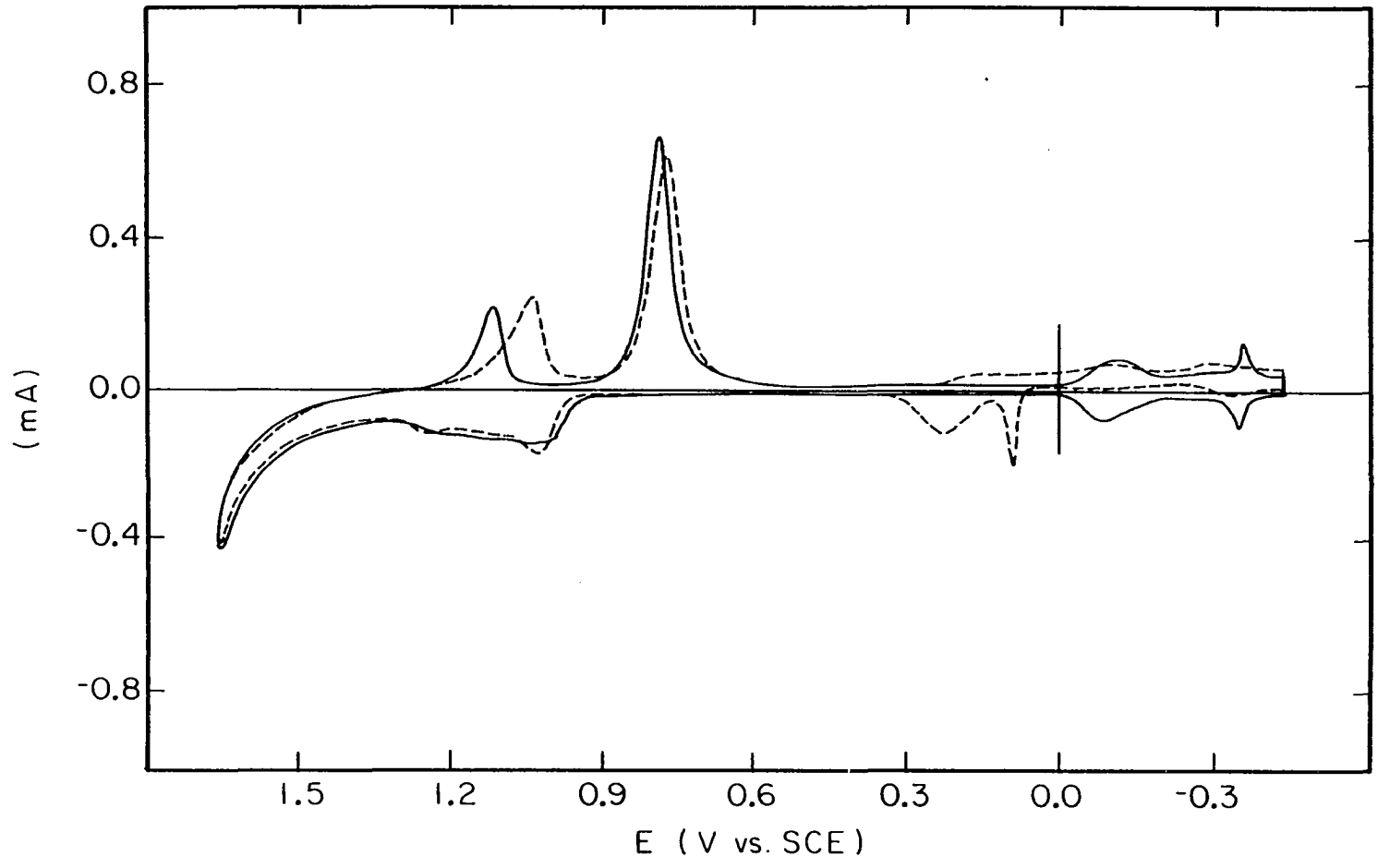
0.8
0.4
0.0
-0.4
-0.8
(mA)
1.5
1.2
0.9
0.6
0.3
0.0
-0.3
E (V vs. SCE)

the reduction of gold oxide, which was formed simultaneously during the anodic deposition of lead dioxide.

The observation of change in the stripping potential of oxides is one method to estimate the stability of the oxide formed on the positive scan of the potential. The stripping peak (dotted line in Figure III-1) obtained for the negative scan is shifted to more negative values in the presence of Bi(III). This strongly indicates that the mixed bismuth-lead oxide formed in the presence of Bi(III) is more stable than pure lead dioxide.

Results obtained by calculating the heterogeneous rate constants for oxidation of selected analytes on the rotated pure lead dioxide and mixed bismuth-lead oxide electrode are summarized in the Appendix. In general, the rate was increased on the mixed oxide. Oxidation of several organic compounds (the methanol and amine series), estimated by amperometric responses (i-t) with rotation rate change of the electrode at constant anodic potential, showed that the oxidation rate was increased. However, the anodic current remained independent of the rotation velocity which means that these electrodic reactions remained kinetically controlled. The most dramatic examples showing the highest effect in electrocatalytic response, are the oxidation of phenols, citric acid and 2-thiophene carboxylic acid. The anodic current for oxidation of these compounds at a constant potential of 1.60 V was independent of the rotation rate for

the pure lead dioxide electrode and its magnitude was very small. These compounds are concluded to be inactive at pure PbO_2. However, anodic currents for oxidation of phenols and 2-thiophene carboxylic acid at the mixed oxide varied linearly with $\omega^{1/2}$. From a plot of i vs. $\omega^{1/2}$, a straight line that intersects the origin was obtained. Since any deviation from the straight line that intersects the origin indicates some kinetic involvment in the electron transfer reaction [6], it is concluded to be that the oxidation of these compounds are made virtually mass-transport limited by the presence of Bi in the mixed oxide. In this case, the kinetics of electron transfer and associated chemical reactions are very rapid compared to the mass transfer process.

The technique of controlled potential coulometric electolysis was applied successfully for determining n, the number of electrons lost per molecule in the anodic electrode reactions [7]. Values of n for several reactions at pure lead dioxide and the mixed lead-bismuth oxide are summarized in Table III-2. The reaction products listed in the final column were estimated from n. In the case of sulphur compounds, production of SO_4^{2-} was verified by observation of the precipitation of white barium sulfate following addition of Ba(II). In many cases, integer values of n were obtained. However, noninteger values of n were also found probably because of secondary chemical reactions during the

Table III-2. Evaluation of the number of electrons (n, equiv mol^{-1}) involved in the oxidation of various compounds by exhaustive controlled potential coulometry[a]

Analyte	n/equiv mol^{-1}[b]		Product[c]
	PbO_2	Bi mixed PbO_2	
Fe^{2+}	1.0±0.1	1.0±0.1	Fe^{3+}
$As(OH)_3$	2.1±0.1	2.0±0.1	$OAs(OH)_3$
Br^-	1.0±0.1	1.0±0.1	$0.5Br_2$
I^-	6.1±0.1	5.9±0.1	IO_3^-
Mn^{2+}	5.0±0.1	5.0±0.1	MnO_4^-
$S_2O_3^{2-}$	7.9±0.1	8.1±0.1	$2SO_4^{2-}$
SCN^-	6.0±0.1	6.0±0.1	$SO_4^{2-} + CN^-$
$H_2N-C(S)-NH_2$	6.8±0.1	5.5±0.8	SO_4^{2-} + $H_2N-C(O)-NH_2$
$H_3C-C(S)-NH_2$	7.9±0.1	5.8±0.1	SO_4^{2-} + $H_3N-C(O)-NH_2$
$H_2C(SH)-CH_2-SO_3H$	5.9±0.1	6.1±0.1	$HO_3S-CH_2-CH_2-SO_3H$
$C_4H_3(S)-CH_2-CO_2H$	6.3±0.1	7.1±0.1	???
$C_6H_5-SO_2H$	1.7±0.1	2.0±0.1	$C_6H_5-SO_3H$
$H_2C(SH)-CH(NH_2)-CO_2H$	6.6±0.1	6.0±0.1	$HO_3S-CH_2-CH(NH_2)-CO_2H$

[a]Conditions: 1.0M $HClO_4$.

[b]Uncertainty is standard deviation from triplicate results.

[c]Products estimated from n; SO_4^{2-} identified by Ba^{2+} test.

Table III-2. (Continued)

Analyte	n/equiv mol^{-1}[b]		Product[c]
	PbO_2	Bi mixed PbO_2	
$H_3C-S-C_6H_4-CO_2H$	2.4±0.2	2.9±0.1	$H_3C-SO_2-C_6H_4-CO_2H$
EDTA	10.0±0.1	10.2±0.1	???
$HO-C(CH_2-CO_2H)_2-CO_2H$	no rxn	2.0±0.2	$2CO_2 + 4HCO_2H$
$HO_2C(HC-OH)_2CO_2H$	6.7±0.1	6.0±0.1	$2CO_2 + 2HCO_2H$
$H_2C(OH)-CO_2H$	no rxn	2.0±0.2	$OHC-CO_2H$
HCO_2H,HCHO	no rxn	no rxn	——
$HO-C_6H_4-OH$	2.1±0.1	2.1±0.1	$(O)C_6H_4(O)$
C_6H_5-OH	4.2±0.1	4.0±0.1	$(O)C_6H_4(O)$
$HO-C_6H_4(CO_2H)-SO_3H$	7.4±0.1	9.3±0.2	SO_4^{2-} + ??
$C_6H_8O_6$	2.8±0.2	4.6±0.1	???

electrolysis. This phenomenon is distinctive for organic molecules.

The current-potential responses on the negative scan for Mn(II), cystine, and As(III) at rotated lead oxide and mixed lead-bismuth oxide electrodes are shown in Figure III-2. The anodic plateau current at the mixed oxide is linearly increased with $\omega^{1/2}$; however, at pure PbO_2, it is not a linear function of $\omega^{1/2}$. This is indicative of a mass-transport limited process only at the mixed oxide.

The observed half-wave potential ($E_{1/2}$) for oxidation of Mn(II) is virtually the same at the two electrode. The half-wave potential should be the same if the energy barriers for charge transfer controlling the oxidation of Mn(II) at the two electrodes are equal. This is concluded to indicate that the rate determining step in the oxidation process, concluded to be oxygen-transfer, does not involve charge transfer. The observed $E_{1/2}$ for oxidation of As(III) at the mixed electrode is nearly the same as for the case of Mn(II), even though the reversible potential is ca. 0.30 V for the As(V)-As(III) couple. The fact that the half-wave potentials are similar for the compounds tested is evidence of a single common rate controlling process. This rate controlling process is concluded to be the generation of active oxygen species at the surface of the oxide electrodes. There is a certain potential to generate active oxygen species. Unless these species are generated, the anodic oxygen-transfer reactions

Figure III-2. I-E curves of PbO_2 and $PbO_2 \cdot Bi_2O_5$ on the negative potential scan in the presence of 1.0mM Mn(II), 1.0mM cystine and 2.5mM As(III)

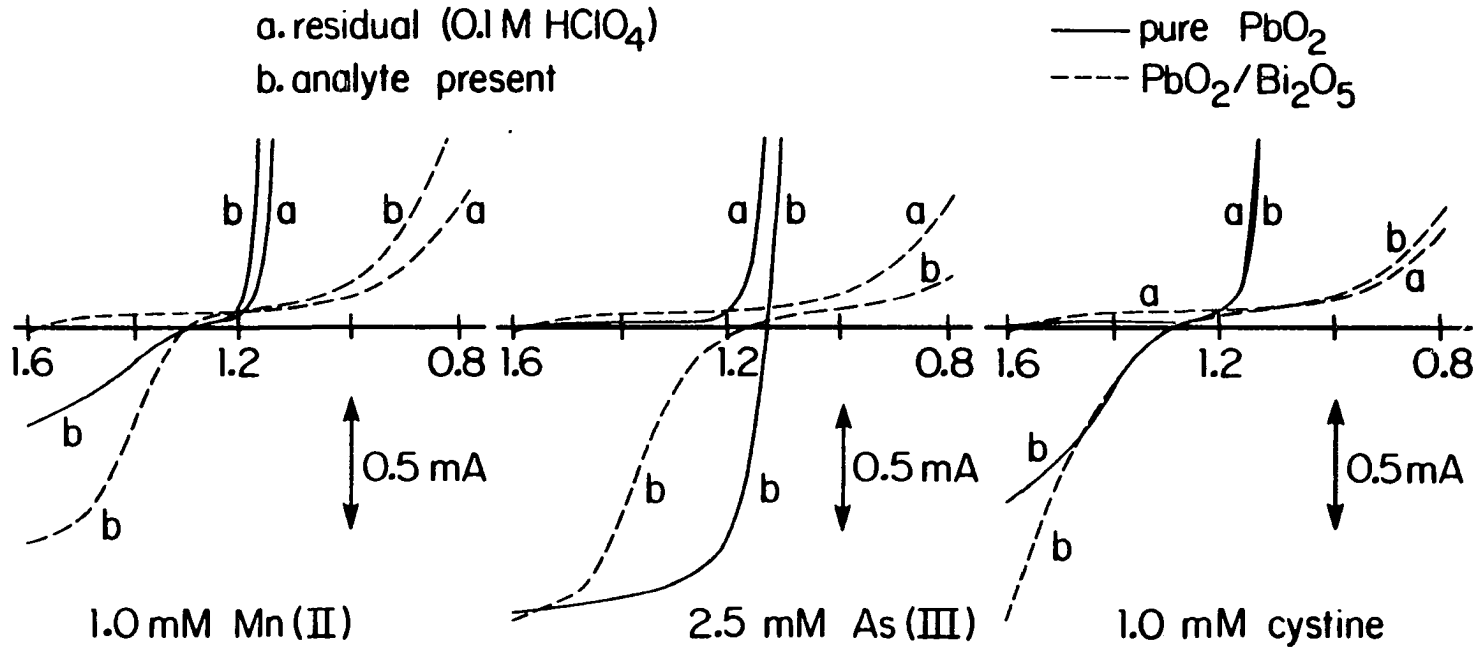
a. residual (0.1 M $HClO_4$)
b. analyte present
—— pure PbO_2
---- PbO_2/Bi_2O_5
1.6
1.2
0.8
0.5 mA
1.0 mM Mn (II)
2.5 mM As (III)
1.0 mM cystine

are not possible even though oxidation reactions are expected to proceed from thermodynamics at lower potential, e.g., consider As(V)-As(III) couple. Therefore, the generation of active oxygen species tends to be characteristic of anodic oxygen-transfer reactions.

D. References

1. Trasatti, S. Electrochim. Acta 1984, 29, 1503.
2. Thomas, J. M.; Thomas, W. J. In "Introduction to the Principles of Heterogeneous Catalysis"; Academic: New York, 1967; Page 270.
3. Delmastro, A.; Maja, M. J. Electrochem. Soc. 1984, 131, 2756.
4. Sharpe, T. S. In "Encyclopedia of Electrochemisty of the Elements"; Bard, A. J., Ed.; Marcel Dekker: New York, 1973.
5. Bard, A. J.; Faulker, L. R. In "Electrochemical Methods"; John Wiley: New York, 1980; Page 291.
6. Bard, A. J.; Faulker, L. R. In "Electrochemical Methods"; John Wiley: New York, 1980; Page 290.
7. Bard, A. J.; Sarthanam, K. S. V. In "Electroanalytical Chemistry"; Bard, A. J., Ed.; Marcel Dekker: New York, 1970; Vol. 4, Page 216.

IV. THE EFFECTS OF FOREIGN IONS ON THE GROWTH OF LEAD DIOXIDE ON A GOLD ELECTRODE

A. Abstract

The effects of cations and anions on the nucleation and growth of lead dioxide were studied at a gold rotated disc electrode. The accumulation of electrodeposited lead dioxide in the presence of a high concentration of As(III) does not proceed because the chemical stripping rate of lead dioxide by As(III) is greater than the deposition rate for PbO_2. For anions, sulfate and nitrate greatly enhance the rate of deposition of lead dioxide whereas phosphate decreases the rate of deposition. It is shown that the growth of PbO_2 on the gold substrate is not a uniform process, but proceeds by preferential island growth.

B. Introduction

There is interest in the development of PbO_2 as an anode electrode material which can be used as an analytical transducer with high electrocatalytic activity for anodic oxygen transfer processes [1]. Lead dioxide is favored as an anode material because of its high electrical conductivity, large oxygen overpotential, and chemical inertness in applications for electrolysis and electrosynthesis [2]. The

deposition of PbO_2 on such substrates as Pt, Ti, tin oxide and graphite have been reported [3-8]. It is known from this literature that the nucleation process plays an important role in the anodic electrodeposition of PbO_2. Some metal ions present in the oxidation of Pb(II) are well incorporated into the PbO_2 matrix during electrodeposition to produce a mixed oxide of improved reactivity and stability in comparison to pure PbO_2 [9]. Other metal ions make the nucleation process difficult or they remain as inert impurities without influencing the deposition process.

In this work, several cations and anions were studied for their effects on the nucleation process in the electrodeposition of PbO_2 on a gold substrate. Nucleation was monitored by voltammetric (i-E) and amperometric (i-t) techniques. Scanning electron micrography was used to examine the electrodeposited oxide films.

C. Experimental

Chemicals. All chemical used were Analytical Grade Reagents from Fisher Scientific or Baker Chemicals. The supporting electrolyte was 1.0M $HClO_4$, and triply distilled water was used to prepare solutions. All test solutions were deaerated by dispersion of N_2 and an inert atmosphere was maintained over the solutions during the electrochemical measurements.

Instrumentation. A rotated gold disc electrode (RDE, 0.496 cm^2), platinum wire and saturated calomel electrode (SCE) were employed as the working, counter and reference electrodes, respectively. The potential and rotation velocity were controlled, respectively, by a potentiostat (Model RDE 3; Pine Instrument Co., Grove city, PA) and a rotater (Model ASR-2; Pine Inst. Co.). Voltammetric (i-E) and amperometric (i-t) response curves during the deposition were recorded on a X-Y recorder (Model 7035B; Hewlett Packard) or a stripchart recorder (Model SR-255B; Heath Schlumberger).

Voltammetry. The electrode potential for all solutions of 1.0M $HClO_4$ was scanned in the range -0.4 V to 1.70 V vs. SCE. The scan rate was varied to observe changes in the stripping peak of PbO_2 appearing at ca. 1.10 V on the negative scan. Any enhancement or deterioration caused by the added impurity in the formation of PbO_2 was evaluated from the change of the stripping peak. Amperometric responses (i-t) were recorded for a step-wise change in potential from a value in the "double layer region" (0.30 V) to a predetermined value (1.55 V) which was sufficiently positive to initiate nucleation of PbO_2. The induction period for nucleation was estimated from the i-t curves.

The thickness of oxide films was controlled by the appropriate choice of values for the applied potential,

deposition time, and rotation velocity of the electrode. The surface morphology and nucleation process of PbO_2 on the gold substrate were observed with scanning electron microscope (SEM; Model 200, Cambridge).

D. Results and Discussion

The first step in the electrodeposition of lead dioxide is known as nucleation. Nucleation is the process leading to formation of the smallest possible stable aggregates of insoluble metal oxide. Scanning electron micrographs in Figure IV-1 show small crystallites resulting from the continued growth of the nuclei of PbO_2. It is clear also from the micrographs that the morphological features of the Au substrate which are the most favorable for nucleation are sharp points or ridges on the Au surface. Extended growth of the crystallites leads to contact between neighboring crystallites and the Au substrate becomes completely eclipsed from the view of the microscope. The extent of deposition was considered satisfactory when voltammetric response in the region of anodic oxygen evolution appeared to be that due soley to PbO_2 and not influenced by Au. When voltammetric data following additional deposition was identical to data obtained prior to the additional deposition, the formation of PbO_2 electrode was considered sufficient to electrochemically eclipse the Au electrode.

Figure IV-1. Scanning electron micrographs of electrodeposited PbO_2 at a Au RDE

Deposition potential: 1.60 V vs. SCE
Rotation velocity of electrode (ω): 900 rev min^{-1}
Deposition time: 2.0 min
Solution: 1.0mM Pb(II) in 1.0M $HClO_4$

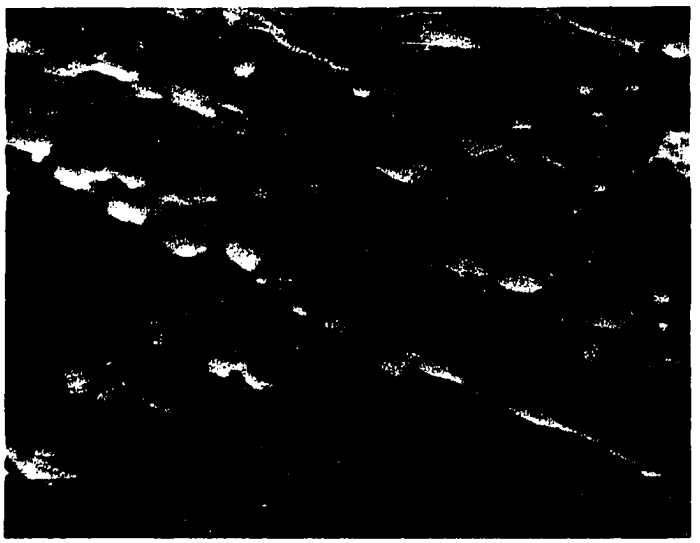

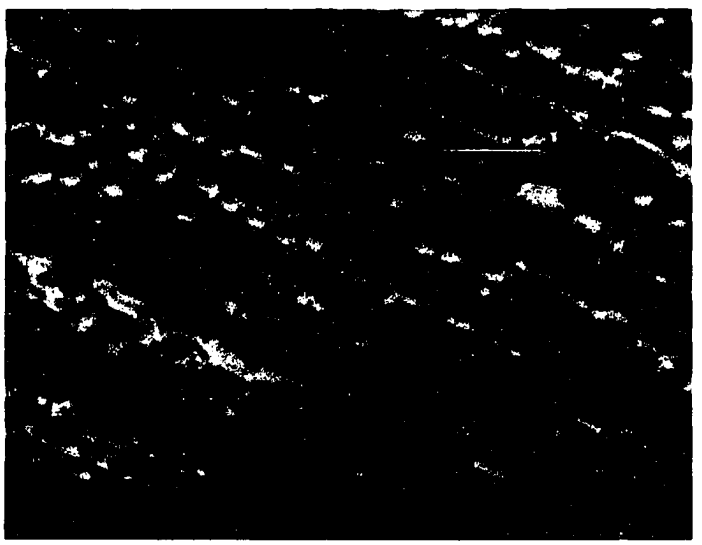

Current-time (i-t) profiles were obtained during the anodic deposition process of pure PbO_2 at a gold rotated disc electrode following a single potential step from 0.30 V to 1.55 V vs. SCE. and are illustrated in Figure IV-2. There are three characteristic regions of the i-t curves. The first region (I) consists of a very large current spike produced by double-layer charging and has a very short time scale. The second region (II) corresponds to the induction period for the nucleation of PbO_2 and has a very low constant current. After the induction period, stable aggregate of PbO_2 nuclei grow, which gives the third region (III) corresponding to the uprising portion in the i-t curves. Steady-state currents (IV) obtained after the rising current in the curves do not linearly depend on the rotation velocity (ω); however, the induction period is increased as the rotation velocity of the electrode increases. Basically, the induction time (t_{ind} for period II) represents a nucleation period which is controlled by nucleation mechanism [10] and depends on the concentration of Pb(II) [11].

Fleischmann and Liler [11] presented a probable mechanism for the nucleation and growth of PbO_2 which is schematically represented as follows:

Figure IV-2. I-t curves for anodic deposition of PbO_2 with a single potential step

Electrode: a Au RDE (0.496 cm^{-2})
Solution: 1.0mM Pb(II) in 1.0M $HClO_4$
Potential changes: 0.30 V ——> 1.55 V vs. SCE
A: 2500 rev min^{-1}
B: 1600 rev min^{-1}
C: 900 rev min^{-1}
D: 400 rev min^{-1}
E: 100 rev min^{-1}

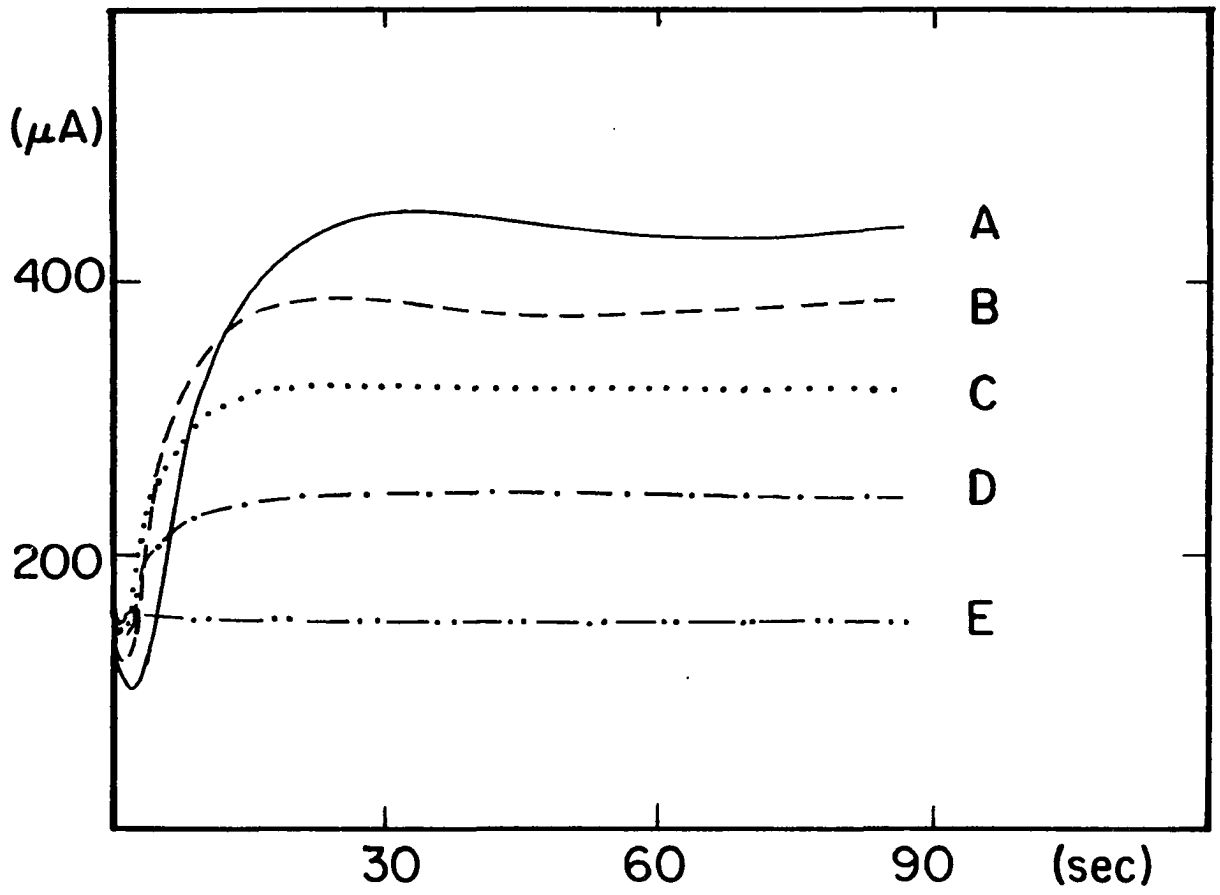
(μA)
400
200
A
B
C
D
E
30
60
90
(sec)

$$H_2O \rightleftharpoons OH^- + H^+ \qquad (1)$$

$$OH^- \rightleftharpoons OH_{ads} + e \qquad (2)$$

$$Pb(II) + OH_{ads} + OH^- \longrightarrow Pb(OH)_2^{2+} + e \qquad (3)$$

$$Pb(OH)_2^{2+} \rightleftharpoons PbO_2 + 2H^+ \qquad (4)$$

$$\text{net: } Pb(II) + 2OH^- \rightleftharpoons PbO_2 + 2H^+ + 2e \qquad (5)$$

As shown in the reactions above, discharge of hydroxide ion and subsequent reaction to form lead hydroxide ions is a necessary step in the formation and growth of PbO_2. Therefore, the change in the induction time with variation in rotation rates of the electrode is concluded to be the result of the change in the residence time of $Pb(OH)_2^{2+}$ at the electrode-solution interface. The longer induction time at the higher rotation rate can be explained by the fact that severe stirring of deposition solution prevents the soluble $Pb(OH)_2^{2+}$ formed in reaction (3) from settling down at the favorable site for nucleation. It was observed that the induction period is decreased as the applied potential increases. The induction period was estimated to be the time interval between the end of the double layer charging current and the beginning of the rising current. It ranges from 200 μsec to 2 sec depending on the applied potential. Because the induction time depends on the rate of discharge of OH^- ions [8] and subsequent adsorption of the OH species according to reaction (2) [12], the decrease in the induction

time with overpotential suggests that a heterogeneous electron-transfer is the rate-limiting step for nucleation.

Many cations, such as As(III), Bi(III), Ag(I), Zn(II), Mo(VI), Mn(II), and Mg(II), added as impurities to the deposition solution were observed to influence the growth rate of PbO_2 and to change the shape of the stripping peak of PbO_2 obtained during the negative scan of the applied potential. However, it is hard to point out that one ion has more effective on the nucleation and growth of PbO_2 than the others because each metal salt available had different anion and the nature and concentration of the anion also affect the processes [7,13]. Particularly, it was observed that metal ions combined with sulfate ions decrease the induction period, thereby, increasing the overall rate of the formation of PbO_2.

Among the cations tested, As(III) was eminent for blocking the nucleation and growth of PbO_2. Current-potential curves (i-E) obtained by cyclic voltammetry are shown in Figure IV-3 for a gold electrode in the presence of Pb(II) only (solid line) or Pb(II) plus As(III) (dashed line) in the deposition solution. The stripping peak of PbO_2 (ca. 1.15 V vs. SCE.) in the curves appeared on the negative scan cannot be observed when As(III) ions are present in the deposition solution. This indicates that lead dioxide on the gold electrode is not readily formed in the presence of As(III) during the positive scan of potential. The

Figure IV-3. I-E curves of Pb(II) and Pb(II) + As(III) in 1.0M $HClO_4$ at a Au RDE

Rotation velocity of electrode (ω): 900 rev min^{-1}
Potential scan rate (ϕ): 6 V min^{-1}
(···): 1.0mM Pb(II)
(——): 1.0mM Pb(II) + 0.04mM As(III)

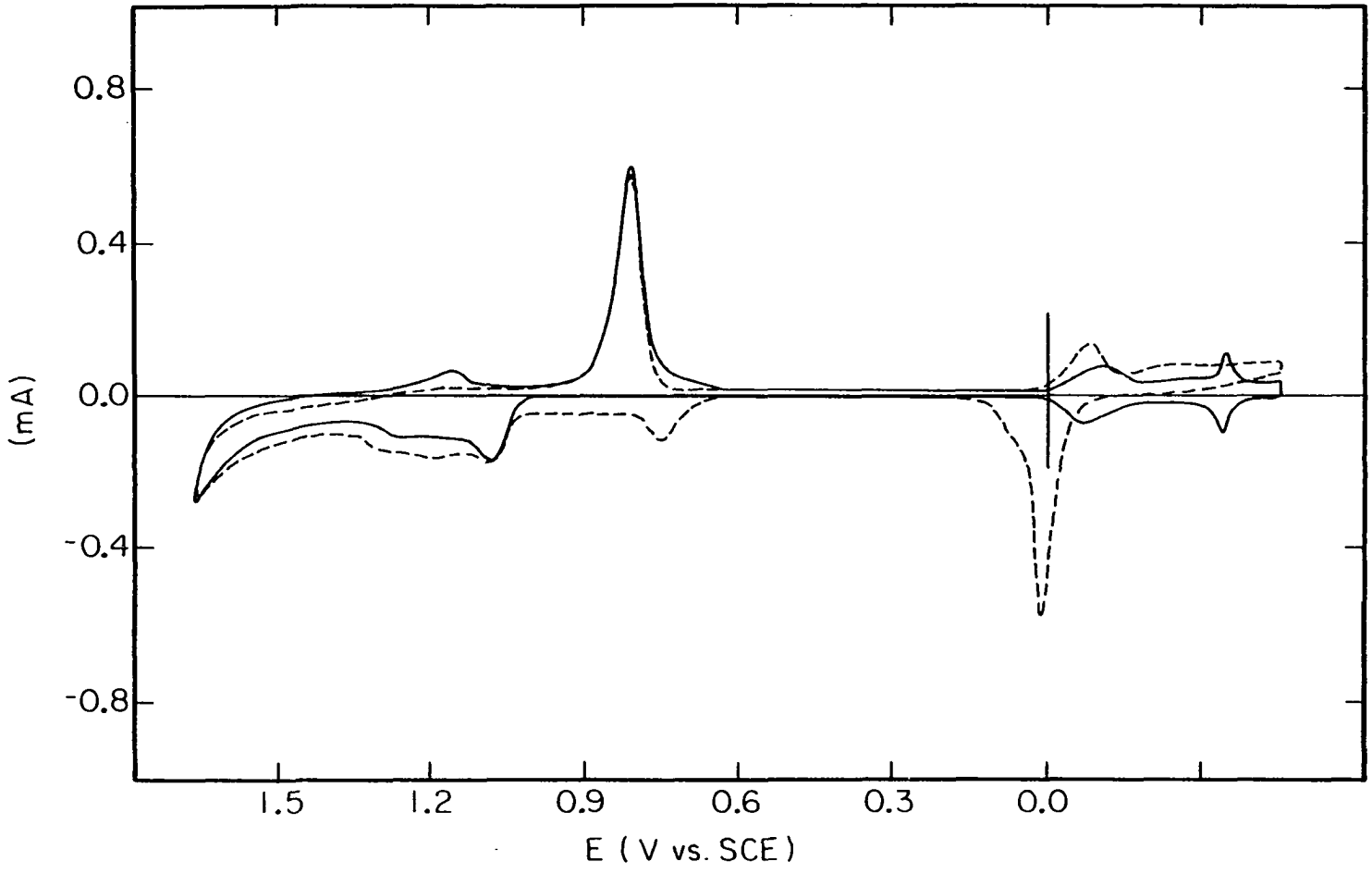
0.8
0.4
0.0
-0.4
-0.8
(mA)
1.5
1.2
0.9
0.6
0.3
0.0
E (V vs. SCE)

inhibition phenomena which shows the longer induction time in the i-t curves also was observed. The relationship between the deposition time and fomation of lead dioxide in the presence of As(III) is summarized in Table IV-1. As shown in the Table, the anodic electrodeposition of PbO_2 on gold substrates is impossible at high level concentration of As(III) although deposition time is increased up to one hour. The inhibition is explained by the fact that chemical stripping of PbO_2 by As(III) and easy oxidation of As(III) at the deposition potential might shield the oxidation of Pb(II) in the competitive oxidative electrodeposition of two species on the gold substrate. Reactions involved in this process can be written as,

$$As(III) \longrightarrow As(V) + 2e \qquad (6)$$

$$PbO_2 + 4H^+ + 2e \longrightarrow Pb(II) + 2H_2O \qquad (7)$$

$$As(III) + PbO_2 + 4H^+ \longrightarrow As(V) + Pb(II) + 2H_2O \qquad (8)$$

Calculated free energy of the reaction (8) from thermodynamic data is $-4.12 * 10^5$ J $mole^{-1}$. Therefore, it is apparent that the deposition or nucleation rate of PbO_2 crystal is far less than the stripping rate at the high level concentration of As(III).

Many anions of sodium salts, such as NaH_2PO_4, NaCl, $NaKC_4H_4O_6$, $NaC_2H_3O_2$, Na_2SO_4, and NaF were used to study the

Table IV-1. Effects of As(III) in the electrodeposition of PbO_2 on a gold disc electrode

Deposition solution	Deposition time (min)	Deposition potential (V vs. SCE)	Formation of PbO_2
1.0mM Pb(II)	10	1.50	no
+	10	1.60	yes
0.08mM As(III)	10	1.65	yes
1.0mM Pb(II)	10	1.60	no
+	10	1.70	no
0.8mM As(III)	30	1.75	no
0.02mM Pb(II)	60	1.65	no
+			
1.0mM As(III)			

anion effects. All compounds has common cations, i.e., sodium ion. By using common cation, any side effects from cation can be minimized.

Among the tested anions, sulfate, nitrate and fluoride ions increases the rate of formation of PbO_2. Especially, the sulfate ions greatly enhance the anodic electrodeposition of PbO_2. Current-potential curves (i-E) obtained by cyclic voltammetry for a gold electrode (Figure IV-4) show that the area of the stripping peak (ca. 1.15 V vs. SCE) representing the dissolution of PbO_2 on the negative scan is much greater in the presence of sulfate ion. This indicates that the rate of formation of PbO_2 is greatly enhanced by the sulfate. It is shown in Figure IV-5 that the induction time for the nucleation of PbO_2 in the presence of As(III) depends on the concentration of sulfate in the presence of As(III) at the same overpotential. The induction time is sharply decreased as concentration of sulfate increases. It can be envisaged that sulfate ions are more likely adsorped than OH^- species at the same potential because of its charge. It makes Pb(II) ions easier to access the double layer charged more negatively for making nuclear sites. Once $PbSO_4$ is formed at the site it can be easily turned into PbO_2 at the applied potential (E_{app}: 1.60 V vs. SCE) because standard electrochemical potential for the following reaction is 1.22 V vs. SCE.

Figure IV-4. I-E curves of Pb(II) and Pb(II) + SO_4^{2-} in 1.0M $HClO_4$ at a Au RDE

Rotation velocity of electrode (ω): 900 rev min^{-1}
Potential scan rate (ϕ): 6 V min^{-1}
(···): 1.0mM Pb(II)
(——): 1.0mM Pb(II) + 0.4mM SO_4^{2-}

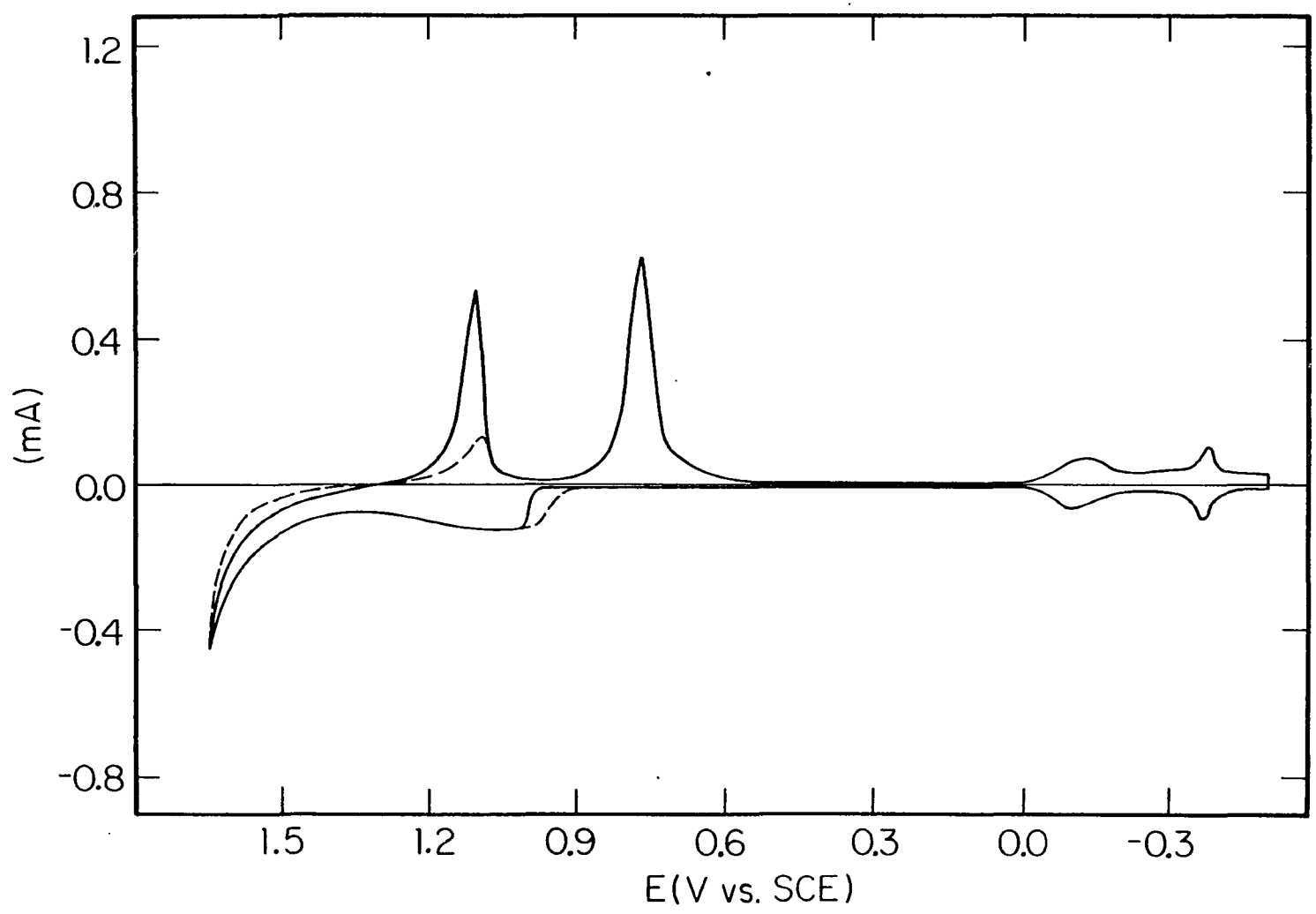
1.2
0.8
0.4
0.0
-0.4
-0.8
(mA)
1.5
1.2
0.9
0.6
0.3
0.0
-0.3
E(V vs. SCE)

Figure IV-5. Changes of induction time as a function of concentration of SO_4^{2-} in the electrodeposition of PbO_2 in 1.0M $HClO_4$

Electrode: a Au RDE (0.496 cm^{-2})
Solution: 1.0mM Pb(II) + 0.02mM As(III) + x mM SO_4^{2-} in 1.0M $HClO_4$
Potential changes: 0.30 V ——> 1.60 V vs. SCE

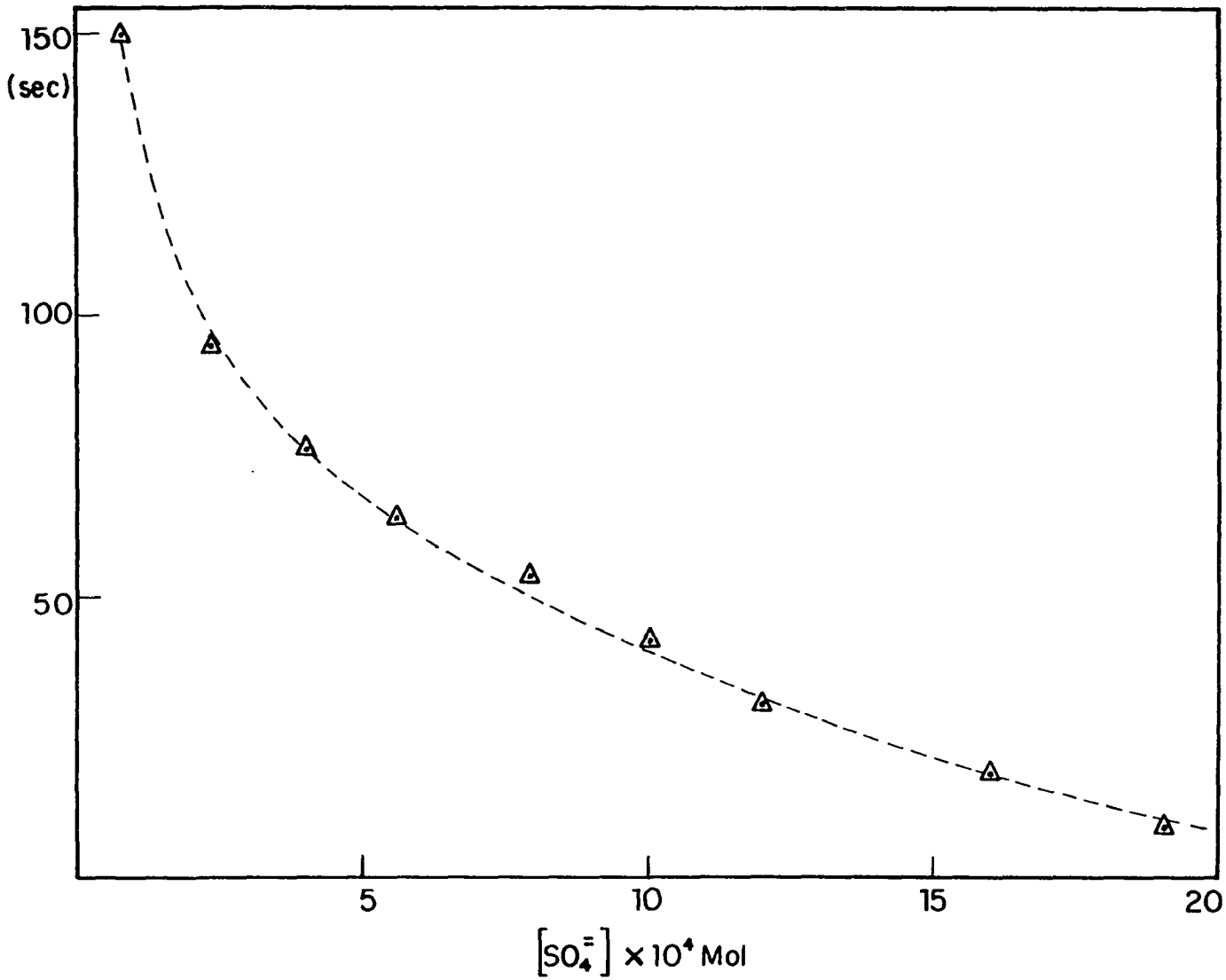
150
(sec)
100
50
5
10
15
20
[SO4=] × 10⁴ Mol

$$2H_2O + PbSO_4 \longrightarrow PbO_2 + 4H^+ + SO_4^{2-} + 2e \qquad (9)$$

Figure IV-6 shows current-time profiles for the formation of PbO_2 in the presence of sulfate (A), As(III) (D), and sulfate plus As(III) (B) in 1.0M $HClO_4$ containing Pb(II) ions (C). The induction time is shorter and the limiting current is larger in the curve B compared to the curve D. The increase in the limiting current and decrease in the induction time for the electrodeposition of PbO_2 are the evidences of enhancing effects of sulfate ions. The sulfate ions are still effective even in the presence of interfering ion such as As(III). That is, the decrease in the rate of anodic deposition by As(III) is compensated by sulfate ions. The trend of enhancing effects was observed for the nitrate and fluoride ion, but their effects are less than that of sulfate ions. It is noticeable that phosphate ions inhibit the formation of PbO_2, probably because a stable oxide of $H[Pb(OH)_2PO_4]$ may be formed at the surface. The oxide is not easily convertible to PbO_2 [8].

In conclusion, among the tested ions, the sulfate ions have the most positive effects on the growth of PbO_2 on the gold electrode and As(III) ions have the most negative effect on the process.

Figure IV-6. I-t curves showing the effects of As(III) and SO_4^{2-} in the electrodeposition of PbO_2 in 1.0M $HClO_4$ on a Au RDE

Electrode: a Au RDE (0.496 cm^{-2})
Rotation velocity of electrode (ω): 900 rev min^{-1}
Potential step: 0.30 V ———> 1.55 V vs. SCE
Solution:
A: 1.0mM Pb(II) + 0.4mM SO_4^{2-}
B: 1.0mM Pb(II) + 0.4mM SO_4^{2-} + 0.02mM As(III)
C: 1.0mM Pb(II)
D: 1.0mM Pb(II) + 0.02mM As(III)

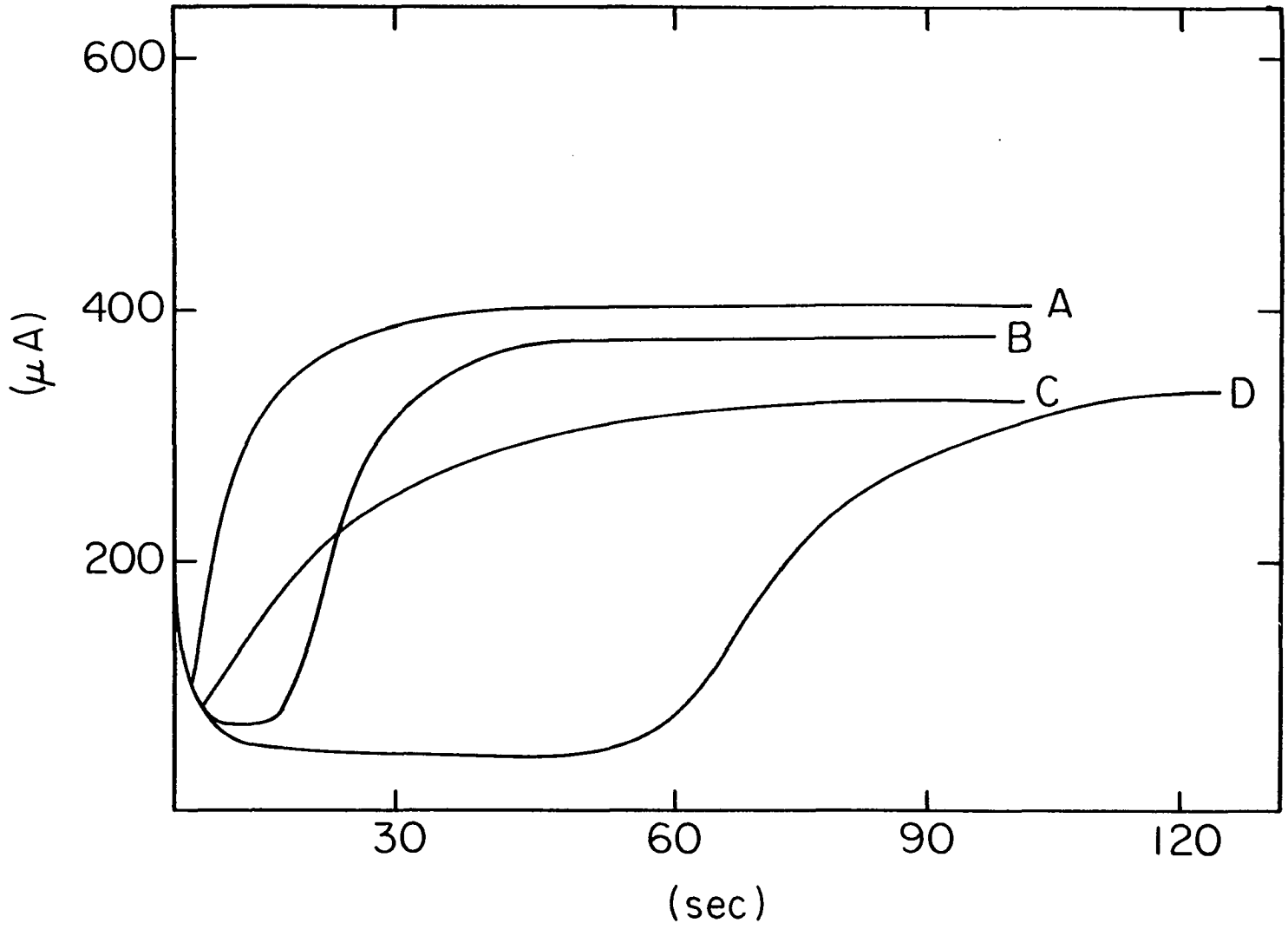
600
400
200
(μA)
A
B
C
D
30
60
90
120
(sec)

E. References

1. Tang, A. P-C.; Johnson, D. C. J. Electrochem. Soc. 1986, 000, 000.

2. Kuhn, A. T. "Electrochemistry of Lead"; Academic: London, 1979.

3. Narasimham, K. C.; Udupa, H. V. K. J. Electrochem. Soc. 1976, 123, 1294.

4. Laitinen, H. A.; Watkins, N. H. J. Electrochem. Soc. 1976, 123, 804.

5. Thanos, J. C. G.; Wabner, D. W. J. Electroanal. Chem. 1985, 182, 25.

6. Barradas, R. G.; Contractor, A. Q. J. Electroanal. Chem. 1981, 129, 327.

7. Beck, F. J. Electroanal. Chem. 1975, 65, 231.

8. Ramamurthy, A. C.; Kuwana, T. J. Electroanal. Chem. 1982, 135, 243.

9. Yeo, I-H.; Johnson, D. C. J. Electrochem. Soc. 1986, 000, 000.

10. Harrison, J. A.; Thirsk, H. R. In "A Guide to the Study of the Electrode Kinetics"; Academic: New York, 1972; Chapter 3.

11. Fleischmann, M.; Liler, M. Trans. Faraday Soc. 1958, 54, 1376.

12. Bagotzky, V. S.; Tarasevich, M. R. J. Electroanal. Chem. 1979, 101, 1.

13. Carr, J. P.; Hampson, N. A. Chem. Rev. 1972, 72, 679.

V. ANODIC OXYGEN-TRANSFER ELECTROCATALYSIS IN OXIDATION OF Mn(II) AND ORGANIC COMPOUNDS AT LEAD DIOXIDE ELECTRODE DOPED WITH GROUP IIIA AND GROUP VA METAL OXIDES

A. Abstract

The heterogeneous rate constant for the anodic oxidation of Mn(II) at PbO_2-based mixed oxide electrodes in 1.0M $HClO_4$ was determined as a function of high doping levels by the oxides of Group IIIA and VA metals. Electrodes were prepared by electrodeposition from solutions containing Pb(II) and the doping metal ions in 1.0M $HClO_4$. Doping with the Group IIIA metal oxides resulted in a slight decrease of the rate constant for Mn(II) oxidation; however, doping with the Group VA metal oxides resulted in significant catalysis of the anodic oxygen transfer reaction as compared to a pure PbO_2 electrode. The rate constant at the mixed oxide deposited from a solution of 1.0mM Bi(III)/1.0mM Pb(II) was at least 25X greater than for pure PbO_2, becoming virtually mass transfer limited at the mixed oxide electrode to rotation rates of 3600 rev min^{-1}. The ratio of [Bi]/[Pb] in the oxide was ca. 0.7.

B. Introduction

In general, anodic oxidation reactions accompanied by transfer of oxygen from water to the reaction produdts are characterized by slow heterogeneous rates at constant (dc) potentials for the popular anode materials (i.e., carbon and noble metals).

Lead dioxide electrodes have been known as to be useful anode for electroanalysis and electrosynthesis and have been studied extensively because of applications in lead-acid storage batteries. Lead dioxide has the desirable electrochemical properties of high electronic conductivity and a large overpotential for anodic evolution of oxygen. However, the available cathodic potential range is seriously restricted because of the large positive value of E° for the PbO_2-Pb(II) half reaction (1.21 V vs. SCE). The electrocatalytic activity of lead dioxide electrodes for supporting anodic reactions had not been studied extensively, when this research began, and appeared to be very limited.

Electrocatalysis at metal oxides doped with small amounts of foreign metals has become of interest. Fishman et al. [1] reported that incorporation of a small amount of platinum into sodium tungsten bronze is effective for electrocatalysis of the cathodic reduction of oxygen. Many workers also found that the catalytic activities of SnO_2, Co_3O_4, and MnO_2 are improved for the anodic evolution of

oxygen and chlorine by doping with foreign metal ions [2-6]. Doping of lead dioxide with antimony was considered to modify the performance of lead acid batteries [7-9] and antimony as an alloying element in the anode grids was found to improve some properties of lead dioxide. Some results of studies of antimony effects on the properties and electrocrystallization of PbO_2 have been reported in the literature [10,11]. Richie et al. [12] suggested that Sb(V) can be adsorbed at growth sites of the lead dioxide crystal surface and can enter the lead dioxide lattice, occupying Pb(IV) sites. Delmastro and Maja [13] have reported some characteristics of PbO_2 doped with many elements (Ag, As, Co, Mn, Ni, Sb, Se, Sn, Te and Zn) which can be present as alloying constituents of the electrode grid and as impurities of the electrolyte in lead-acid batteries. These authors studied the dopant ion effects on the structure of lead dioxide, nonstoichiometry, crystal morphology, self-discharge rate.

In this work, high levels of Group IIIA and VA metal oxides were introduced into electrodeposited PbO_2 as dopants in an attempt to modify the electrocatalytic reactivity of pure β-PbO_2. The concentration of doping metal ions in the deposition solution was increased up to the concentration of Pb(II) in the deposition solution. The electrocatalytic reactivity of β-PbO_2 electrodes doped with metal ions was tested with simple model reactions, such as oxidation of Mn(II) and some organic compounds whose reactions were assumed to involve the anodic transfer of oxygen.

This work was based on the anticipation that incorporation into the slightly distorted rutile structure of β-PbO_2 of metals oxides having stoichiometry different from PbO_2 can alter the activity of surface oxygen and, thereby, should have a significant effect on the heterogeneous rates of anodic reactions controlled by the rate of oxygen transfer. At the electrode potential used for deposited of PbO_2 in 1.0M $HClO_4$ (1.60V vs. SCE), the doping metals were expected from thermodynamics to be converted to their highest oxidation states in the double-layer region at the electrode surface. Provided these metal ions substitute for Pb(IV) in the PbO_2 matrix, it was anticipated that doping with oxides having stoichiometry M_2O_3 ($MO_{1.5}$) can produce mixed oxides which are deficient in surface oxygen, i.e., $PbO_2.MO_x (x < 2)$. Doping with oxides having stoichiometry M_2O_5 ($MO_{2.5}$) was expected to produce mixed oxide with excess surface oxygen, i.e., $PbO_2.MO_x (x > 2)$. The oxidation of Mn(II) in 1.0M $HClO_4$ was chosen as a test reaction because four oxygens were assumed to be transferred in the oxidation reaction to produce MnO_4^-. Furthermore, the heterogeneous rate for Mn(II) oxidation at pure electrodeposited β-PbO_2 electrodes was determined to be slow.

C. Experimental

Chemicals and others. All chemicals were Analytical Reagents from Fisher Scientific Co., Baker Chemicals or Aldrich Chemical Co. The metal salts and oxides used were: $Pb(NO_3)_2$, $Ga(NO_3)_3 \cdot H_2O$, In_2O_3, $Tl(NO_3)_3 \cdot 3H_2O$, As_2O_5 and $Bi(NO_3)_3 \cdot 5H_2O$. Water was deionized and triply distilled, and the supporting electrolyte was 1.0M $HClO_4$. Nitrogen was dispersed through the solution in the cell to remove dissolved oxygen prior to electrodeposition of the oxides and the kinetic measurements; and an inert atmosphere of nitrogen was maintained over the solution during all experiments. The reference electrode was a saturated calomel electrode (SCE).

Preparation of lead dioxide. The pure and doped electrodes were prepared by applying a constant potential to a gold rotated disc substrate ($0.496 cm^2$) in 1.0M $HClO_4$ containing Pb(II) with Group IIIA and VA metal ions. The potential was controlled at a value of 1.60 V vs. SCE with a potentiostat (Model RDE3, Pine Instrument Co.) for ten minutes at a rotation velocity of 900 rev min^{-1}. For the preparation of pure PbO_2 electrodes the deposition solution contained only 1.0mM Pb(II) ions. For the doped PbO_2 electrode, the solution contained 1.0mM Pb(II) ions plus various concentration of metal ions, e.g., Tl(III), In(III), Ga(III), As(V) and Bi(III). In the case of Bi(III), it was observed

that at least some of the Bi(III) ions could be oxidized to the higher oxidation state of Bi(V). The thickness of the electrodeposited lead dioxides was estimated from the product i·t (coulombs) and the density of PbO_2, and was estimated to be ca. 6,000 A. Oxide layers of this minimum thickness had a uniform appearance of being shiny and black. Increase of oxide thickness beyond this minimal value had negligible effect on values of rate constants determined.

Measurement of activities of the electrodes. In order to compare the activities of pure and doped lead dioxide electrodes, oxidations of Mn(II) and some organic molecules were chosen as model reactions. The prepared electrodes were immersed into a 1.0M $HClO_4$ solution while the potential was maintained at 1.60 V vs. SCE, where the model compounds can be oxidized to the higher oxidation state or decomposed. This detection potential is the same as was used for electrodeposition of the oxides. This value is near the positive limit of the accessible potential range set by rapid evolution of O_2 at PbO_2 electrodes in 1.0M $HClO_4$. The rotation velocity of the electrode was kept at 3600 rev min^{-1} to provide for rapid mixing when a test compound was introduced into the cell. The amperometric response was measured for six values of rotation rate (3600, 2500, 1600, 900, 400, and 100 rev min^{-1}). Plots of $1/i$ vs. $1/\omega^{1/2}$ were made to calculate the heterogeneous rate constants for oxidation of the test compounds.

Stability of the electrodes. The electrode prepared under a given set of conditions was cathodically stripped away by scanning the potential from the positive limit (1.60 V vs. SCE) to a negative value of ca. 0.0 V. No test compounds were present in the electrolyte solution used for the stripping process.

X-ray fluorescence. Several mixed bismuth-lead dioxide electrodes were prepared to determine the amount of Bi in the oxide. Ratios of $C^b_{Bi(III)}/C^b_{Pb(II)}$ in the deposition solutions were 0.5, 0.7, 1.0. The electrodes were analyzed with X-ray fluorescence instrument (Model 440, Nuclear Semiconductor). Standard samples were prepared from pure PbO_2 and Bi_2O_3 to calibrate the analytical process. The atomic ratio of Bi/Pb in the standard samples were 0.33, 1.0, 3.0.

Determination of valence state of Bi. The valence state of bismuth in the mixed oxide was determined by an amperometric method. Cathodic currents were measured as a function of rotation rate (ω) during cathodic deposition of Bi(III) as Bi metal on a rotated gold disc electrode. The plot of $1/i$ vs. $1/\omega^{1/2}$ was linear with a slope given by Levich's equation [14].

$$\text{slope} = 1/0.62nFAC^b\nu^{-1/6}D^{2/3} \qquad (1)$$

The value of the diffusion coefficient (D) was determined by substituting known values of n, F, A, C^b, and $\nu^{-1/6}$ into the equation above. The number of electrons (n) invloved in this process was assumed to be three. The same procedure was applied for the determination of diffusion coefficient of Pb(II); the value of n was assumed to be two. The values of diffusion coefficient obtained were used for calculation of the number of electrons involved in the anodic deposition of the pure PbO_2 and mixed bismuth-lead dioxide.

From the slopes of the plot of 1/i vs. $1/\omega^{1/2}$, substituting values of D obtained previously into equation (1), yielded the values of n in the electrodeposition of pure PbO_2 and the mixed oxide. Thus, it was predicted that the difference of n values obtained for the two processes was due to oxidation of Bi(III).

D. Results and Discussion

Plots of i vs. $\omega^{1/2}$ are shown in Figure V-1 for the oxidation of Mn(II) at the electrodeposited PbO_2 and mixed-oxide electrodes. The activity of pure PbO_2 was enhanced by the presence of the Group VA metals, i.e., As(V) and Bi(III). Conversely, the activity was decreased by the presence of Group IIIA metals, i.e., Ga(III), In(III) and Tl(III).

The concept of "oxygen-rich" and "oxygen-deficient" oxide electrodes is proposed to explain the enhanced and

Figure V-1. Plots of i vs. $\omega^{1/2}$ for oxidation of 1.0mM Mn(II) in 1.0M $HClO_4$ at electrodes of PbO_2 mixed with metal oxide

Conditions for electrodeposition of mixed-oxide electrodes.
Deposition potential: 1.60 V vs. SCE
Rotation velocity of electrode (ω): 900 rev min^{-1}
Deposition time: 10.0 min
Solution: 1.0M $HClO_4$
a: 0.1mM Bi(III) + 1.0mM Pb(II)
b: 0.1mM As(III) + 1.0mM Pb(II)
c: 1.0mM Pb(II)
d: 0.1mM Tl(III) + 1.0mM Pb(II)

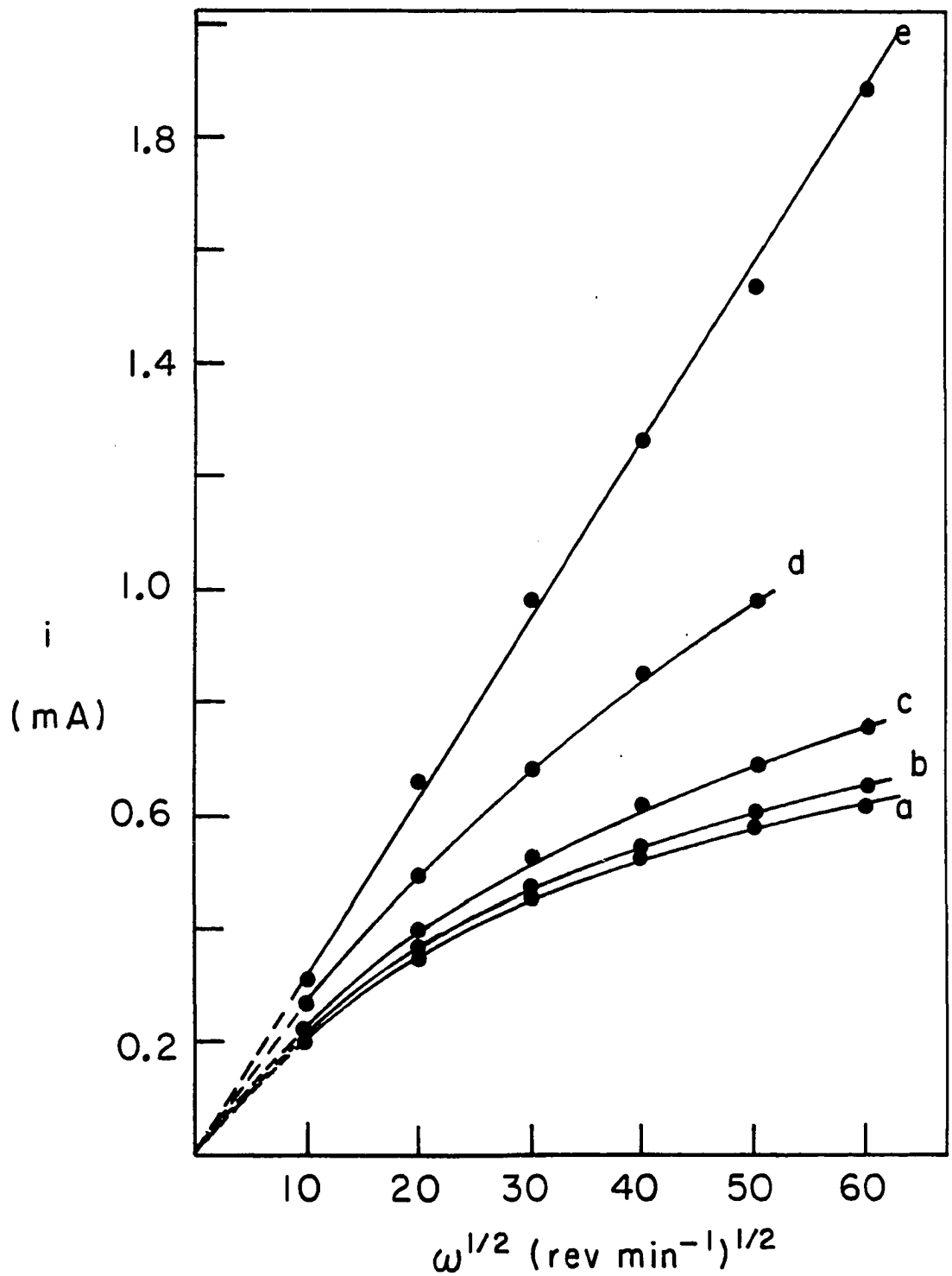
e
d
c
b
a
1.8
1.4
1.0
0.6
0.2
i
(mA)
10
20
30
40
50
60
ω^1/2 (rev min^-1)^1/2

inhibited electrocatalytic reactivity for anodic oxygen-transfer reactions. That is, it is proposed that the doped PbO_2 electrodes can contain more oxygen or less oxygen at the surface than the pure PbO_2 electrode due to the non-stoichiometric environment of the metal oxides used as doping agents. Accordingly, anodic oxygen-transfer reactions are expected to be electrocatalyzed at oxygen-rich, mixed oxide electrode having the empirical formula designated mixed-oxides $PbO_2.MO_x (x > 2)$, e.g., PbO_2/As_2O_5, PbO_2/Bi_2O_5. Anodic oxygen-transfer reactions are expected to be slow at oxygen-deficient, mixed-oxide electrode having the empirical formula $PbO_2.MO_x (x < 2)$, e.g., PbO_2/Ga_2O_3, PbO_2/In_2O_3 and PbO_2/Tl_2O_3 (Table V-1). Electrodeposition of the mixed oxide using As(III) was very difficult, as mentioned in Chapter III, presumably because the rate of chemical stripping of PbO_2 by As(III) is faster than the rate of anodic deposition of Pb(II). For the case of Bi, aqueous solutions of Bi(V) are unstable and deposition from a solution containing Bi(III) offered none of the difficulties observed for As(III).

Anodic currents for the electrodeposition of the pure lead dioxide and the mixed bismuth-lead dioxide from 1.0M $HClO_4$ containing only Pb(II) or Pb(II) with Bi(III) were measured as a function of rotation rate (ω) to determine valence state of Bi. It was assumed that the difference in anodic currents of the two processes was due to oxidation of

Table V-1. Mixed oxide electrode materials based on the PbO_2 matrix

Group IIIA	Group IVA	Group VA
Ga	Ge	As
(Ga_2O_3)		(As_2O_5)
In	Sn	Sb
(In_2O_3)		(Sb_2O_5)
Tl	Pb	Bi
(Tl_2O_3)	(PbO_2)	(Bi_2O_5)
oxygen-deficient oxides $PbO_2 \cdot MO_{1.5}$		oxygen-rich oxides $PbO_2 \cdot MO_{2.5}$

Bi(III) during the electrodeposition. From the slopes of the plot of $1/i$ vs. $1/\omega^{1/2}$, substituting values of D obtained previously into equation (1), yielded the values 2.2 and 3.7 for n in the electrodeposition of pure PbO_2 and the mixed oxide, respectively. Thus, the contribution to the n value by oxidation of Bi(III) is 1.5. If all Bi(III) ions were oxidized to Bi(V) during the electrodeposition of the mixed oxide, then apparent n value contributed by oxidation of Bi(III) should be 2.0. Hence, it is estimated that some pentavalent Bi is generated in the deposition of the mixed oxide. From the apparent n value, it is designated that the approximate stoichiometry of the mixed oxide is $pbO_2 \cdot BiO_x (x > 2)$. The electrodeposition of mixed antimony-lead oxides from solutions containing Sb(III) or Sb(V) was impossible because the hydroxides of Sb(III) and Sb(V) are precipitated even in highly acidic solutions.

The plots of $1/i$ vs. $1/\omega^{1/2}$ for data shown in Figure V-1 are linear, as shown in Figure V-2, and values of the heterogeneous rate constants (k) calculated from the intercepts according Koutecky-Levich equation are given in Table V-2. From these data, it is apparent that oxygen-transfer reactivity of the oxygen-deficient electrodes is less than that of pure electrodeposited PbO_2. The activity of the oxygen-rich electrodes is significantly greater than for PbO_2 with the rate being virtually transport limited at the $PbO_2 \cdot BiO_x (x > 2)$ electrode deposited from the solution

Figure V-2. Plots of $1/i$ vs. $1/\omega^{1/2}$ for oxidation of 1.0mM Mn(II) in 1.0M $HClO_4$ at electrodes of PbO_2 mixed with metal oxide

Conditions for electrodeposition of mixed-oxide electrodes.
Deposition potential: 1.60 V vs. SCE
Rotation velocity of electrode (ω): 900 rev min^{-1}
Deposition time: 10.0 min
Solution: 1.0M $HClO_4$
a: 0.1mM Bi(III) + 1.0mM Pb(II)
b: 0.1mM As(III) + 1.0mM Pb(II)
c: 1.0mM Pb(II)
d: 0.1mM Tl(III) + 1.0mM Pb(II)

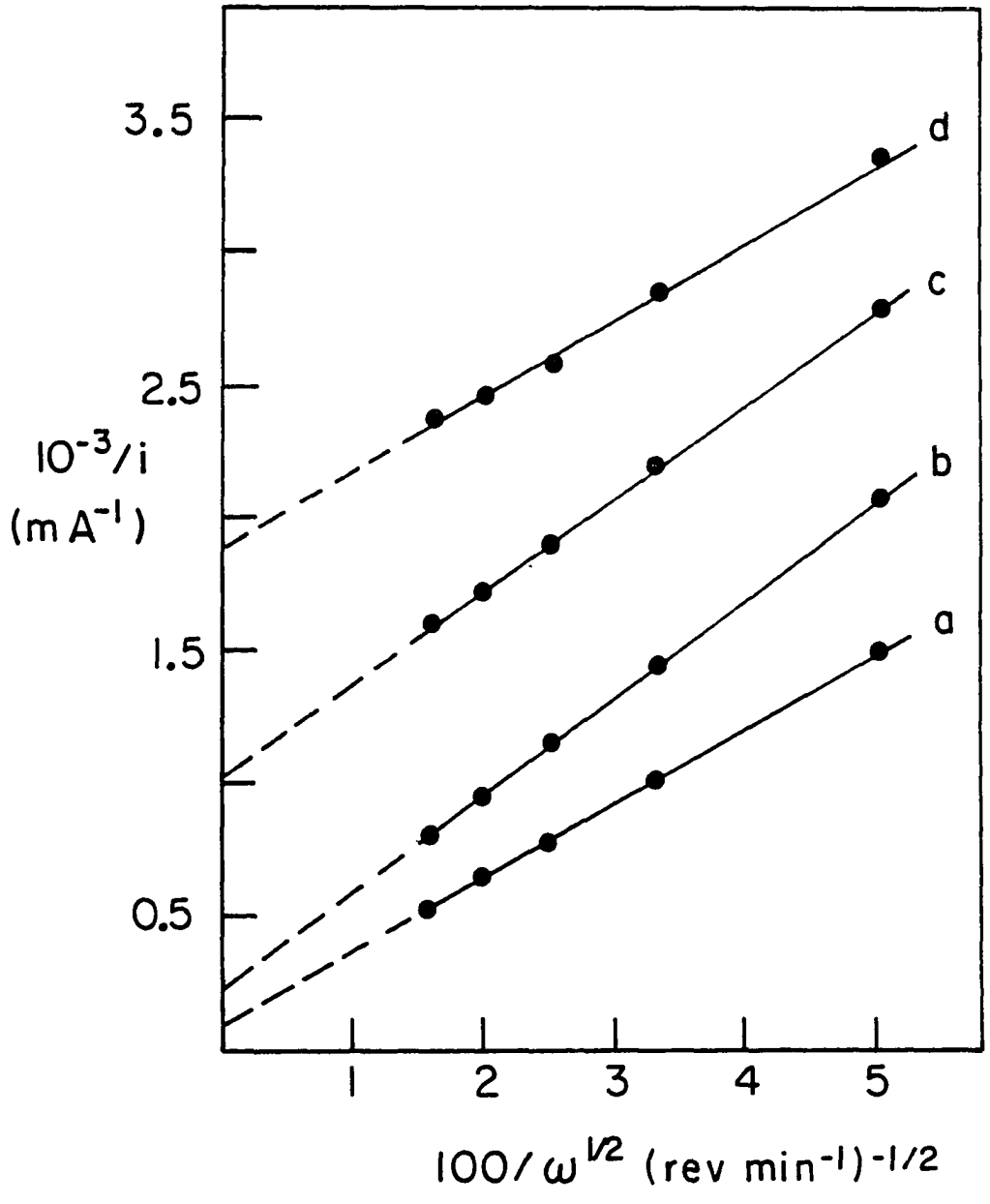
3.5
2.5
1.5
0.5
$10^{-3}/i$
$(m A^{-1})$
d
c
b
a
1
2
3
4
5
$100/\omega^{1/2}$ (rev $min^{-1})^{-1/2}$

Table V-2. Rate constants for oxidation of Mn(II) at rotated disc electrodes of metal-oxide mixed PbO_2

$$Mn(II) + 4H_2O \longrightarrow MnO_4^- + 8H^+ + 5e$$

Doping ion	Concentration[a] (mM)	k (cm sec^{-1})[b]
——	——	4.1×10^{-3}
Tl(III)	0.10	2.3×10^{-3}
In(III)	1.0	3.4×10^{-3}
Ga(III)	1.0	3.5×10^{-3}
As(V)	0.10	2.0×10^{-2}
As(V)	1.0	5.7×10^{-2}
Bi(III)	0.10	6.9×10^{-2}
Bi(III)	1.0	$> 1 \times 10^{-1}$[c]

[a]Electrodes deposited from 1.0 mM Pb(II) in 1.0 M $HClO_4$.

[b]Kinetic measurements in 1.0 mM Mn(II) in 1.0 M $HClO_4$.

[c]Effectively mass transport controlled.

containing 1.0mM Bi(III) and 1.0mM Pb(II). This corresponds to an increase of ca. 25X in the rate constant compared to pure electrodeposited PbO_2.

The final product of oxidation of Mn(II) was confirmed to be MnO_4^- by the determination of n = 5 using exhaustive electrolysis. Furthermore, the color of the solution of Mn(II) was slowly changed to be purple by the electrocatalysis, which is the characteristic color of MnO_4^- solution.

The heterogeneous rate constant for oxidation of Mn(II) was determined also as a function of the concentration of Bi(III) in the solution of 1.0mM Pb(II) used for electrodeposition of the oxygen-rich electrodes. Representative plots of i vs. $\omega^{1/2}$ and 1/i vs. $1/\omega^{1/2}$ are shown in Figure V-3 and in Figure V-4. From these plots, it is obvious that the rate for oxidation of Mn(II) increases as concentration of Bi(III) is increased in the deposition solution. The reaction becomes virtually mass-transport limited rate at the mixed oxide electrode prepared with $C^b_{Bi(III)}/C^b_{Pb(II)} = 0.1$. In Figure V-5, it is shown a plot of -log {i} vs. -log $\{C^b_{Bi(III)}/C^b_{Pb(II)}\}$ for the deposition media. Clearly the greatest relative effect of added Bi(III) is observed for $0.01 < [C^b_{Bi(III)}/C^b_{Pb(II)}] < 0.1$. The activities of these oxygen-rich electrodes for oxidation of Mn(II) reaches a maximum value at the electrodes prepared from solutions having $C^b_{Bi(III)}/C^b_{Pb(II)} > 0.1$.

Figure V-3. Plots of i vs. $\omega^{1/2}$ for oxidation of 1.0mM Mn(II) in 1.0M $HClO_4$ at mixed $Pb(Bi)O_2$ electrodes

Conditions for electrodeposition of the mixed-oxide electrodes.
Deposition potential: 1.60 V vs. SCE
Rotation velocity of electrode (ω): 900 rev min^{-1}
Deposition time: 10.0 min
Solution: 1.0M $HClO_4$
a: 1.0mM Pb(II) + 0.0mM Bi(III)
b: 1.0mM Pb(II) + 0.005mM Bi(III)
c: 1.0mM Pb(II) + 0.01mM Bi(III)
d: 1.0mM Pb(II) + 0.05mM Bi(III)
e: 1.0mM Pb(II) + 0.1mM Bi(III)

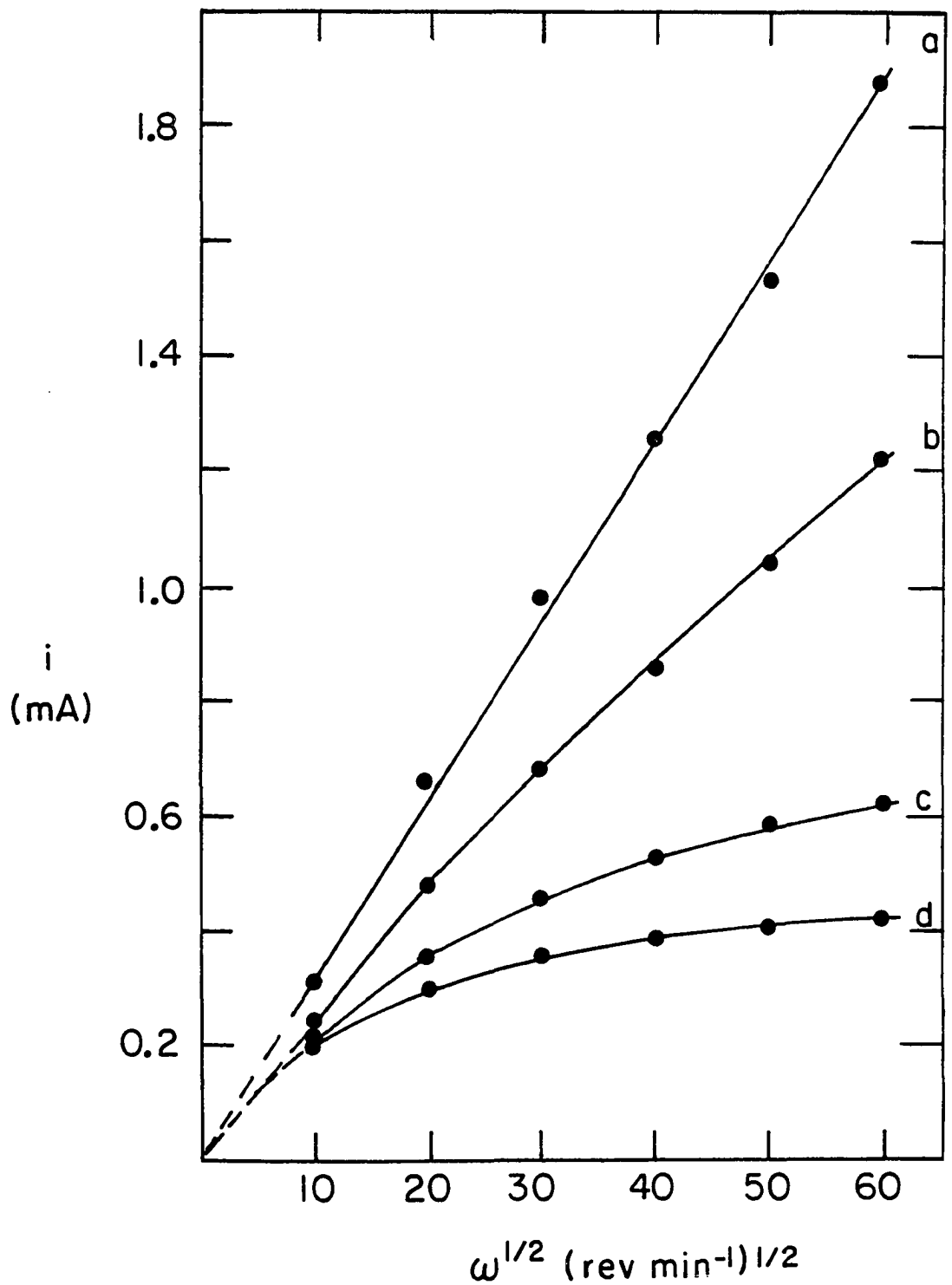
a
b
c
d
1.8
1.4
1.0
0.6
0.2
i
(mA)
10
20
30
40
50
60
ω^1/2 (rev min-1)1/2

Figure V-4. Plots of $1/i$ vs. $1/\omega^{1/2}$ for oxidation of 1.0mM Mn(II) in 1.0M $HClO_4$ at mixed $Pb(Bi)O_2$ electrodes

Conditions for electrodeposition of mixed-oxide electrodes.
Deposition potential: 1.60 V vs. SCE
Rotation velocity of electrode (ω): 900 rev min^{-1}
Deposition time: 10.0 min
Solution: 1.0M $HClO_4$
a: 1.0mM Pb(II) + 0.0mM Bi(III)
b: 1.0mM Pb(II) + 0.005mM Bi(III)
c: 1.0mM Pb(II) + 0.01mM Bi(III)
d: 1.0mM Pb(II) + 0.05mM Bi(III)
e: 1.0mM Pb(II) + 0.1mM Bi(III)

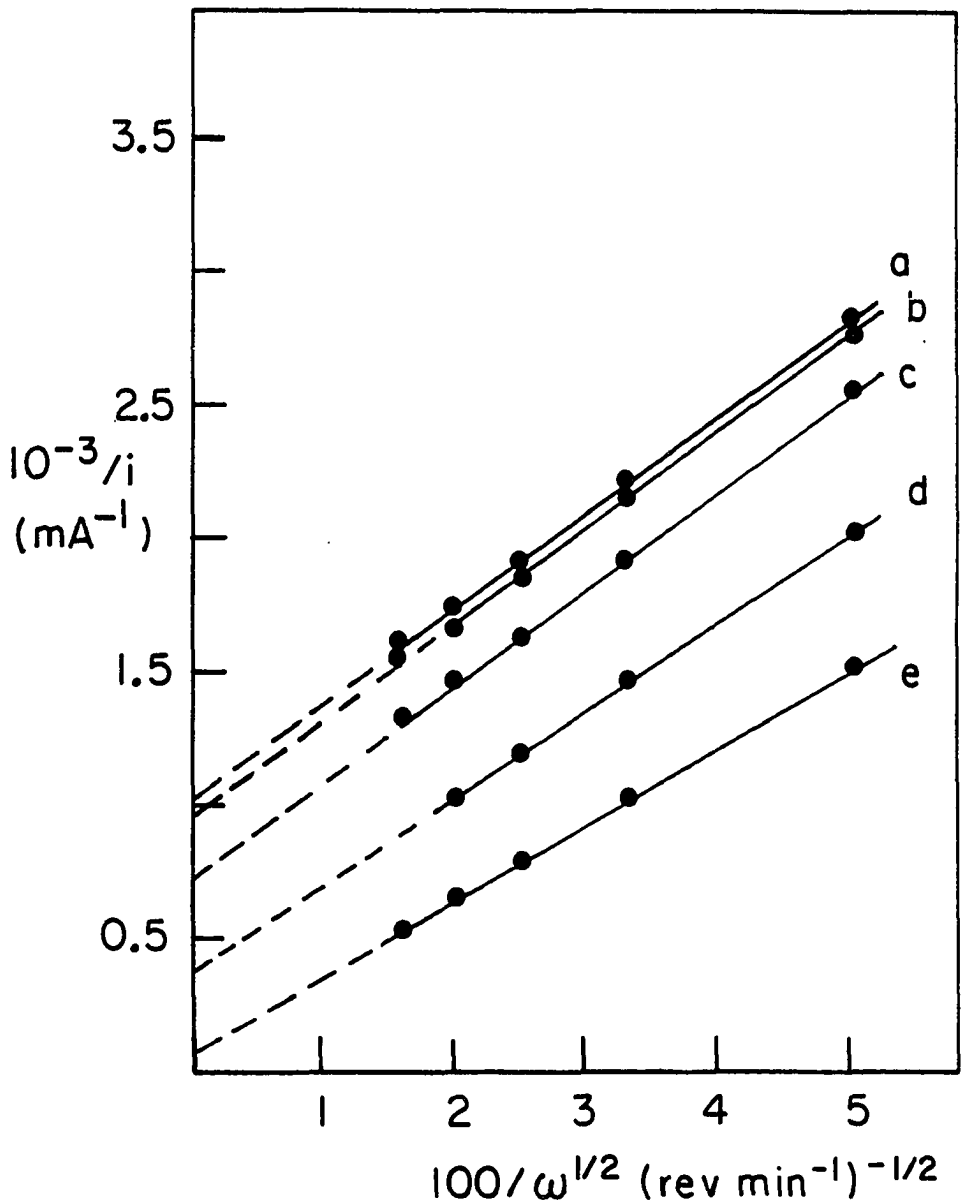
3.5
2.5
1.5
0.5
$10^{-3}/i$
(mA^{-1})
a
b
c
d
e
1
2
3
4
5
$100/\omega^{1/2}$ (rev $min^{-1})^{-1/2}$

Figure V-5. Plot of $-\ln \{i\}$ vs. $-\ln [C^{b}_{Bi(III)}/C^{b}_{Pb(II)}]$

Conditions for the measurement of anodic current.
Detection potential: 1.60 V vs. SCE
Rotation velocity of electrode (ω): 2500 rev min^{-1}
Solution: 1.0mM Mn(II) in 1.0M $HClO_4$

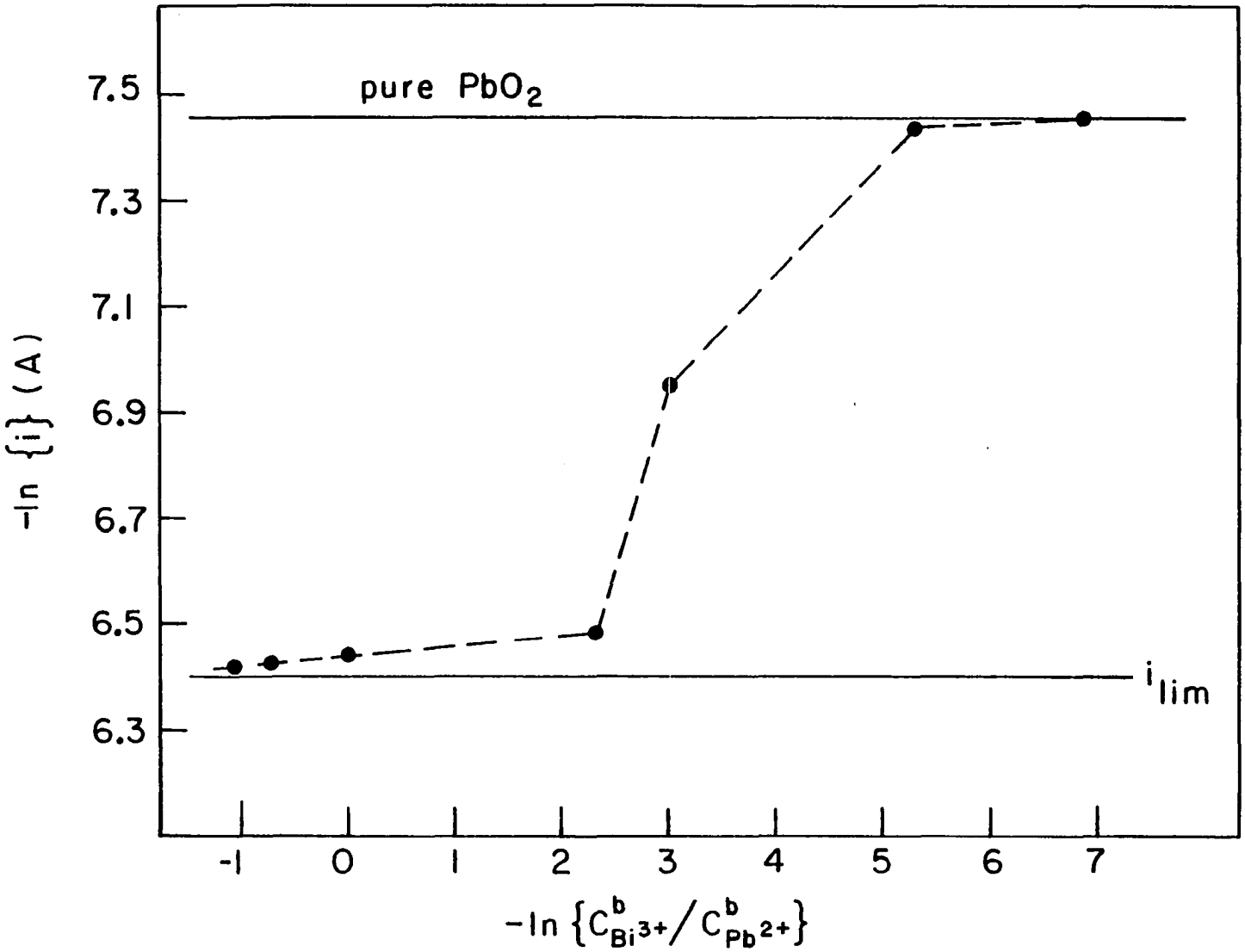
pure PbO_2
7.5
7.3
7.1
6.9
6.7
6.5
6.3
$-\ln \{i\}$ (A)
i_{lim}
-1
0
1
2
3
4
5
6
7
$-\ln \{C^b_{Bi^{3+}} / C^b_{Pb^{2+}}\}$

The atomic ratio Bi/Pb in the mixed oxide electrodes was determined by X-ray fluorescence. The X-ray fluorescence experiment showed that the ratio of Bi/Pb in the mixed oxides was not exactly matched to the ratio of $C^b_{Bi(III)}/C^b_{Pb(II)}$ in the deposition solution. However, as the concentration of Bi in the deposition solution was increased the concentration of Bi in the oxide electrode was increased. The results for the three electrodes analyzed are shown in Table V-3 as a function of $C^b_{Bi(III)}/C^b_{Pb(II)}$. The ratio Bi/Pb was ca. 0.7 for $C^b_{Bi(III)}/C^b_{Pb(II)} = 1.0$.

The values of the heterogeneous rate constant measured for numerous other oxygen-transfer reactions were determined to be larger at the $PbO_2 \cdot BiO_x (x > 2)$ electrode, as compared to PbO_2. Representative examples are given in Table V-4. Most dramatic is the oxidation of phenol to benzoquinone, which is barely perceptible at pure electrodeposited PbO_2 electrodes under these conditions. This corresponds to an increase in k of more than 100X. For oxidation of Mn(II), the activity of the electrodes is not changed by the variation of deposition potential and by the presence or absence of oxygen when the electrodes are prepared.

Results of linear sweep voltammetry are shown in Figure V-6 for PbO_2 and $PbO_2 \cdot BiO_x (x > 2)$ electrodes. Curves a-c correspond to the negative scan of electrode potential to determine the effect of doping on the potential at which cathodic dissolution of the oxide occurs. Increasing the

Table V-3. Ratio Bi/Pb in the mixed oxide[a] of $PbO_2 \cdot BiO_x$ ($x > 2$) as determined by X-ray fluorescence analysis

$C^b_{Bi(III)}/C^b_{Pb(II)}$	Bi/Pb
0.50mM/1.0mM	0.42
0.70mM/1.0mM	0.56
1.00mM/1.0mM	0.67

[a]The mixed bismuth-lead oxide electrode was prepared by electrodeposition in 1.0M $HClO_4$.

Table V-4. Rate constants for oxidation of selected organic compounds at rotated disc electrodes of pure PbO_2 and mixed $Pb(Bi)O_2$[a]

Compound	$10^3 \cdot k$ (cm s^{-1}) [b]	
	pure	Bi-mixed
manganese (II)	4.1(1)	> 100 [c]
sulfosalicyclic acid	4.5(9)	11(2)
phenol	no rxn.	> 100 [c]
hydroquinone	9.7(4)	29(12)
cystine	9.0(4)	15(4)
thiophenacetic acid	1.4(3)	22(12)

[a]Lead dioxide deposited from 1.0 mM Pb(II) in 1.0M $HClO_4$; mixed bimuth-lead dioxide deposited from 1.0 mM Pb(II) with 1.0 mM Bi(III) in 1.0 M $HClO_4$.

[b]Uncertainty given for 90% confidence interval. Measurements done for 1.0 mM analyte in 1.0 M $HClO_4$.

[c]Effectively mass-transport limited.

Figure V-6. Linear sweep voltammograms obtained on the negative potential scan in 1.0M $HCLO_4$

Conditions for electrodeposition of mixed-oxide electrodes.
Deposition potential: 1.60 V vs. SCE
Rotation velocity of electrode (ω): 900 rev min^{-1}
Deposition time: 20.0 min
Solution: 1.0M $HClO_4$
a, d: 1.0mM Pb(II)
b: 1.0mM Pb(II) + 0.1mM Bi(III)
c: 1.0mM Pb(II) + 1.0mM Bi(III)
Concentration of analyte
0.0mM Mn(II) for curves a, b and c
1.0mM Mn(II) for curves d and e

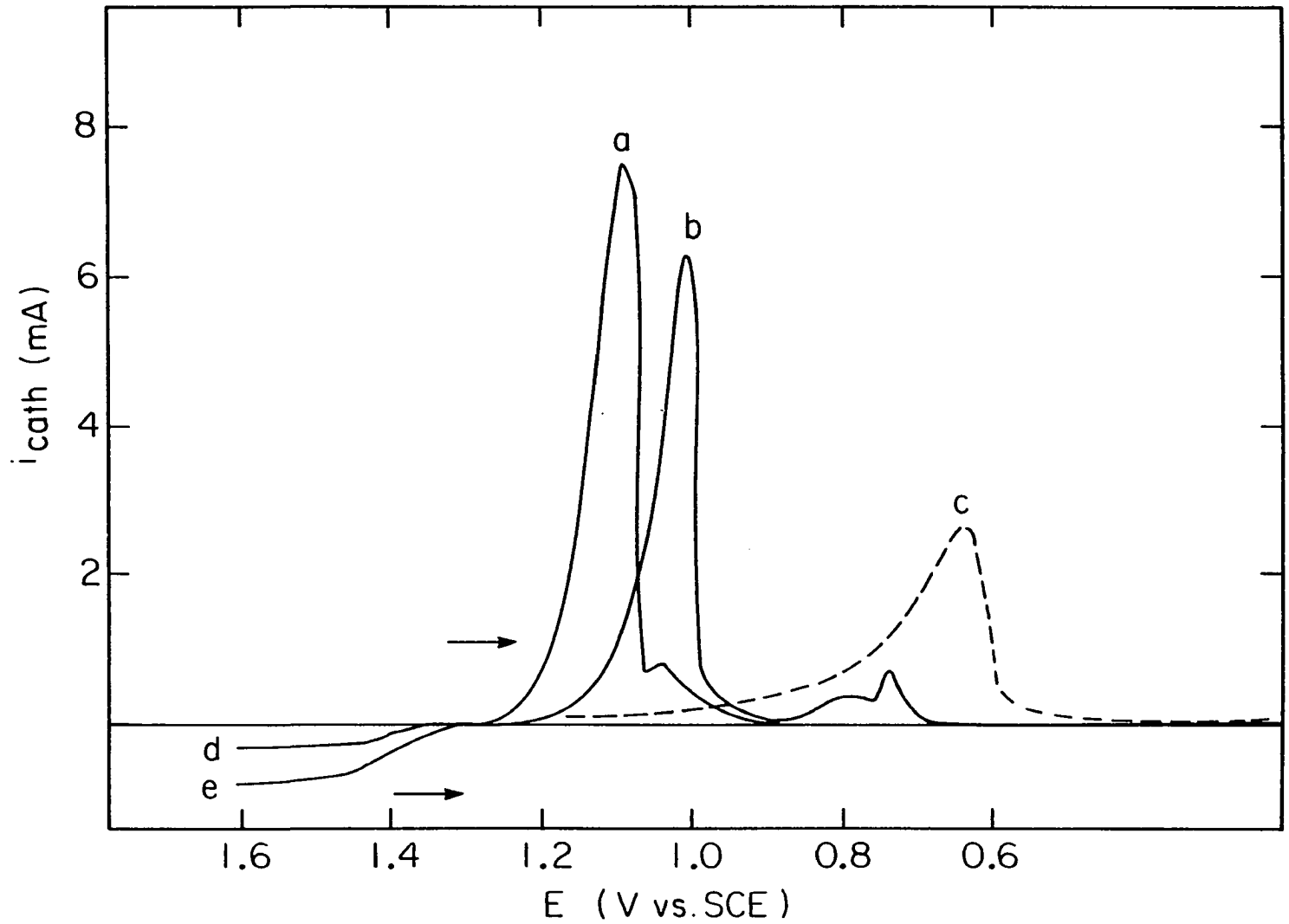
8
6
4
2
i_{cath} (mA)
a
b
c
d
e
1.6
1.4
1.2
1.0
0.8
0.6
E (V vs. SCE)

level of Bi in the mixed oxide clearly increases the stability of the electrode. The maximum negative shift in the cathodic peak of ca. 0.5 V corresponds to ca. 20 Kcal mol^{-1} greater stability of $PbO_2 \cdot BiO_x (x > 2)$, calculated for n = 2 eq mol^{-1}. The stability increases as the concentration of Bi(III) increases in the deposition solution.

The same electrodes were prepared and allowed to be reacted with 4.0mM As(III) for 30 minutes with 2500 rev min^{-1}. The electrodes were transferred to fresh electrolyte and was stripped away in the absence of analytes. Voltammetric responses (i-E) of the stripping were recorded. Comparing the shapes of stripping peaks of between the mixed oxide electrode treated with As(III) and the electrode without As(III) treatment, the shapes of i-E curves obtained for mixed bismuth-lead oxide electrodes were not changed even though the mixed oxide was exposed in such a severe corrosive condition. Hence, the oxide containing much Bi ion in the deposition solution is more resistive toward the corrosion by As(III). This represents a significant advantage in that the voltammetric range is increased for the $PbO_2 \cdot BiO_x (x > 2)$ electrode and the rate of chemical corrosion by chemical reducing agents under open circuit conditions (i = 0) is expected to decrease. Electrodes of the type $PbO_2 \cdot MO_x (x < 2)$ yield i-E curves with virtually no shift in the cathodic peak potential, as compared to pure PbO_2.

Curves d and e in Figure V-6, obtained on the negative scan, compare the reactivity of PbO_2 and $PbO_2 \cdot BiO_x (x > 2)$ electrodes for oxidation of Mn(II). The value of $E_{1/2}$ is approximately 1.4 V vs. SCE for both electrodes, which corresponds closely to the predicted reversible $E_{1/2}$ of 1.26 V vs. SCE at pH 0. The potential 1.60 V chosen for kinetic studies corresponds to a region of minimal potential dependence for the anodic i-E wave without significant background current. Voltammetric curves for solutions of MnO_4^- contained no cathodic waves apart from the peaks shown in curves a-c for dissolution of PbO_2 and $PbO_2 \cdot BiO_x (x > 2)$. Clearly, the oxygen-rich mixed-oxide electrode is observed only to promote the anodic process for this redox couple. Attempts to determine if the oxygen-deficient oxides are catalytically active for reduction of MnO_4^- were not successful because the mixed oxide dissolved cathodically in the region of potential where reduction of MnO_4^- is expected.

E. Conclusion

In general, so-called "oxygen-rich" mixed-oxide electrodes, corresponding to an empirical formula of the type $PbO_2 \cdot MO_x (x > 2)$, are concluded to significantly increase rates of anodic oxygen-transfer reactions as illustrated here mainly for oxidation of Mn(II) to MnO_4^- at $PbO_2 \cdot BiO_x (x > 2)$. The increased rate of oxygen-transfer reactions is concluded

to be the direct result of the high density of surface sites corresponding to Bi(V) centers at which excess surface oxygen can exist. The excess oxygen is not stabilized with the same lattice energy associated with the surface of pure electrodeposited PbO_2. The $PbO_2 \cdot BiO_x (x > 2)$ does not react in the manner of a true catalyst in that only the anodic partial reaction for the Mn(II)-MnO_4^- redox couple is enhanced, and we characterize this electrode as being an "anodic semicatalyst". This would correspond formally to a highly asymmetric activation barrier with $\alpha_c << \alpha_a$ and $\alpha_a = n - \alpha_c \approx 5$ for oxidation of Mn(II). It is also anticipated that the oxygen-deficient mixed oxides might function as semicatalysts for cathodic oxygen-transfer reactions.

F. References

1. Fishman, J. F.; Henry, J. F.; Tessor, S. Electrochim. Acta 1969, 14, 1314.
2. Chertykovtseva, T. A.; Shub, D. M.; Veselovski, V. I. Electrokhimiya 1978, 14, 1260.
3. Chertykovtseva, T. A.; Skuridina, Z. D.; Shub, D. M.; Veselovski, V. I. Electrokhimiya 1978, 14, 1412.
4. Iwakura, C.; Inai, M.; Tamura, H. Chem. Lett. 1979, 225.
5. Morita, M; Iwakura, C.; Tamura, H.; Electrochim. Acta 1979, 24, 639.
6. Morita, M; Iwakura, C.; Tamura, H.; Electrochim. Acta 1980, 25, 1341.
7. Burbank, J. J. Electrochem. Soc. 1964, 111, 1112.

8. Swets, D. E. J. Electrochem. Soc. 1973, 120, 925.

9. Muskalick, N. J. J. Electrochem. Soc. 1975, 122, 19.

10. Caldara, F.; Delmastro, A.; Gracchia, G.; Maja, M. J. Electrochem. Soc. 1980, 127, 1869.

11. Boggio, A.; Maja, M.; Penazzi, N. J. Power Sources 1983, 9, 221.

12. Ritchie, E. J.; Burbank, J. J. Electrochem. Soc. 1970, 117, 299.

13. Delmastro, A.; Maja, M. J. Electrochem. Soc. 1984, 131, 2756.

14. Bard, A. J.; Faulkner, L. R. "Electrochemical Methods"; John Wiley: New York, 1980; Page 288.

VI. CHARACTERIZATION OF MIXED BISMUTH-LEAD DIOXIDE ELECTRODES

A. Abstract

The structures of electrochemically deposited films of lead dioxide and mixed bismuth-lead dioxide were studied by X-ray diffraction (XRD). The results indicate the unit cell has a slightly distorted rutile structure for both the pure PbO_2 and mixed oxide. As the ratio of Bi/Pb is increased, the unit cell parameters are increased only slightly. The bismuth is concluded to substitute for Pb(IV) in the rutile structure of PbO_2. Crystal sizes of the electrodeposited pure β-PbO_2 and the mixed oxide were observed by scanning electron micrographs (SEM) and also evaluated from the peaks width of XRD pattern. It is suggested that some vacancies in the cation sites are necessary to preserve electroneutrality of the mixed oxide.

B. Introduction

The crystal structures of lead dioxides have been studied extensively primarily due to its use in lead-acid storage batteries [1-5]. Two crystal modifications of PbO_2 are known: α-PbO_2 and β-PbO_2. The basic structural building block is a distorted octahedron of oxygen atoms surrounding a

lead atom in both forms. In β-PbO_2 (the "rutile" form), neighboring octahedra form a linear chain by sharing opposite edges, as shown in Figure VI-1. The chains propagate along the tetragonal c axis and are interconnected by sharing oxygen atoms. In α-PbO_2 (the orthorhombic form), the octahedra are arranged in a zig-zag manner by sharing alternate edges, as shown in Figure VI-1. The connection among the chains in α-PbO_2 is more complicated than in β-PbO_2. So far, no structure determination of either form has been reported for single crystals.

The effects on morphology and self-discharge rates of lead-acid batteries due to doping of PbO_2 was investigated by Delmastro and Maja [6]. The effects of impurities on the lead acid batteries performence have appeared in the literatures [7-11]. Some authors have tried to characterize the positive plate of lead acid batteries containing antimony with SEM, X-ray diffraction [12] and electrochemical measurements [13].

Thanos and Wabner [14] studied electrodeposited PbO_2 on titanium prepared at different values of temperature. They observed that the electrode plated at higher temperature contained more β-PbO_2 than α-PbO_2, and exhibited preferred orientation with the (110) crystal face parallel to the geometrical plane of the electrode. They also investigated the change of surface texture in different electrolytes during the electrolysis [15].

Figure VI-1. Two crystal forms of α-PbO_2 and β-PbO_2

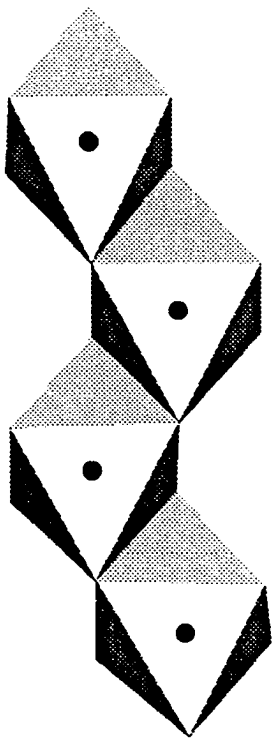

α-PbO_2
(orthorhombic)

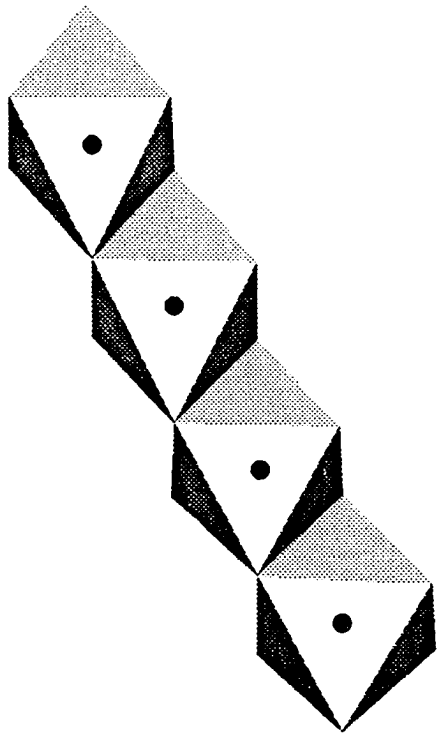

β-PbO_2
(rutile)

Electrodeposited α-PbO_2 and β-PbO_2 show preferred orientation effects, whereas the chemically prepared samples do not [16]. Hill et al. [17] studied the structual parameters of β-PbO_2 prepared chemically or obtained from batteries, in an attempt to correlate structure with the decline of battery performance.

In Chapter V, It was reported that lead dioxide mixed with Group VA and IIIA metal ions has more or less electrocatalytic activity than electrodeposited pure PbO_2. Especially, the lead dioxide doped with bismuth has a significantly increased reactivity for the oxidation of Mn(II) and several other organic compounds.

Here, the properties of this mixed oxide electrode obtained by electrochemical deposition on a gold substrate were studied with X-ray diffraction (XRD), scanning electron microscopy (SEM) and Auger electron spectroscopy (AES).

C. Experimental

Chemicals. All chemicals were Analytical Reagents from Aldlich Chemicals and Baker Chemicals: $Pb(NO_3)_2$, $Bi(NO_3)_3$. The supporting electrolyte was 1.0M $HClO_4$. Triply distilled water was used in preparing all solutions.

Instrumentation. The instruments have been described in Chapter III. Two types of gold electrode were used as

ubstrates to prepare pure and mixed bismuth-lead dioxide. A gold electrode without Teflon (ACMDI 6070 Au, Pine Instrument Co.) was designed for use in XRD studies to eliminate interferences from the Teflon which produces a broad diffraction pattern of its own. The electrode without the Teflon was used also for AES studies. The conventional type of gold disc electrode with a Teflon shroud (AFMT28Au, Pine Instrument Co.) was used for SEM.

X-ray diffraction. Lead dioxide and mixed bismuth-lead dioxide films were prepared on a gold electrode by electrochemical deposition as described in Chapter V. The deposition time was approximately 20 min in this case. The amount of Bi in the mixed oxide was controlled by variation of concentration of Bi(III) in the deposition solution. The ratios of concentrations for two ions, $C^b_{Bi(III)}/C^b_{Pb(II)}$, in the solution were 0.0, 0.1, 0.2, 0.3, 0.5, 0.7 and 1.0. Random powder samples of oxides prepared for $C^b_{Bi(III)}/C^b_{Pb(II)}$ = 0.0 and 1.0 were prepared by stripping the deposit from the gold electrode surface either mechanically or by applying a negative potential to strip the deposit after the deposition was complete. Pellets of such oxides were dried and ground into fine powder.

The random powder samples were spread on a silicon single crystal of 2.4 cm diameter and mounted on a powder diffractometer. Other electodes were directly transferred to

the diffractometer and mounted. The diffractometer used for all these diffraction experiments was an automated Picker powder diffractometer (Ames Laboratory of the U.S.D.O.E., Iowa State University, Ames, Iowa) equipped with a diffracted-beam graphite monochromator. A θ-θ stepscan procedure was employed with 2θ steps of 0.04° over the 4.04 - 50.00° range using MoKα radiation. The step counting time used was 30 sec per step for those of $C^b_{Bi(III)}/C^b_{Pb(II)}$ = 0.2, 0.3, and 1.0, and 10 sec per step for all others.

Scanning Electron Microscopy (SEM). The crystallinity of pure lead dioxide and mixed bismuth-lead dioxide electrode was observed by taking SEM photos with Scanning Electron Microscope (Model 200, Cambridge). Samples were prepared by the same method described as above for the pure PbO_2 and the mixed oxide electrode of $C^b_{Bi(III)}/C^b_{Pb(II)}$ = 1 on a gold disc electrode (AFMT28Au, Pine Instrument Co.). The interaction of Teflon with electron beam created fuzzy image of the sample. This problem was removed by covering the Teflon portion of the electrode with aluminum foil. The energy of the electron beam was 20.00 KeV. The sample was tilted 30° with respect to the direction of the electron beam to obtain a clearer perspective of the size of the individual crystallites.

Auger Electron Spectroscopy (AES). The bulk composition of pure and mixed lead dioxide electrodes was examined by Auger Electron Spectroscope (Physical Electronics Industries Inc., PHI Model 11-500A). The surface of the mounted samples of PbO_2 on a gold substrate were cleaned with a low energy electron beam to eliminate possible contaminations from handling of the samples. The intensity of Auger electrons was recorded as a function of the depth in the oxide layer so that the distribution of the ratio Pb/Bi in the bulk of the oxide could be determined. Layers of the oxide examined were removed before investigating the next layer by sputtering with a high energy electron beam (2 KV, 50μA).

D. Results and Discussion

In order to monitor the properties of the crystalline particles (e.g., preferred orientation and particle size) as well as atomic parameters, X-ray diffraction experiments were carried out on the random powder samples and on the electrodeposited pure β-PbO_2 and mixed Bi-Pb dioxide electrodes on a gold substrate.

For the mixed oxide, it was expected that the mixed oxides would have a structure corresponding to a metal-substituted lead dioxide or they might belong to some new structural type(s). In the case of metal substitutions, these might be random substitutions, or substitutions which

give rise to short-range or long-range ordering. Long-range orderings of lead and bismuth atoms are very difficult to detect using XRD because the X-ray scattering powers of Pb and Bi are very close to each other. On the other hand, if some new structures were produced as a result of doping or mixing, it was expected that these could be characterized via powder pattern indexings and subsequent structure determination.

A theoretically calculated XRD pattern of β-PbO2 is shown in Figure VI-2. The observed diffraction patterns of the powder of β-PbO_2, electro-deposited pure PbO_2, and mixed Bi-Pb dioxide are shown in Figure VI-3 through Figure VI-11. All the diffraction patterns were readily identified as that of β-PbO_2 by simple comparison of the peak positions with the theoretical pattern for β-PbO_2. Mixed oxides prepared for $0 < C^b_{Bi(III)}/C^b_{Pb(II)} \leq 0.3$ contained additional small peaks which were identified as coming from α-PbO_2. Since the samples deposited on gold electrodes were not thick enough to inhibit scattering of MoKα radiation by the substrate, the diffraction patterns included the contribution from elemental gold phases as well.

The X-ray diffraction patterns do not contain any new peaks other than those for α/β-PbO_2 and Au phases, and the powder diffraction profile of the the mixed oxide $C^b_{Bi(III)}/C^b_{Pb(II)} = 1.0$ resembles that of pure PbO_2 electrode. This excludes a possible model of new structure

Figure VI-2. Calculated X-ray diffraction pattern of β-PbO_2

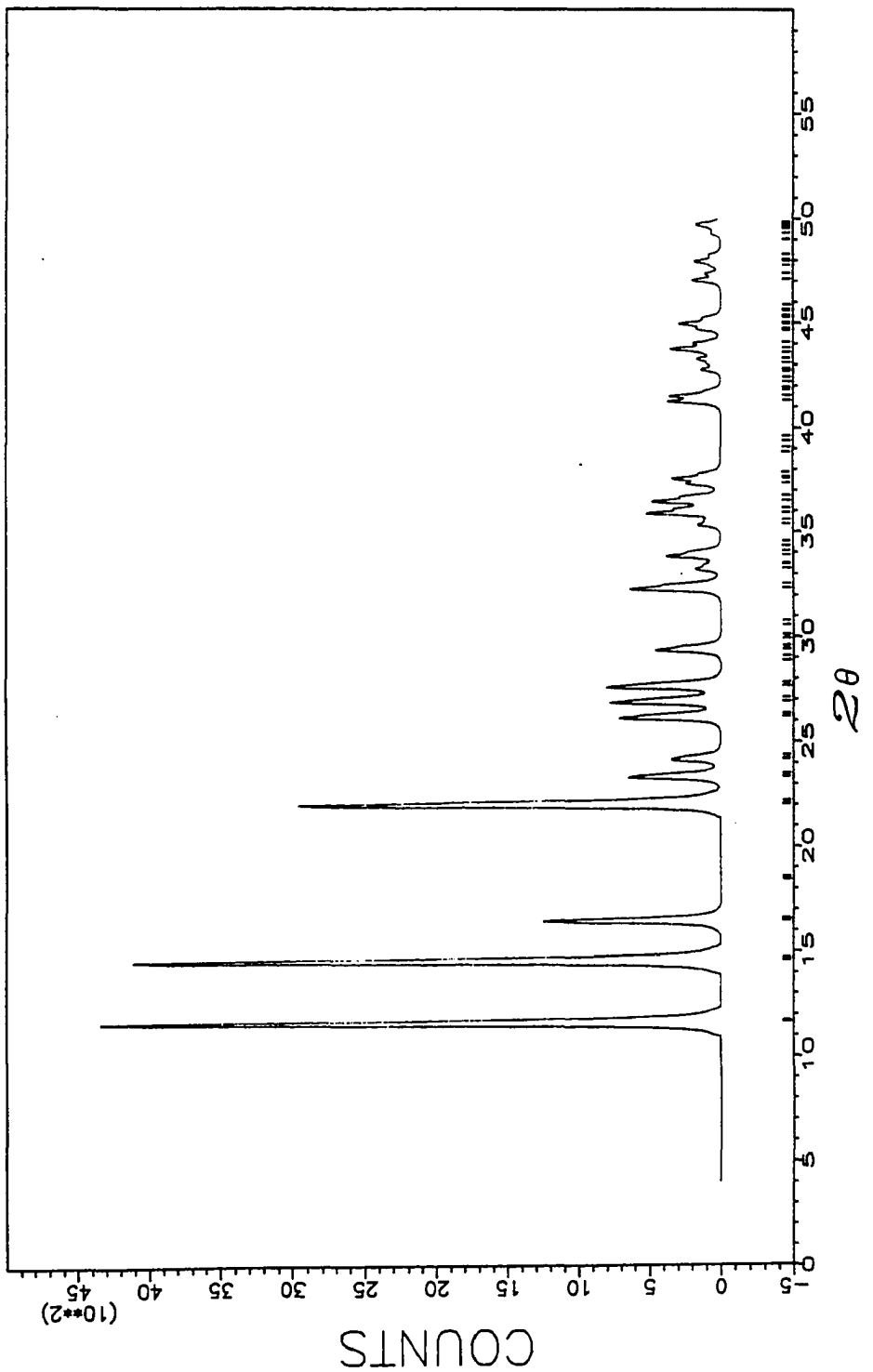
COUNTS
(10**2)
45
40
35
30
25
20
15
10
5
0
-5
0
5
10
15
20
25
30
35
40
45
50
55
2θ

Figure VI-3. X-ray diffraction pattern of powdered β-PbO_2 obtained from electrodeposition

Conditions for electrodeposition of PbO_2 electrodes.
Deposition potential: 1.60 V vs. SCE
Rotation velocity of electrode (ω): 900 rev min^{-1}
Deposition time: 20.0 min
Solution: 1.0mM Pb(II) in 1.0M $HClO_4$

2θ
COUNTS
(10**2)

Figure VI-4. X-ray diffraction pattern of electrodeposited β-PbO_2 obtained from electrodeposition

Conditions for electrodeposition of PbO_2 electrodes.
Deposition potential: 1.60 V vs. SCE
Rotation velocity of electrode (ω): 900 rev min^{-1}
Deposition time: 20.0 min
Solution: 1.0mM Pb(II) in 1.0M $HClO_4$

2θ
0
5
10
15
20
25
30
35
40
45
50
55
COUNTS
(10**2)
-3
0
3
6
9
12
15
18
21

Figure VI-5. X-ray diffraction pattern of mixed $Pb(Bi)O_2$ electrode: $C^b_{Bi(III)}/C^b_{Pb(II)}$ = 0.1 in the deposition solution

Conditions for electrodeposition of the mixed-oxide electrodes.
Deposition potential: 1.60 V vs. SCE
Rotation velocity of electrode (ω): 900 rev min^{-1}
Deposition time: 20.0 min

COUNTS
(10**2)
2θ

Figure VI-6. X-ray diffraction pattern of mixed $Pb(Bi)O_2$ electrode: $C^b_{Bi(III)}/C^b_{Pb(II)} = 0.2$ in the deposition solution

Conditions for electrodeposition of the mixed-oxide electrodes.
Deposition potential: 1.60 V vs. SCE
Rotation velocity of electrode (ω): 900 rev min^{-1}
Deposition time: 20.0 min

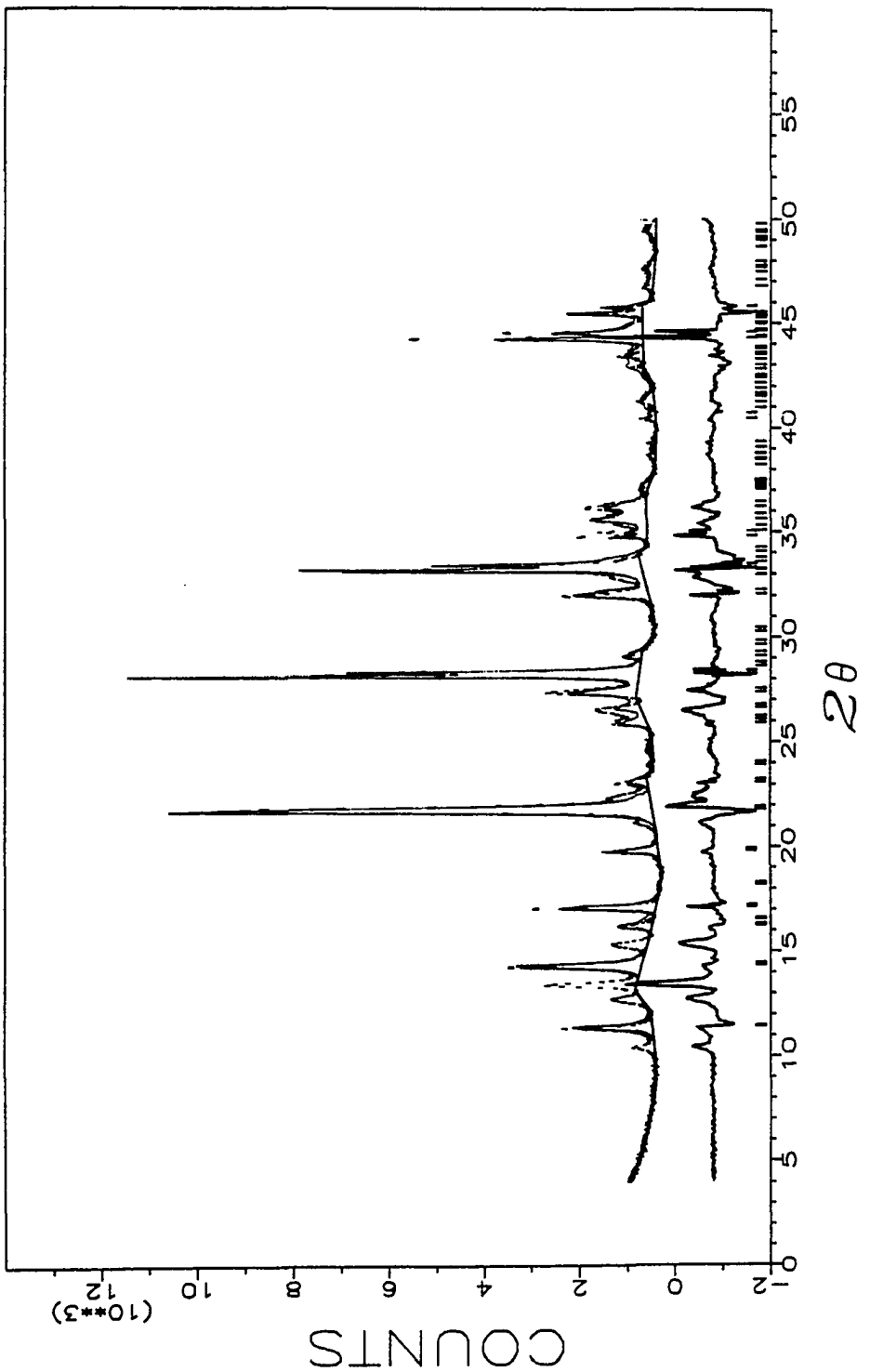
COUNTS
(10**3)
0
2
4
6
8
10
12
0
5
10
15
20
25
30
35
40
45
50
55
2θ

Figure VI-7. X-ray diffraction pattern of mixed $Pb(Bi)O_2$ electrode: $C^b_{Bi(III)}/C^b_{Pb(II)}$ = 0.3 in the deposition solution

Conditions for electrodeposition of the mixed-oxide electrodes.
Deposition potential: 1.60 V vs. SCE
Rotation velocity of electrode (ω): 900 rev min^{-1}
Deposition time: 20.0 min

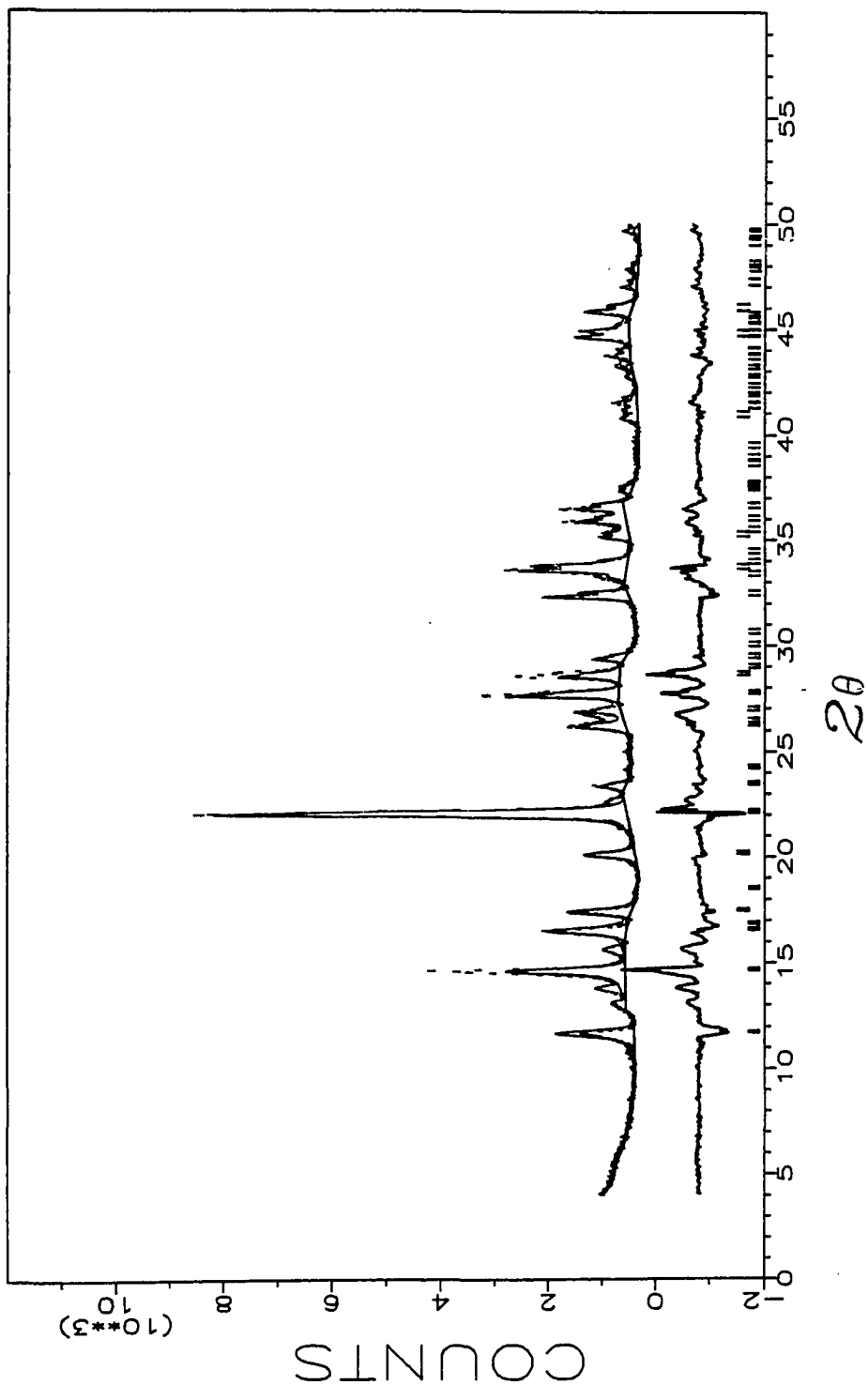
COUNTS
(10**3)
10
8
6
4
2
0
-2
0
5
10
15
20
25
30
35
40
45
50
55
2θ

Figure VI-8. X-ray diffraction pattern of mixed $Pb(Bi)O_2$ electrode: $C^b_{Bi(III)}/C^b_{Pb(II)}$ = 0.5 in the deposition solution

Conditions for electrodeposition of the mixed-oxide electrodes.
Deposition potential: 1.60 V vs. SCE
Rotation velocity of electrode (ω): 900 rev min^{-1}
Deposition time: 20.0 min

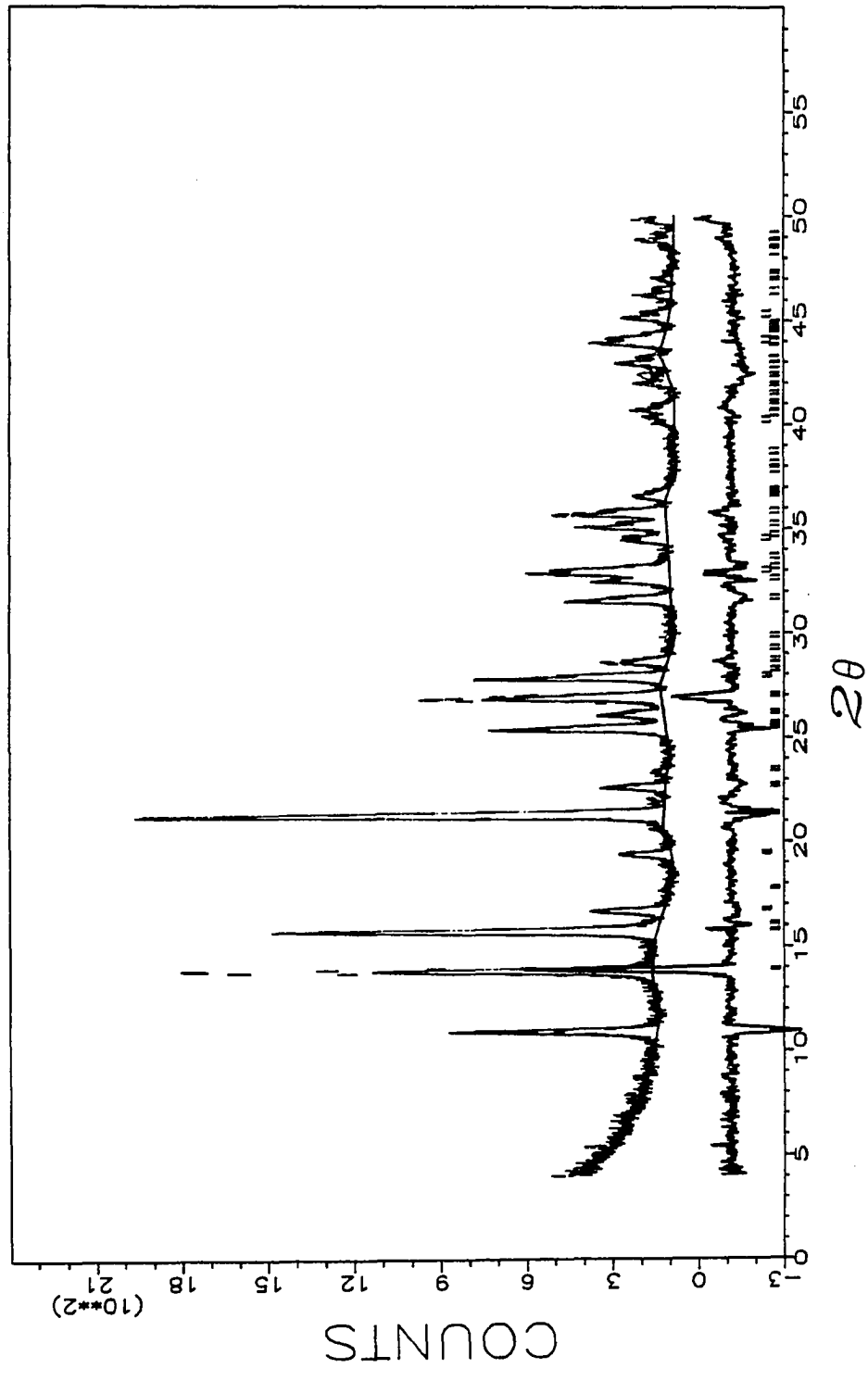
COUNTS
(10**2)
0
3
6
9
12
15
18
21
0
5
10
15
20
25
30
35
40
45
50
55
2θ

Figure VI-9. X-ray diffraction pattern of mixed $Pb(Bi)O_2$ electrode: $C^b_{Bi(III)}/C^b_{Pb(II)}$ = 0.7 in the deposition solution

Conditions for electrodeposition of the mixed-oxide electrodes.
Deposition potential: 1.60 V vs. SCE
Rotation velocity of electrode (ω): 900 rev min^{-1}
Deposition time: 20.0 min

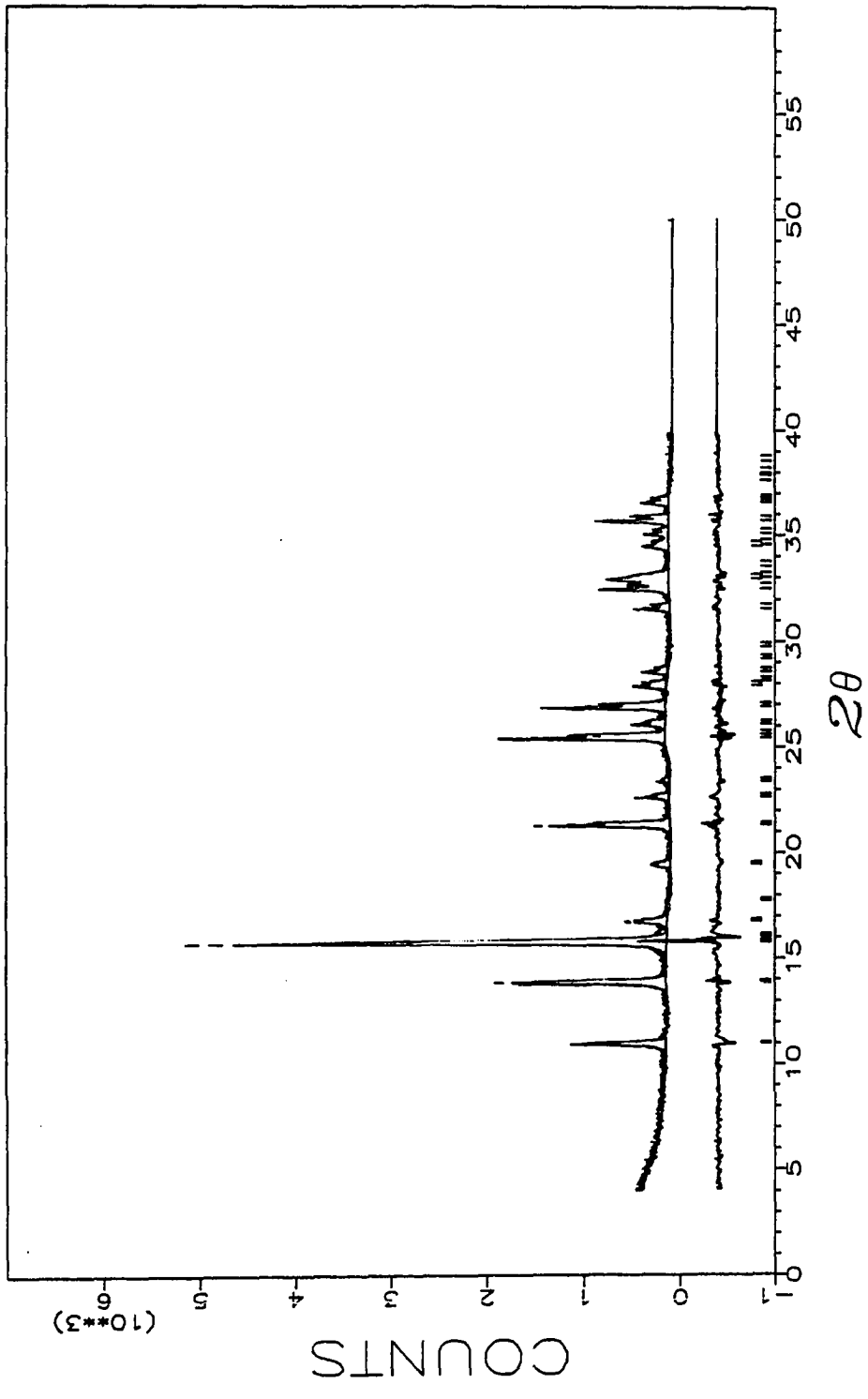
COUNTS
(10**3)
6
5
4
3
2
1
0
-1
0
5
10
15
20
25
30
35
40
45
50
55
2θ

Figure VI-10. X-ray diffraction pattern of mixed $Pb(Bi)O_2$ electrode: $C^b_{Bi(III)}/C^b_{Pb(II)}$ = 1.0 in the deposition solution

Conditions for electrodeposition of the mixed-oxide electrodes.
Deposition potential: 1.60 V vs. SCE
Rotation velocity of electrode (ω): 900 rev min^{-1}
Deposition time: 20.0 min

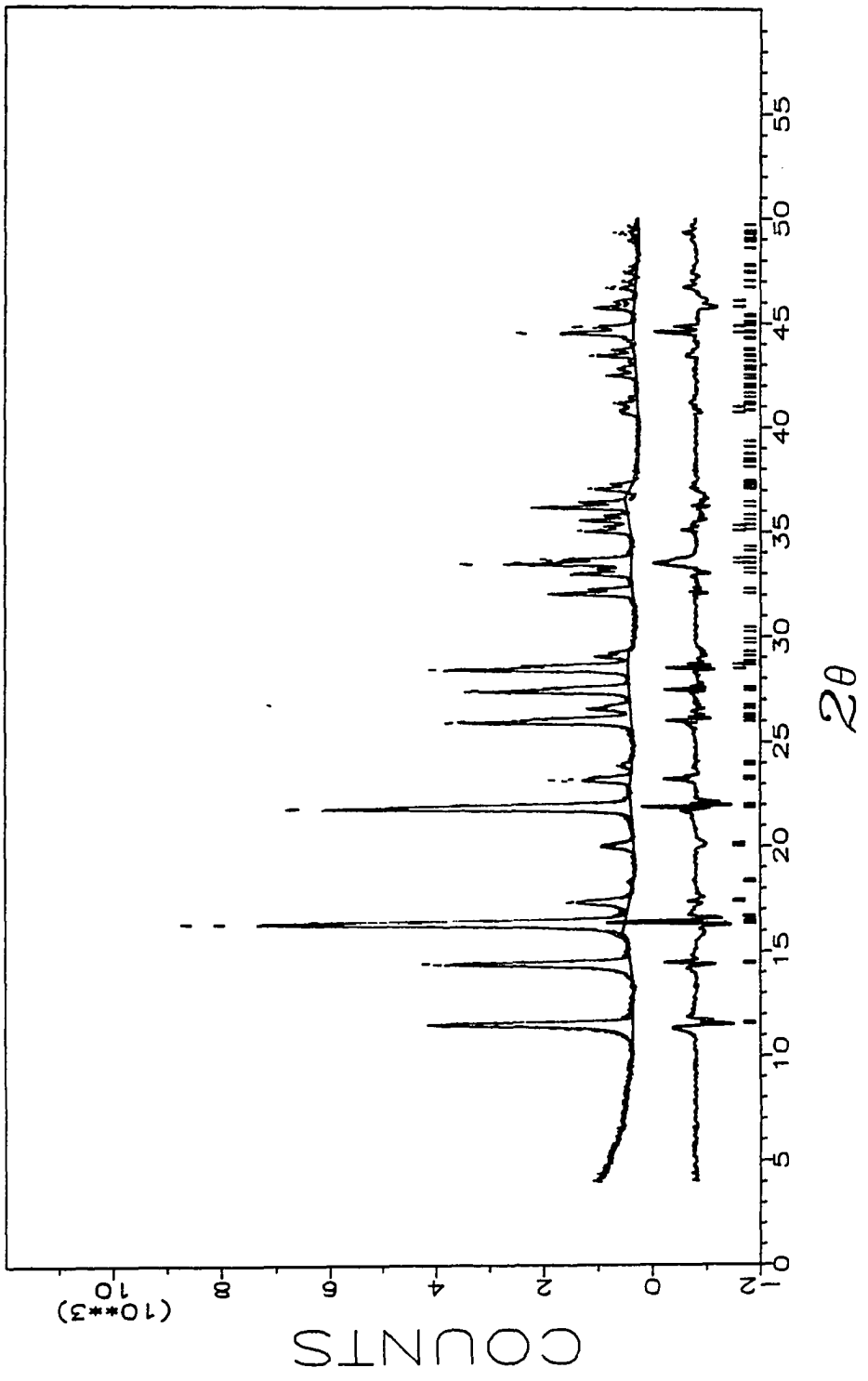
COUNTS
(10**3)
10
8
6
4
2
0
2
0
5
10
15
20
25
30
35
40
45
50
55
2θ

Figure VI-11. X-ray diffraction pattern of powdered mixed $Pb(Bi)O_2$ electrode: $C^b_{Bi(III)}/C^b_{Pb(II)} = 1.0$ in the deposition solution

Conditions for electrodeposition of PbO_2 electrodes.
Deposition potential: 1.60 V vs. SCE
Rotation velocity of electrode (ω): 900 rev min^{-1}
Deposition time: 20.0 min

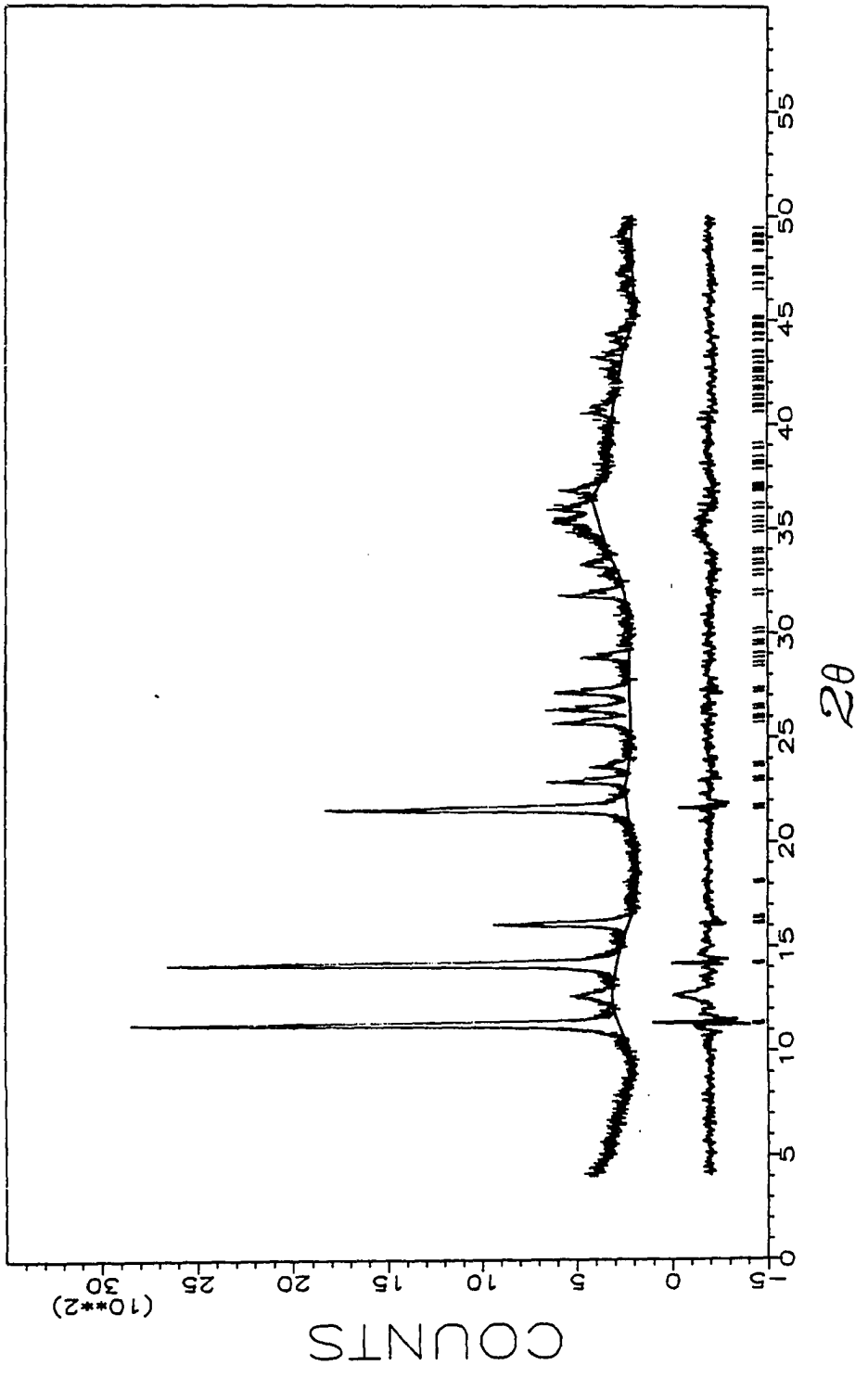
COUNTS
(10**2)
-5
0
5
10
15
20
25
30
0
5
10
15
20
25
30
35
40
45
50
55
2θ

of the oxide. Since the X-ray scattering powers of Pb and Bi, whether in neutral or ionic oxidation states, are very close to each other, long-range ordering, if any, is very difficult to detect.

Table VI-1 shows the increase in the unit cell volume as the concentration of bismuth increases. It is known that lead and bismuth have different ionic radii: Pb(IV) = 0.775, Bi(V) = 0.76 and Bi(III) = 1.03 A [18]. If all the Bi atom in the lattice are pentavalent, the volume must decrease as the ratio Bi/Pb increases. Since this is not the case observed, some fraction of the Bi in the lattice must be in trivalent state. For rutile structures, an empirical relationship between unit cell volume (V) and the cationic radius (r) holds, normally:

$$V = 41.8987 + 88.2806 \cdot r^3 \qquad (1)$$

In equation (1), r is the average cationic radius and can be estimated as follows:

$$r^3 = (1-x)\cdot(r_{Pb(II)})^3 + x\cdot[(1-y)\cdot(r_{Bi(III)})^3 + y\cdot(r_{Bi(V)})^3] \qquad (2)$$

where x is the total concentration of bismuth in the electrode and y is the mole fraction of bismuth in the form of pentavalent state defined by

Table VI-1. Variations of lattice parameters of β-PbO_2 as functions of the ratio of Bi(III)/Pb(II) in the solution

$C^b_{Bi(III)}/C^b_{Pb(II)}$	a = b	c	V	y[a]
0[b]	4.9542(7)	3.3846(6)	83.07(3)	——
0	4.9561(11)	3.3789(12)	83.00(5)	——
0.1	4.9478(14)	3.3819(17)	82.79(6)	1.02
0.2	4.9633(7)	3.3951(8)	83.64(3)	0.86
0.3	4.9632(7)	3.3978(7)	83.70(3)	0.89
0.5	4.9719(6)	3.4070(6)	84.22(3)	0.89
0.7	4.9798(4)	3.4165(4)	84.72(2)	0.88
1.0	4.9855(3)	3.4249(4)	85.13(1)	0.87
1.0[b]	4.9882(5)	3.4251(4)	85.22(2)	0.86

[a]y = [Bi(V)]/([Bi(V)]+[Bi(III)]) = mole fraction of Bi(V) of the total Bi in the mixed oxides.

[b]Powder samples.

$$y = [Bi(V)]/([Bi(V)]+[Bi(III)]). \quad (3)$$

Since the former can be estimated from X-ray fluorescence analyses on the electrodes (Table V-2), the latter can be easily calculated via:

$$y = \frac{(r_{Bi(III)})^3 - [r^3 - (1-x)\cdot(r_{Pb(IV)})^3]/x}{[(r_{Bi(III)})^3 - (r_{Bi(V)})^3]} \quad (4)$$

The results are shown in the last column of Table VI-1. Interestingly, y values are within 0.86 - 0.89 for most of the samples except for the electrode of $C^b_{Bi(III)}/C^b_{Pb(II)}$ = 0.1. At this concentration ratio, the calculation seems to indicate virtually no Bi(III) present in the electrode. If this is true, it gives rise to the radius for Bi(V) ion as 0.75 A.

The result that the mole fraction of Bi(V) is ca. 0.87 was obtained by XRD studies. This indicated that 87% of the total Bi was oxidized to Bi(V) in the anodic depostion process. Similar result was obtained by electrochemical measurements. Amperometric studies indicated that Bi(III) is oxidized with n = ca. 1.5 $\pm$ 0.2 simultaneously with electrodeposition in the mixed oxide in Chapter V. This number translates into 75% of the total Bi being oxidized to Bi(V). It should be noted that the interpretation of the X-

ray results is subject to the definition of the cationic radii. Although the calculated values do not agree, both X-ray analysis and electrochemical measurements indicated the presence of smaller amounts of Bi(III) compared to Bi(V) in the lattice.

One of the distinct features in the diffraction patterns of the electrode samples compared to those of the powder samples is that relative intensities among reflections in the former are different from those of the latter. For example, the (110) peak at $2\theta = 10.5°$ and the (011) peak at $2\theta = 14.5$ are the strongest in the powder samples (Figures VI-3 and VI-11), while they are relatively weaker than other peaks such as the (121) peak at $2\theta = 22.3°$ in Figure VI-7 and the (020) peak at $2\theta = 15.8°$ in Figure VI-9. This intensity variation is interpreted in terms of preferred orientation of the electrodeposited crystalline particles. The (121) plane shows strongly preferred orientation parallel to the substrate surface for samples with a low Bi/Pb ratio. The (020) plane shows a highly preferred orientation parallel with the substrate surface for high Bi/Pb ratios.

It is shown in Figure VI-12 that the variation in the integrated intensities of (110), (011), (020), (121) reflections as functions of ratio of the $C^b_{Bi(III)}/C^b_{Pb(II)}$ in the deposition solution. Clearly, the preferred

Figure VI-12. Intensity variations of (110), (011), (020) and (121) reflections as a function of bismuth concentration in the mixed $Pb(Bi)O_2$ electrode

Conditions for electrodeposition of the mixed-oxide electrodes
Deposition potential: 1.60 V vs. SCE
Rotation velocity of electrode (ω): 900 rev min^{-1}
Deposition time: 20.0 min
Solution: 1.0M $HClO_4$
$C^b_{Bi(III)}/C^b_{Pb(II)}$ = 0.0, 0.1, 0.2, 0.3, 0.5, 0.7 and 1.0 in the deposition solution

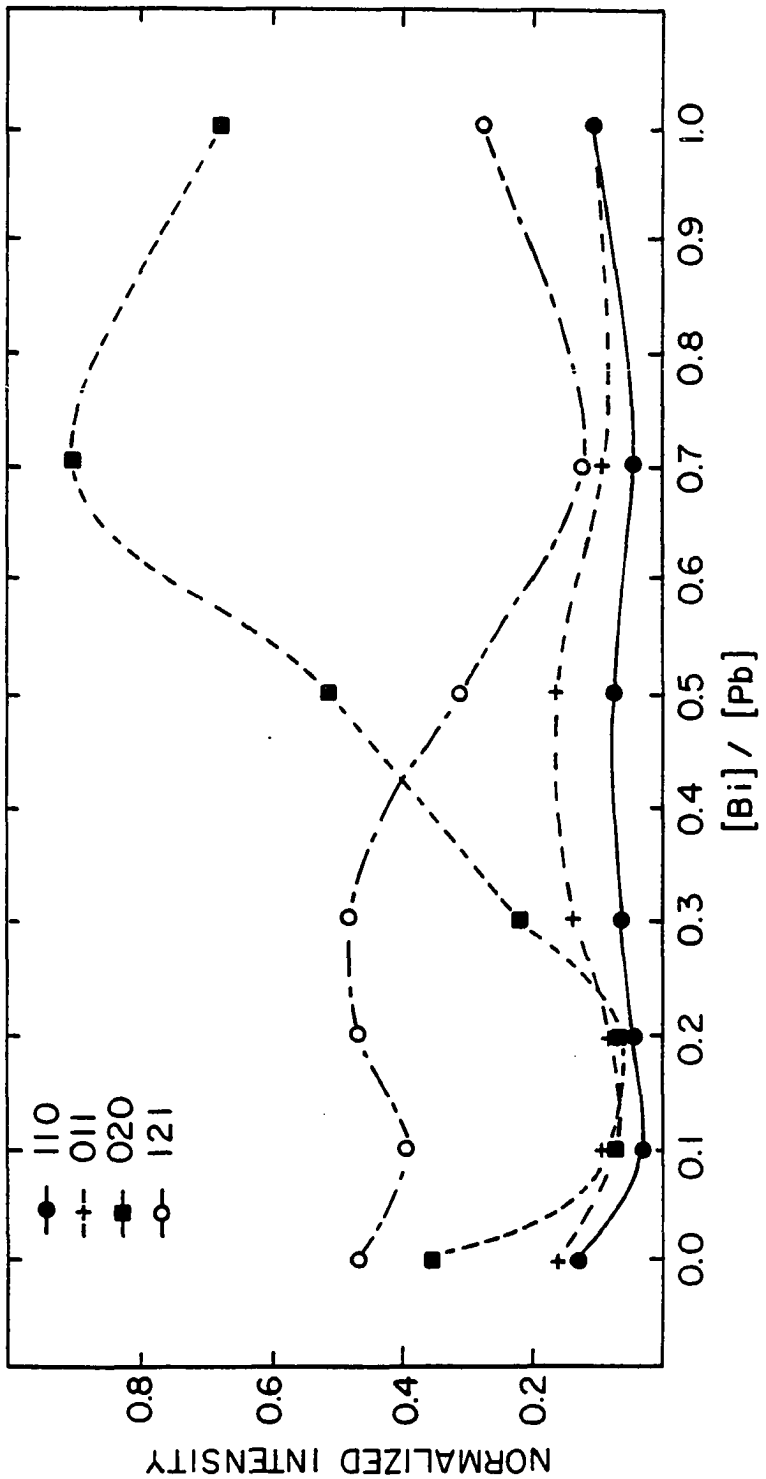
NORMALIZED INTENSITY
0.2
0.4
0.6
0.8
[Bi] / [Pb]
0.0
0.1
0.2
0.3
0.4
0.5
0.6
0.7
0.8
0.9
1.0
110
011
020
121

orientation of the (020) is maximal when $C^b_{Bi(III)}/C^b_{Pb(II)}$ = 0.7. This indicates that the crystals of the electrodeposited PbO_2 in the presence of bismuth are grown in a way such that the (020) face is preferentially orientated parallel to the electrode surface.

Observed half-widths of diffraction peaks at half-maximum intensity can be used to compared the crystalline particle size [19]. The width of the diffraction peaks of the mixed bismuth-lead dioxide is narrower than that for pure PbO_2. The width decreases as $C^b_{Bi(III)}/C^b_{Pb(II)}$ increases, with minimum at $C^b_{Bi(III)}/C^b_{Pb(II)}$ = 0.7. Scanning electron micrographs (SEM) are shown in Figure VI-13 for a pure PbO_2 and a mixed Bi-Pb dioxide for $C^b_{Bi(III)}/C^b_{Pb(II)}$ = 1.0. Clearly, the mixed electrode shows larger particle size. It can be argued that the crystalline particle size increases until $C^b_{Bi(III)}/C^b_{Pb(II)}$ reaches 0.7, and then starts to decrease as more Bi is added. As shown in the SEM photos, the crystals of pure PbO_2 have much smaller dimensions, compared to those for the mixed oxide. Therefore, it can be concluded that bismuth ions decrease the nucleation rate of PbO_2 and, thereby, increase the growth rate of the crystals.

The sputtering experiments with Auger electron spectroscopy strongly suggest that bismuth ions in the mixed oxide are randomly and uniformly distributed in depth and in width. That is, bismuth ions randomly substitute into Pb sites in the lattice of rutile structure.

Figure VI-13. Scanning electron micrographs of electrodeposited pure PbO_2 (A) and mixed $Pb(Bi)O_2$ (B) on a Au RDE

Conditions for electrodeposition of the oxides.
Deposition potential: 1.60 V vs. SCE
Rotation velocity of electrode (ω): 900 rev min^{-1}
Deposition time: 10.0 min
Solution: 1.0M $HClO_4$
Pure PbO_2: 1.0mM Pb(II)
Mixed oxide: 1.0mM Pb(II) + 0.1mM Bi(III)

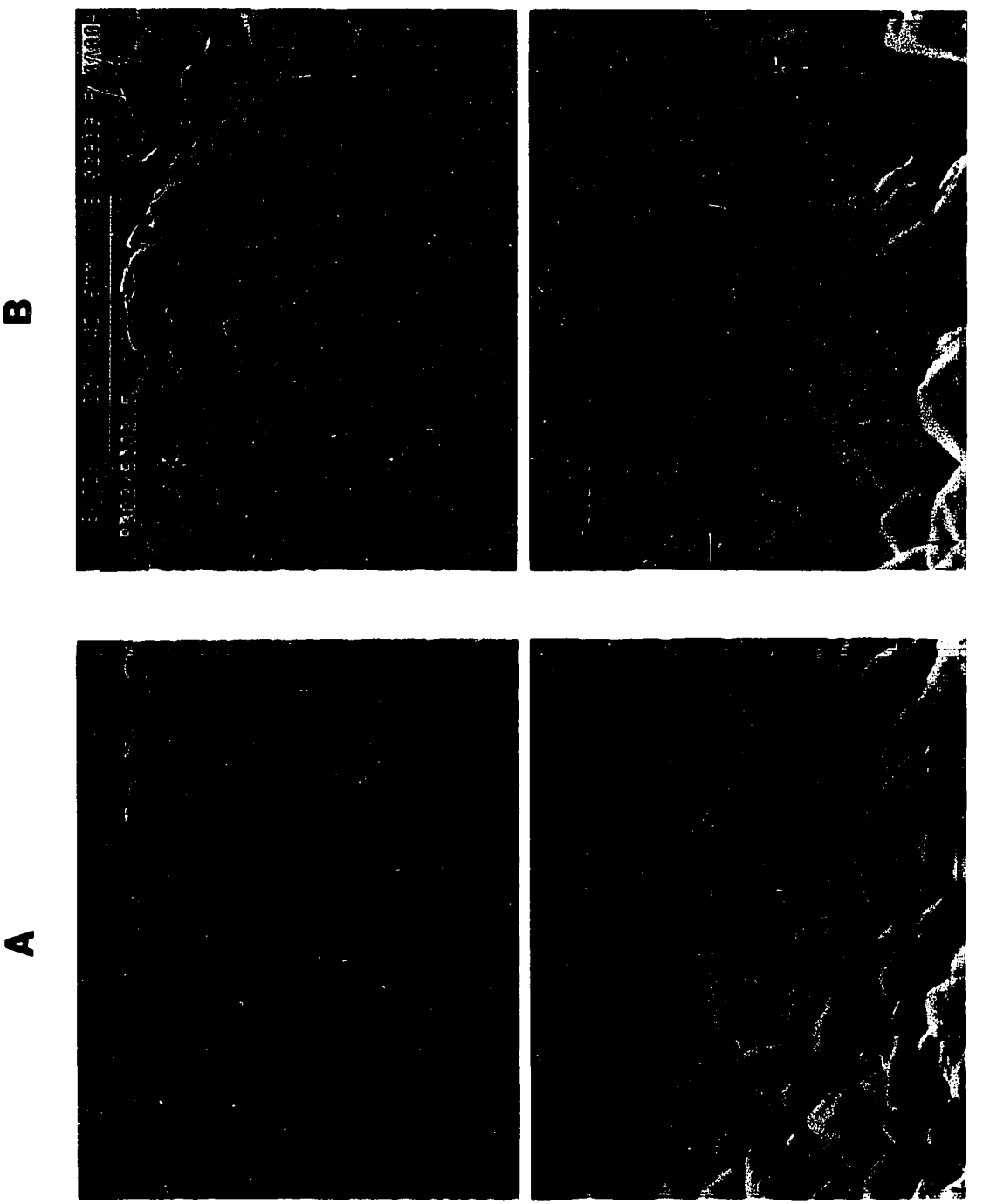
B
A

Considering the charge valence of the mixed oxide, the extra charges from the substitution of Bi(V) for Pb(IV) should be compensated by either extra anions or less substitution of Bi(V) in every Pb(IV) sites. Possible anions are oxygen, Cl^-, and ClO_4^- because electrolyte was 1.0M $HClO_4$ in the deposition process. Auger electron intensity for chloride was observed indicating the presence of this element (or ion) in the mixed oxides. However, the intensity decreased and finally was not observed as electron beam was scanned deeper into the bulk phase of the oxide. Therefore, it is hard to believe that Cl^- ions are present to maintain charge balance of extra positive charge from the Bi(V) substitution.

From the experimental results of AES and XRD it can be concluded that cation site in the mixed oxide could be a Pb(IV), Bi(III), Bi(V), or remain as vacancy to maintain charge valence in the bulk of the mixed oxide. The substituted Bi(V) ions may have more oxygens at the surface to accommodate local charge valence.

In conclusion, bismuth ions substitute for lead ions in the mixed oxides without significant distortion of lattice of rutile structure. It also affects the nucleation and growth of the oxide, which results in the change of crystal size and surface morphology of the mixed oxide.

E. References

1. Hill, R. J. J. Power Sources 1983, 9, 55.

2. Santorio, A.; D'Antonio, P.; Caulder, S. M. J. Electrochem. Soc. 1983, 130, 1451.

3. Varma, R.; Eckert, J.; Maroni, V. A.; Goldstons, J. A.; Giordano, C.; Cehelnik, T.; Kumar, R.; Siegel, S.; Tani, B. In "Proceedings of the Symposium on Advances in Lead-Acid Batteries"; Bullock, K. R. et al., Eds; Electrochem. Soc. Inc.: Pennington, New Jersey, 1984; Page 44.

4. Miyazaki, K.; Sumida, M. In "Proceedings of the Symposium on Advances in Lead-Acid Batteries"; Bullock, K. R. et al., Eds; Electrochem. Soc. Inc.: Pennington, New Jersey, 1984; Page 78.

5. Varma, R. In "Proceedings of the Symposium on Advances in Battery Material and Processes"; Mcbreen, J. et al., Eds; Electrochem. Soc. Inc.: Pennington, New Jersey, 1984; Page 267.

6. Delmastro, A.; Maja, M. J. Electrochem. Soc. 1984, 131, 2756.

7. Crennel, J. T.; Milligan, A. G. Trans. Faraday Soc. 1931, 27, 103.

8. Haring, H. E.; Thomas, U. B. J. Electrochem. Soc. 1935, 68, 293.

9. Byfield, J. W. R. J. Electrochem. Soc. 1941, 79, 259.

10. Mahato, B.; Tiedemann, W. J. Electrochem. Soc. 1983, 130, 2139.

11. Caldara, F.; Delmastro, A.; Fracchia, G.; Maja, M. J. Electrochem. Soc. 1980, 127, 1869.

12. Burbank, J. J. Electrochem. Soc. 1964, 111, 1112.

13. Ritchi, E. J.; Burbank, J. J. Electrochem. Soc. 1970, 117, 299.

14. Thanos, J. C. G.; Wabner, D. W. J. Electroanal. Chem. 1985, 182, 25.

15. Thanos, J. C. G.; Wabner, D. W. J. Electroanal. Chem. 1985, 182, 37.

16. Bagshaw, N. E.; Clarke, R. L.; Halliwell, B. J. Appl. Chem. 1966, 16, 180.

17. Hill, R. J.; Madsen, I. C. J. Electrochem. Soc. 1984, 131, 1486.

18. Shannon, R. D. Acta Crystallogr. 1976, A32, 751.

19. Rosauer, E. A. In "Instruments for Material Analysis"; Iowa State University: Ames, 1981; Page 99.

VII. CORRELATION OF OXYGEN EVOLUTION OVERPOTENTIAL AND ELECTROCATALYSIS AT LEAD DIOXIDE AND MIXED BISMUTH-LEAD DIOXIDE ELECTRODES

A. Abstract

The relationship between the oxygen evolution overpotential and the rate constant for electrocatalytic oxidation of 2-thiophene carboxylic acid (2-TCA) was studied at rotated disc electrodes made from mixed bismuth-lead dioxides. The density of oxygens per metal site on principal faces of the rutile structure was calculated from pictorial representations of the structure drawn by Oak Ridge Thermal Ellipsoid Plot Program (ORTEP). From the results, it is observed that the (020) face has the largest oxygen density and this face is preferentially oriented parallel to the substrate surface by the electrochemical deposition. Voltammetric studies demonstrate that the electrode which has the minimal overpotential for oxygen evolution has the greatest reactivity for the anodic oxygen-transfer reaction for 2-TCA. The optimum concentration ratio of Bi(III):Pb(II) in the deposition solution is 0.7 for generating the mixed oxide with the highest reactivity.

B. Introduction

It is known that oxides can serve as electrode materials in various electrochemical systems, mostly for the performance of anodic processes [1]. Partial catalytic oxidations on mixed oxide catalysts are important in industrial organic chemical processes as the conversion of methanol to formaldehyde, ethylene to ethylene oxide or propylene to acrylonitrile [2]. However, it is not clear why multicomponent metal oxides are effective for the selective oxidation of hydrocarbons. Therefore, the question always arises: What is the main component or functionality at the oxide surface to cause such a catalytic oxidation and what change can be made to such an oxide to enhance the reactivity for the oxidation of organic molecules? Many researchers have tried to understand catalytic behavior in connection with a particular structure or the type of oxygen species in a metal oxide [3-6].

Oxygen evolution at the surface of an oxide electrode can be considered to be competitive with electrocatalytic oxygen-transfer reactions. A general reaction scheme showing this idea can be envisaged as follows:

$$S + H_2O \longrightarrow S[O] + 2H^+ + 2e \qquad (1)$$

$$S[O] + R \longrightarrow S + RO \qquad (2)$$

or

$$2S[O] \longrightarrow 2S + O_2 \qquad (3)$$

In equations (1-3), S is electrode surface, [O] is the labile surface oxygen which can be involved in anodic oxygen-transfer reaction (equation 2) or oxygen evolution (equation 3), R is an electroactive reactant and RO is the reaction product.

Some authors have suggested that the bond strength of oxygen adsorbed at the metal surface controls the oxygen overpotential (η) for the oxide [7,8]. However, others have suggested that it is the bond strength of oxygen adsorbed at the metal oxide which is the factor to be considered [9,10].

Adzic et al. have investigated the effects of crystallographic orientation on the oxidation of HCOOH and CH_3OH at Pt electrode surfaces [11,12]. They observed that these oxidation processes are highly dependent on the surface orientation of single crystal electrodes. The highest activity was found for the (111) orientation and the lowest for the (100). Therefore, it was concluded that crystallographic orientation could be important in controlling electrocatalytic oxygen-transfer reaction rates as well as oxygen evolution overpotential at mixed oxide electrodes.

In Chapter V and VI, it was reported that mixed bismuth-lead dioxide electrodes exhibit a large increase in the

oxidation rate for Mn(II) and organic compounds in comparison to electrodeposited β-PbO_2. Furthermore, the mixed oxide has a preferential orientation of the (020) face parallel to the surface of the substrate electrode.

In this chapter, an attempt is made to show some relationships between oxygen evolution overpotential and heterogeneous rate constants for oxidation of 2-thiophene carboxylic acid (2-TCA). Changes of oxygen evolution overpotential are explained on the basis of changes in the density of surface oxygen atoms in a specific face of the oxide electrode. The heterogeneous rate constants were determined from Koutecky-Levich plots [13].

C. Experimental

Reagents. All chemicals were Analytical Reagents from Fisher Scientific, Aldrich Chemicals or Baker Chemicals: $Pb(NO_3)_2$, $Bi(NO_3)_3$, 2-thiophene carboxylic acid. The supporting electolyte was 1.0M $HClO_4$ and the electrochemical measurements were performed in deaerated solutions under a nitrogen atmosphere.

Instrumentation. The instrumentation was described in Chapter III.

Preparation of electrodes. Lead dioxide electrodes doped with bismuth oxide were prepared on a gold rotated disc electrode (RDE, 0.496 cm^2) by electrodeposition at 1.60 V vs. SCE. The concentration of Bi(III) in the deposition solution containing 1.0mM Pb(II) was changed from 0.0 mM to 1.0 mM. Values of the concentration ratio, $C^b_{Bi(III)}/C^b_{Pb(II)}$, were 0.0, 0.3, 0.5, 0.7 and 1.0. The electrodeposited oxides from the five solutions were used for the measurement of oxygen evolution overpotential at constant current and electrocatalytic reactivity for oxidation of 2-TCA at 1.60 V vs. SCE.

Voltammetry. The steady-state values of anodic currents for the oxygen evolution reaction at gold, electrodeposited pure β-PbO_2 and mixed bismuth-lead dioxide electrodes were measured by applying constant potentials ranging from 1.50 V to 1.75 V vs. SCE. at 50 mV intervals. Tafel slopes and Tafel intercept for the oxygen evolution were calculated from the Tafel plot, i.e., a plot of η vs. log {i}. In a second set of experiments, constant anodic currents (50 and 25 μA) were applied to the electrodes in 1.0M $HClO_4$ and values of potential corresponding to each current were recorded.

The reactivities of the electrodes were compared by measuring anodic current for oxidation of 0.1mM 2-thiophene carboxylic acid. The rotation velocity of the electrode was changed in a stepwise fashion abd values of 1/i were plotted

vs. $1/\omega^{1/2}$. The heterogeneous rate constants were calculated from the intercepts obtained by linear regression analysis of the data used for making the plots.

D. Results and Discussion

Plots of i vs. $\omega^{1/2}$ are shown in Figure VII-1 for the oxidation of 2-thiophene carboxylic acid at electrodeposited pure lead dioxide and mixed bismuth-lead dioxide electrodes prepared for different values of $C^b_{Bi(III)}/C^b_{Pb(II)}$. Particularly, the oxidation rate of this compound at the pure PbO_2 electrode is so slow, i.e., kinetically controlled, that the anodic current is independent of rotation rate.

The values of heterogeneous rate constants calculated from the intercept of 1/i vs. $1/\omega^{1/2}$ plots at the mixed oxide electrodes are given in Table VII-1. From these data, it is apparent that the catalytic oxidation rate increased as the concentration of bismuth was increased in the deposition solution. The value of the heterogeneous rate constant increased to $C^b_{Bi(III)}/C^b_{Pb(II)} = 0.7$, and then decreased. The ratio of Bi:Pb is 0.7 in the deposition solution for producing the mixed oxide with highest reactivity. The electrocatalytic reactivities of these electrodes can not be differentiated by comparing values of heterogeneous rate constants for oxidation of Mn(II) because that reaction is vitually at a mass-transport limited rate at all of the electrodes containing Bi.

Figure VII-1. Plots of i vs. $\omega^{1/2}$ for oxidation of 2-thiophene carboxylic acid at pure PbO_2 and mixed $Pb(Bi)O_2$ electrode

Conditions for electrodeposition of mixed-oxide electrodes:
Deposition potential: 1.60 V vs. SCE
Rotation velocity of electrode (ω): 900 rev min^{-1}
Deposition time: 20.0 min
Solution: 1.0M $HClO_4$
(°): 1.0mM Pb(II) + 0.0mM Bi(III)
(+): 1.0mM Pb(II) + 0.3mM Bi(III)
(□): 1.0mM Pb(II) + 0.5mM Bi(III)
(0): 1.0mM Pb(II) + 0.7mM Bi(III)
(×): 1.0mM Pb(II) + 1.0mM Bi(III)

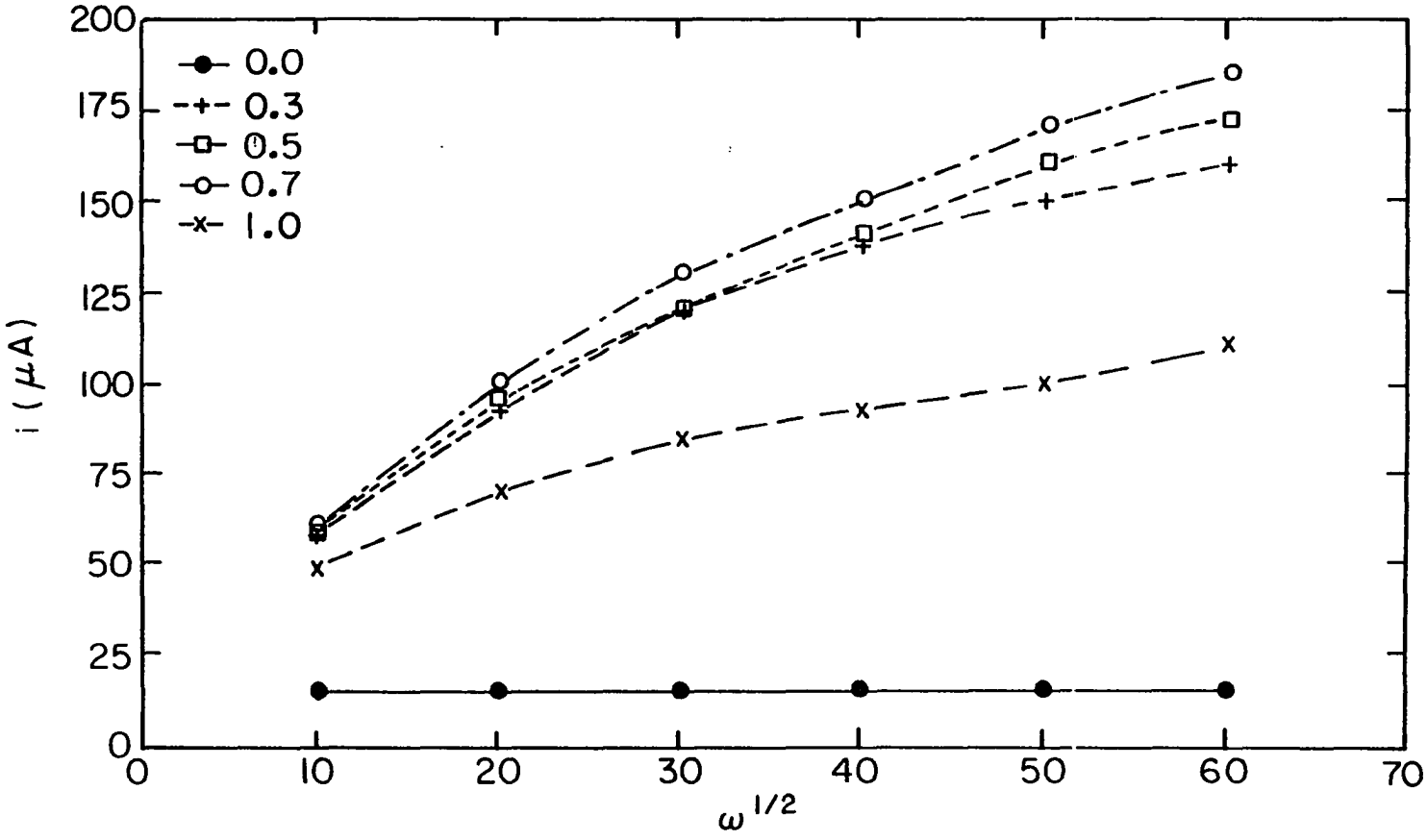
200
175
150
125
100
75
50
25
0
0
10
20
30
40
50
60
70
i (μA)
ω 1/2
0.0
0.3
0.5
0.7
1.0

Table VII-1. Heterogeneous rate constant for oxidation of 2-thiophene carboxylic acid

$C^b_{Bi(III)}/C^b_{Pb(II)}$	Rate constants (x 10^3) (cm sec^{-1})
0.0	0.39
0.3	6.77
0.5	7.47
0.7	8.27
1.0	3.80

In the previous chapter, analysis of X-ray diffraction (XRD) patterns shows that the degree of preferred orientation of the (020) face parallel with the substrate surface is increased as the concentration of bismuth increases and reaches its maximum for the electrode prepared from the deposition solution of $C^b_{Bi(III)}/C^b_{Pb(II)} = 0.7$. This is also the electrode composition giving the highest catalytic reactivity. Furthermore, it is concluded that this composition results in the maximum fraction of the (020) face existing at the electrode-solution interface when the anodic oxygen-transfer reactions occur.

It was concluded that the rate of anodic oxygen-transfer reactions could be a function of the electrochemical activity of surface oxygen at the oxide electrode. Hence, the surface concentration of oxygen as well as the metal-oxygen bond energy at the surface can be critical factors in the electrocatalysis.

The density of oxygen on a particular face was calculated from pictures of the rutile structure drawn by the Oak Ridge Thermal Ellipsoid Plot Program (ORTEP) [14]. The pictures of seven principal faces, e.g., (100), (010), (110), (101), (011), (001) and (111) are shown in Figure VII-2. Rectangular planes in the pictures represent the surface of the electrode. In the rutile structure, two axes (a, b) of unit cell have the same dimension so that (100) and (010) faces have same configuration of oxygen/metal at the surface

Figure VII-2. Seven principal faces ([100], [010], [001], [101], [011], [110] and [111]) of the rutile structure drawn by ORTEP

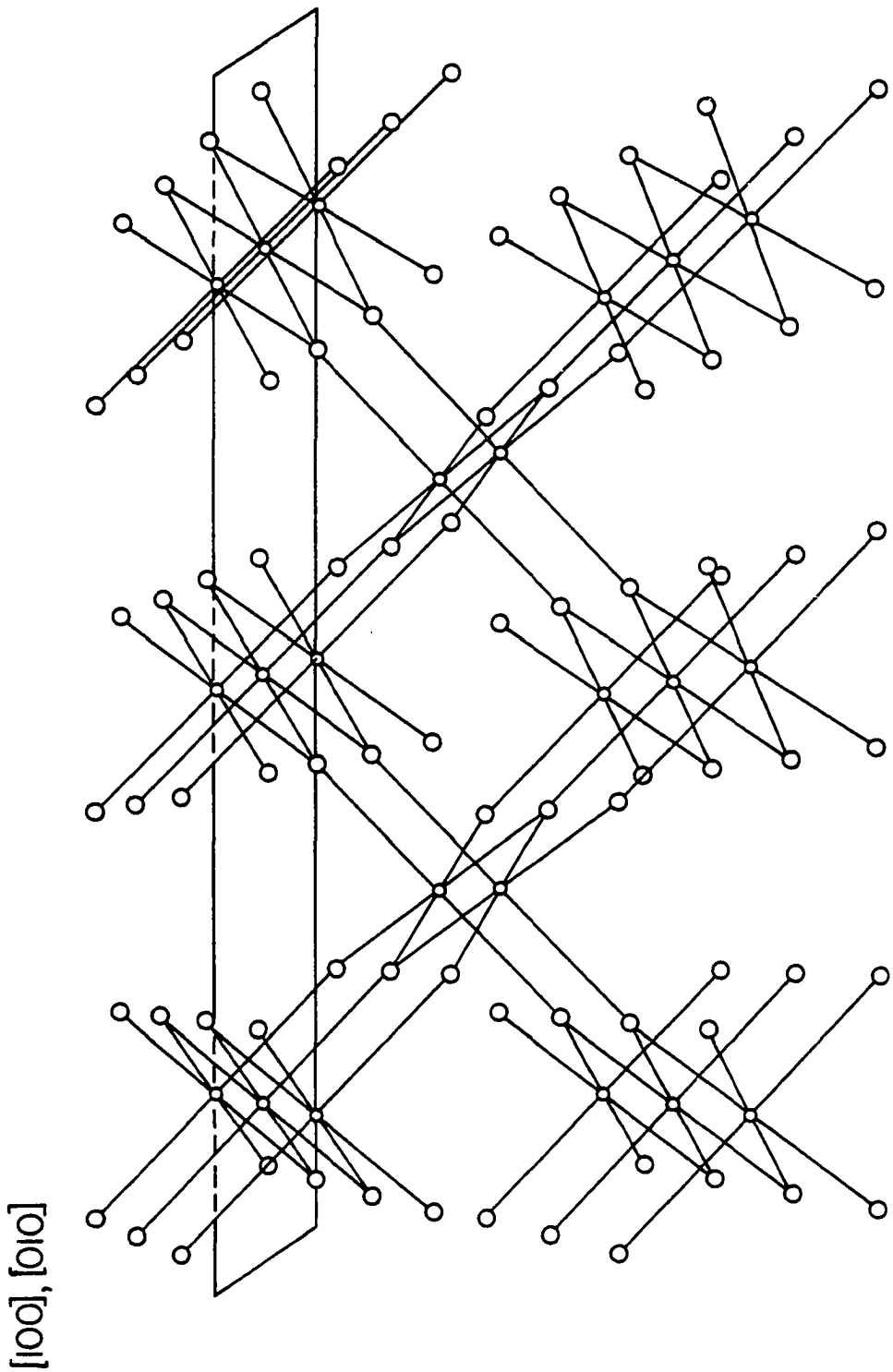
[100], [010]

[001]

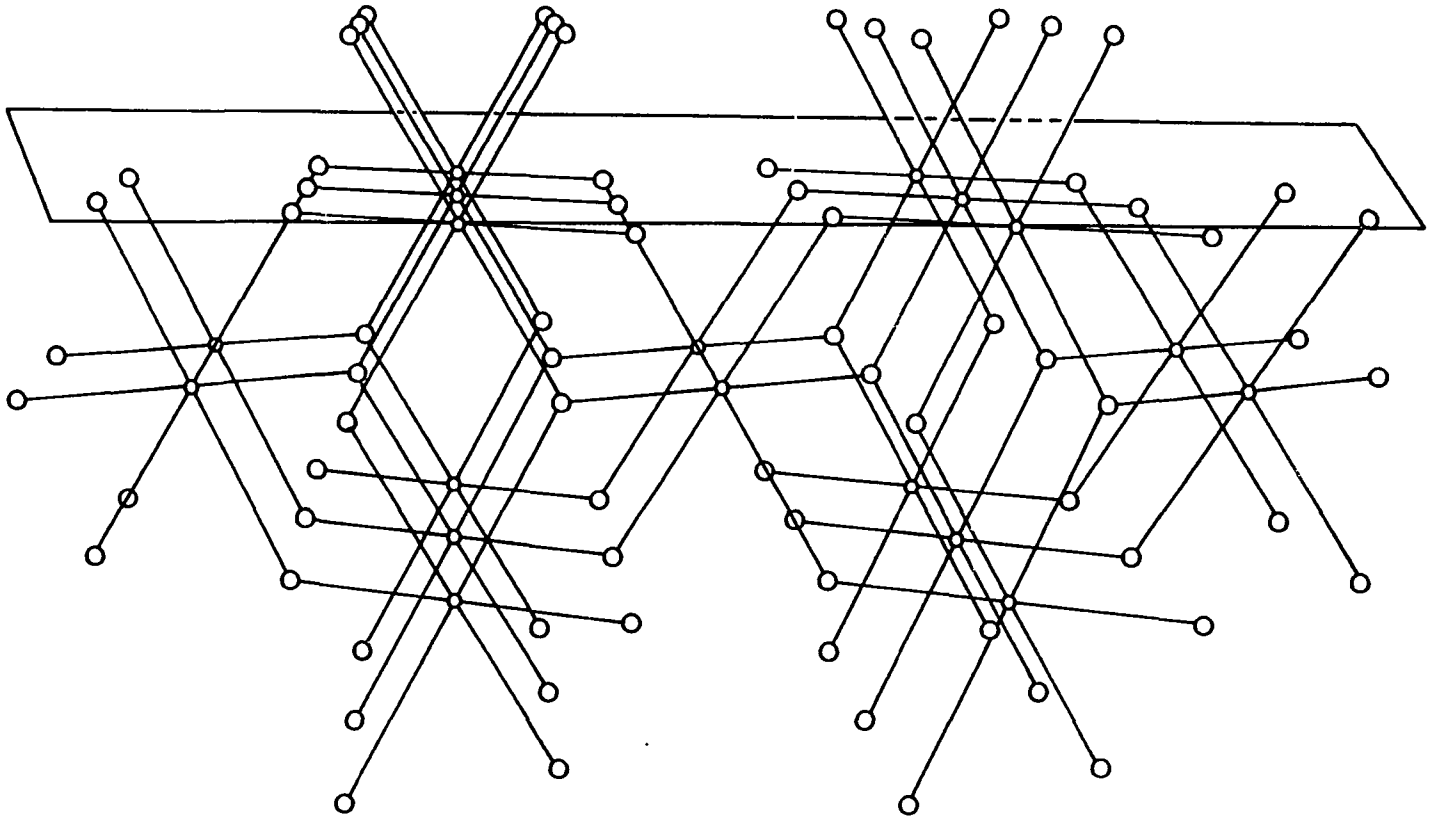

Figure VII-2. continued

[011],[101]

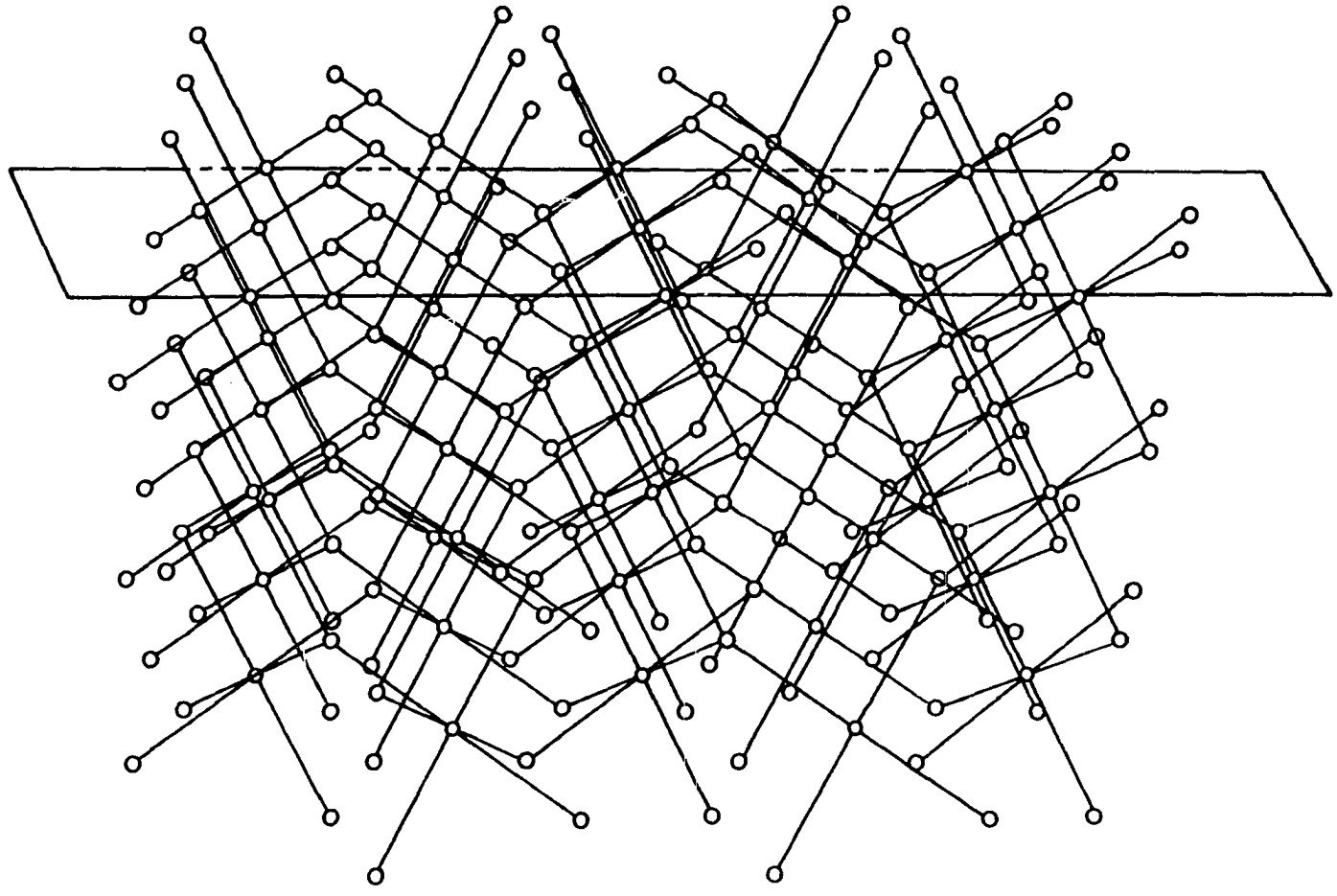

Figure VII-2. continued

[110]

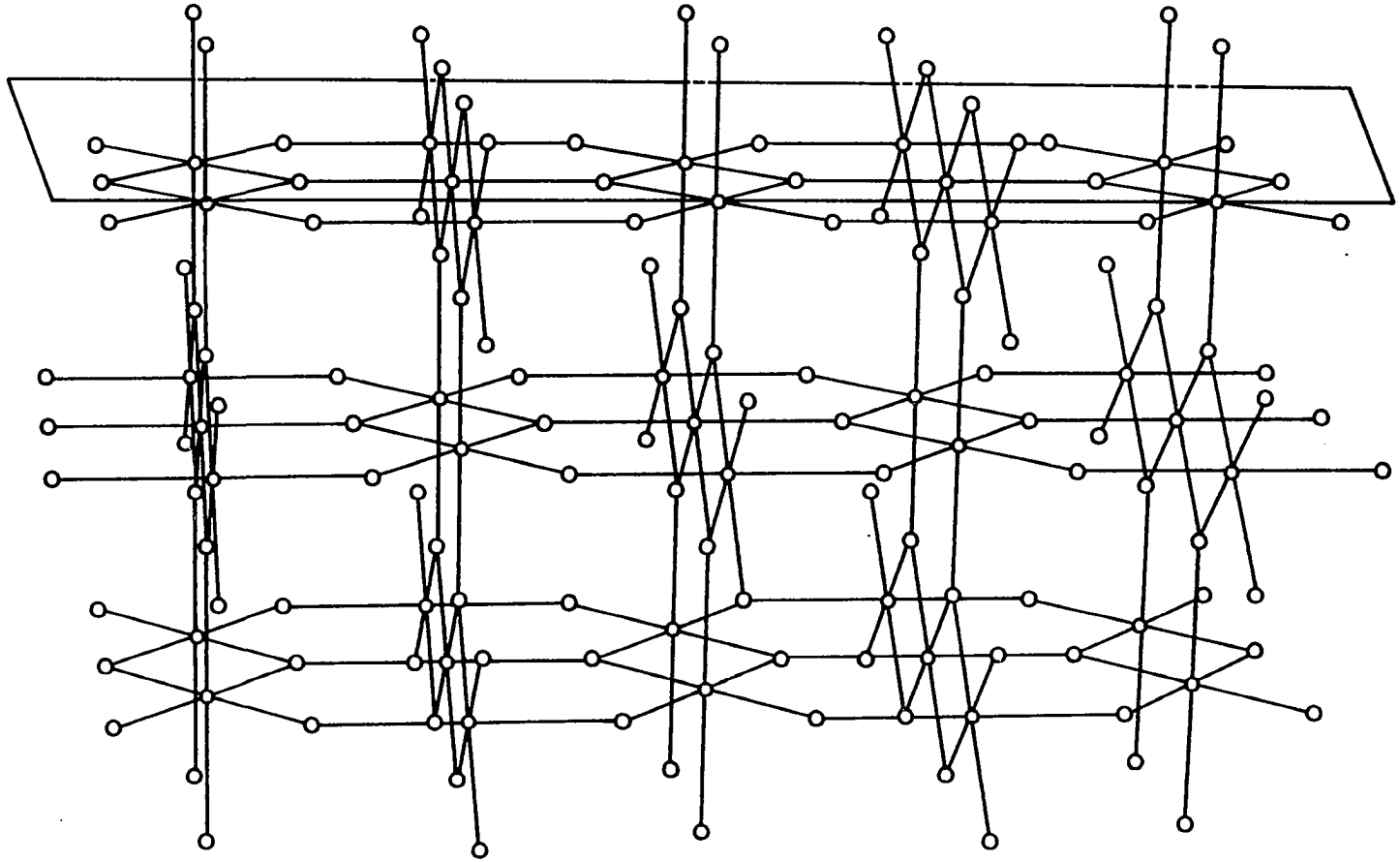

Figure VII-2. continued

[III]

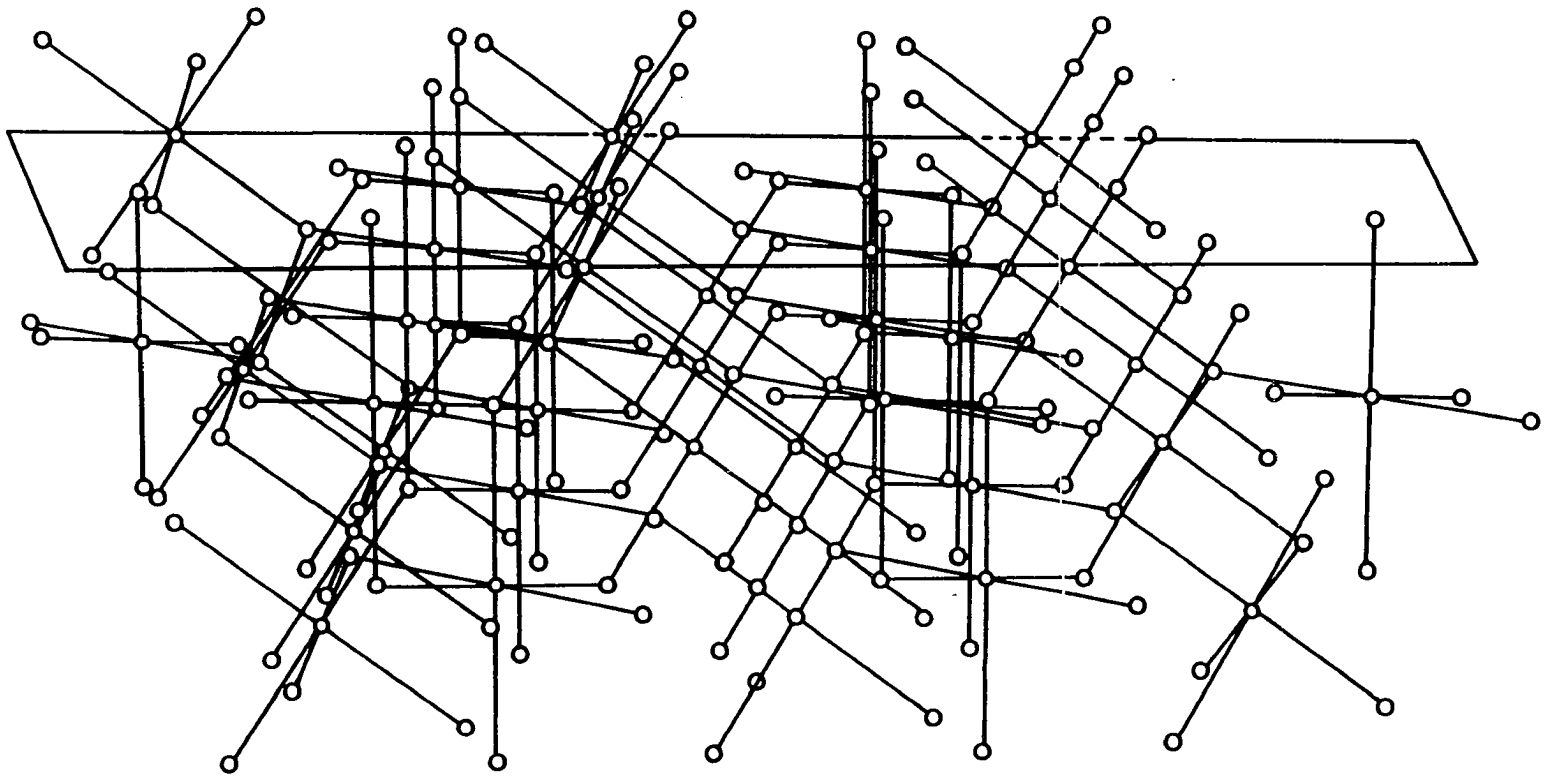

Figure VII-2. continued

and have the same geometrical area. Likewise, the (011) and (101) faces have the same configuration and area. The number of surface oxygens is different on each face and two types of oxygen exist on the surface, i.e., bridging oxygen and single-bonded oxygen. It is reported [15] that bond length between Pb metal and bridging oxygen (equatorial oxygen in the octahedral structure) is 2.150 A and bond length between Pb metal and isolated oxygen (axial oxygen) is 2.169 A. Because the difference in Pb-O bond length is less than 1 % it is impossile to predict which bond length is larger at the oxide surface when exposed to a solution.

The results of the calculated density of surface oxygen are summarized in Table VII-2. From these data, it is obvious that the (010) face has the greatest density of oxygen per metal atom per unit area. This face is identical to the (020) face that is preferentially oriented parallel to the surface of electrodeposited mixed bismuth-lead dioxide electrode. Therefore, it is concluded that during the electrodeposition, the oxide grows in such a fashion so as to produce a large activity of oxygen at the surface of electrode.

Tafel plots for oxygen evolution at the gold, the electrodeposited PbO_2 and the mixed-oxide electrode are shown in Figure VII-3. The values of Tafel slopes obtained from the Tafel plots were 0.09 V, 0.11 V and 0.13 V at the gold, pure PbO_2 and the mixed oxide, respectively. These values

Table VII-2. Density of oxygen atoms per metal atom per unit area of principal crystal faces for the rutile structure

Crystal faces	Area[a]	Ratio of oxygen per metal	Density of oxygen atoms per metal atom per unit area (A^{-2})
(100),(010)[b]	ac	2	0.120
(001)	ab	2	0.082
(011),(101)	$(a^2+c^2)^{1/2}\cdot a$	2	0.067
(110)	$\sqrt{2}ac$	1	0.042
(111)	$(a^2+2c^2)^{1/2}\cdot a$	2	0.059

[a]a, b, and c represent the unit cell dimensions (a = b = 4.942 A, c = 3.382 A).

[b]In the rutile structure, the (100) and (010) faces have same configuration of oxygen/metal at the surface and the same geometrical area.

Figure VII-3. Tafel plots for anodic evolution of O_2 at gold, electrodeposited pure PbO_2 and mixed $Pb(Bi)O_2$ electrode

Conditions for electrodeposition of oxide electrodes.
Deposition potential: 1.60 V vs. SCE
Rotation velocity of electrode (ω): 900 rev min^{-1}
Deposition time: 20.0 min
Solution: 1.0M $HClO_4$
A: 1.0mM Pb(II) + 1.0mM Bi(III)
B: 1.0mM Pb(II)
C: gold oxide electrode

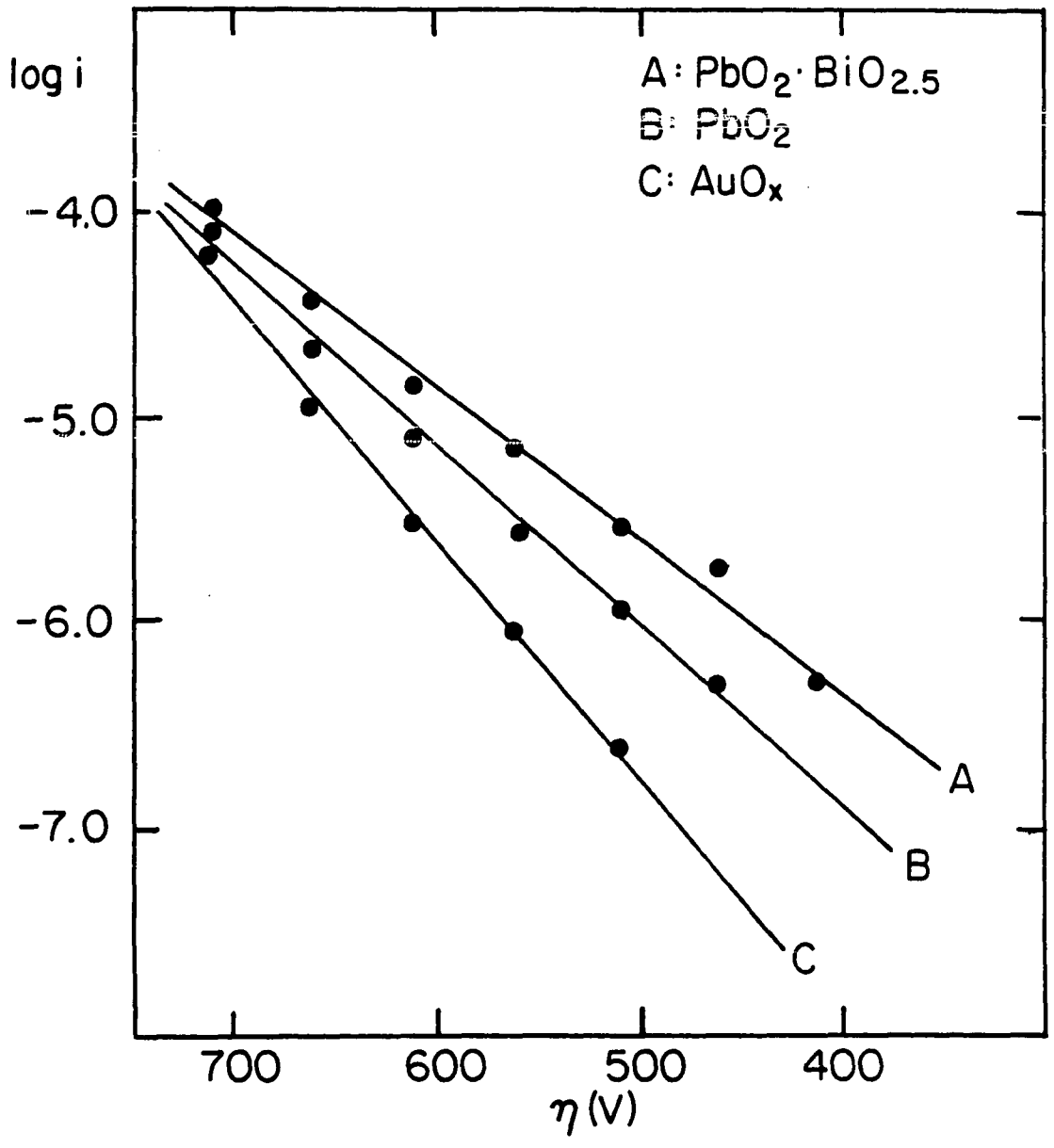
log i
A: $PbO_2 \cdot BiO_{2.5}$
B: PbO_2
C: AuO_x
-4.0
-5.0
-6.0
-7.0
700
600
500
400
η (V)
A
B
C

are concluded to not be significantly different from the normal Tafel slope of 0.12 in acidic solution for the oxygen evolution reaction. Therefore, it is concluded that only one electron is involved in the rate limiting step at these electrodes. The larger value of exchange current obtained for the mixed oxide indicates that the mixed oxide has a better catalytic surface for the oxygen evolution. As shown in the Figure VII-3, the oxygen overpotential at the same current density is the smallest for the mixed oxide. Because oxygen evolution is related to the activity of oxygen at the surface of an electrode and/or the bond strength of surface oxygen, the smaller value of oxygen overpotential is an indirect evidence that the mixed oxide has a larger activity of surface oxygen or of oxygen species with weak bond strength.

Current-potential (i-E) curves recorded for oxygen evolution at pure PbO_2 and mixed bismuth-lead dioxide electrodes are shown in Figure VII-4. Curves A-D were obtained from the positive scan of electrode potential in 1.0M $HClO_4$. Values shown in the figure represent the concentration ratio of $C^b_{Bi(III)}/C^b_{Pb(II)}$ in the deposition solution used for the preparation of the mixed-oxide electrodes. The shapes of the curves for the mixed-oxide are not changed in comparison to that for pure PbO_2, but the overpotential for oxygen evolution decreases as the amount of bismuth is increased. Plotting the potential for oxygen

Figure VII-4. Polarization curves for the oxygen evolution at pure PbO_2 and mixed $Pb(Bi)O_2$ electrodes in 1.0M $HClO_4$

Conditions for electrodeposition of mixed-oxide electrodes.
Deposition potential: 1.60 V vs. SCE
Rotation velocity of electrode (ω): 900 rev min^{-1}
Deposition time: 20.0 min
Solution: 1.0M $HClO_4$
A: 1.0mM Pb(II) + 0.0mM Bi(III)
B: 1.0mM Pb(II) + 1.0mM Bi(III)
C: 1.0mM Pb(II) + 0.5mM Bi(III)
D: 1.0mM Pb(II) + 0.7mM Bi(III)

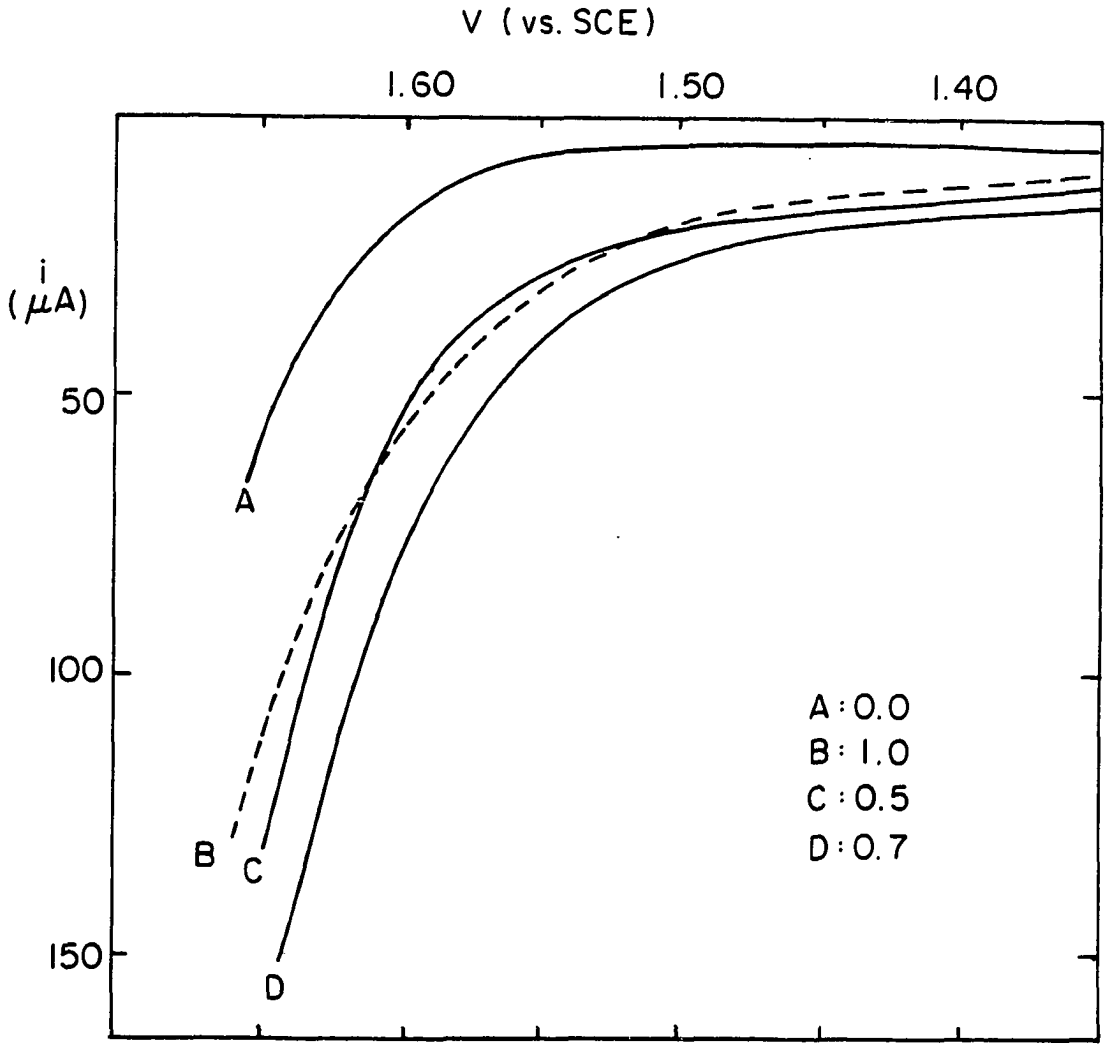
V (vs. SCE)
1.60
1.50
1.40
i
(μA)
50
100
150
A
B
C
D
A : 0.0
B : 1.0
C : 0.5
D : 0.7

evolution at constant anodic currents of 50μA and 25μA (Figure VII-5) shows that the smallest value of the oxygen evolution overpotential is obtained at the mixed oxide electrode prepared with $C^b_{Bi(III)}/C^b_{Pb(II)}$ = 0.7. Values of Tafel slopes and exchange current which were obtained from Tafel plots for oxygen evolution at the electrodes mixed with Bi are summarized in Table VII-3. The fact that the Tafel slopes are virtually identical indicates that the mechanism of oxygen evolution is not changed. However, the exchange current has a maximum value at the electrode of made from the $C^b_{Bi(III)}/C^b_{Pb(II)}$ = 0.7. The electrocatalytic activity for oxidation of 2-TCA is also the highest at this electrode. The same trend is observed for oxidation of 3-thiophene malonic acid (TMA). From the comparison with the results of calculated density of surface oxygen, the degree of preferred orientation at the surface of the mixed oxide electrode and the values of heterogeneous rate constants observed for oxidation of 2-TCA, it can be concluded that the surface of the electrode oriented toward the face containing more oxygen has more chance in producing molecular oxygen, i.e., oxygen evolution, in the absence of analyte. In the presence of analyte, the bonded oxygens at the surface are available for oxygen-transfer to the analytes reaching the electrode surface. However, the availability of the surface oxygens is also dependent on the properties of analyte itself as shown in the oxidation of Mn(II) and other organic compounds. For

Figure VII-5. Changes of potentials for oxygen evolution at constant current (25μA [——] and 50μA [···]) for pure PbO_2 and mixed $Pb(Bi)O_2$ electrodes in 1.0M $HClO_4$

Conditions for electrodeposition of five mixed-oxide electrodes.
Deposition potential: 1.60 V vs. SCE
Rotation velocity of electrode (ω): 900 rev min^{-1}
Deposition time: 20.0 min
Solution: 1.0M $HClO_4$
A: 1.0mM Pb(II) + 0.0mM Bi(III)
B: 1.0mM Pb(II) + 0.3mM Bi(III)
C: 1.0mM Pb(II) + 0.5mM Bi(III)
D: 1.0mM Pb(II) + 0.7mM Bi(III)
E: 1.0mM Pb(II) + 1.0mM Bi(III)

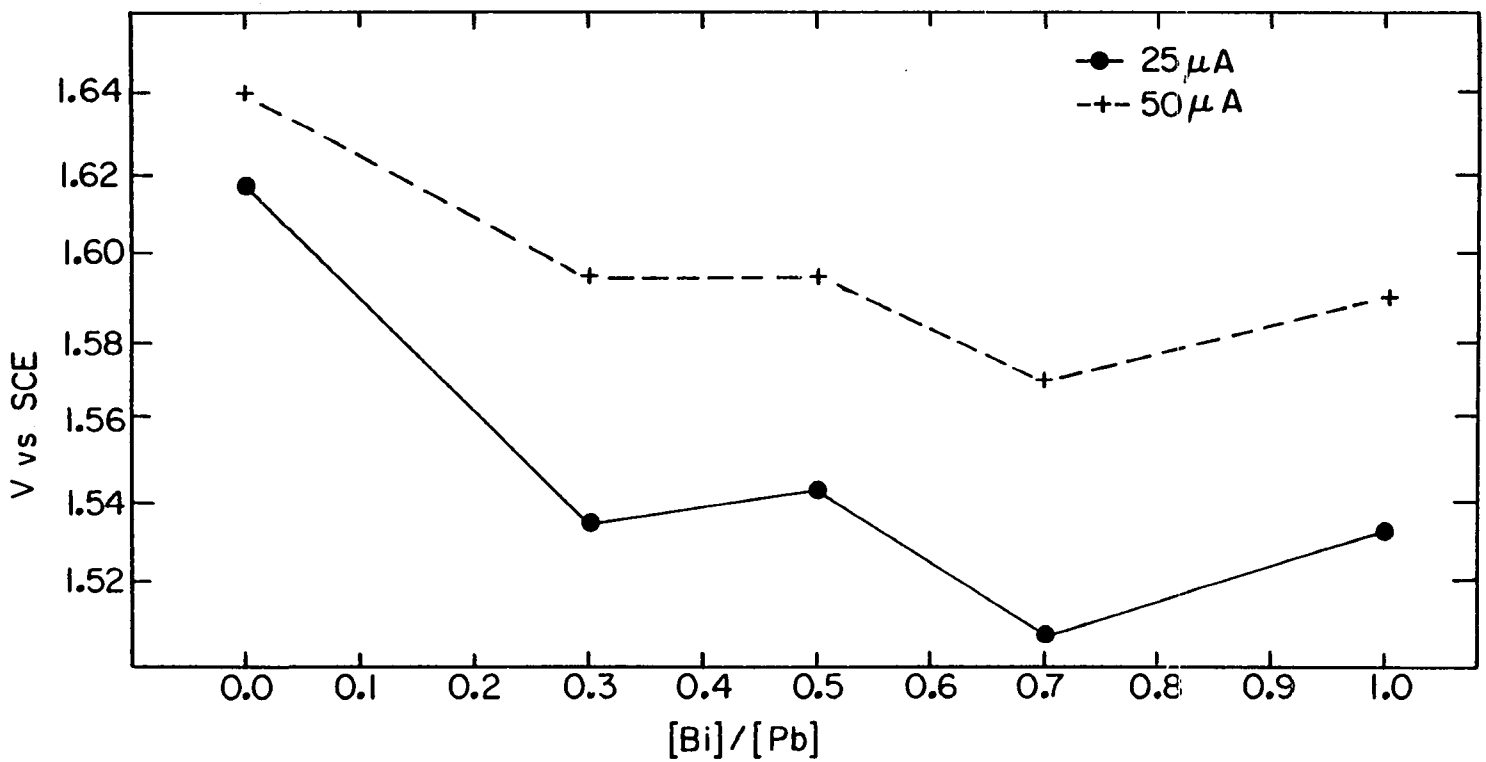
25 μA
50 μA
1.64
1.62
1.60
1.58
1.56
1.54
1.52
V vs SCE
0.0
0.1
0.2
0.3
0.4
0.5
0.6
0.7
0.8
0.9
1.0
[Bi]/[Pb]

Table VII-3. Kinetic parameters of the oxygen evolution reaction at mixed $Pb(Bi)O_2$ electrodes

$C^b_{Bi(III)}/C^b_{Pb(II)}$	Tafel slopes	Exchange currents (ln i)
0.0	0.114	-10.42
0.3	0.108	-9.980
0.5	0.113	-9.732
0.7	0.128	-8.927
1.0	0.128	-8.934

the analyte that is hard to be oxidized such as 2-TCA, the increase in the number of surface oxygens is considered to be an important factor to increase the rate of electrocatalytic oxygen-transfer reactions.

Considering oxygen evolution and electrocatalytic oxygen-transfer reactions, bonds between the oxide and the active surface oxygen are formed and broken repeatedly during the anodic reactions. Therefore, the number of oxygens available, i.e., the density of active oxygen, and the metal-oxygen bond strength at the surface of electrodes are two important factors to be considered in the explanation of any changes in the rate of heterogeneous catalytic oxidation. Some authors have explained electrocatalysis in terms of the bond strength between the electrode surface and the reaction intermediate [16,17]. However, it is very difficult to evaluate the electrocatalytic activity without "in situ" measurement of bond strength. Trasatti [10] plotted values of overpotential for oxygen evolution against the enthalphy of transition (ΔH_t) of oxides from a lower to a higher oxidation state and obtained a so-called "volcano shaped plot". The plot was used to explain relationship between the overpotential for oxygen evolution and the enthalpy of transition of oxides. He suggested that this plot was applicable for prejudging new oxide materials as possible commercial anodes for economically efficient oxygen evolution [18].

Along with these concepts, the transition enthalphy of some oxides was calculated from thermodynamic data [19-21] and the values are given in Table VII-4 and plotted in Figure VII-6. In Figure VII-6, the solid and dashed lines are identical to those of Trasatti as have already been shown in Figure II-2. From the plot, it is expected that the oxygen evolution overpotential at mixed lead dioxides containing Tl, As, Sb and Bi will be lower than at pure PbO_2. This agrees with the experimental observation as shown in Figure VII-7. However, it cannot be explained from this plot why the electrocatalytic activity for oxidation of Mn(II) at PbO_2 doped with Tl decreases [22] if better catalytic activity is predicted only by the prediction of a lower overpotential of oxygen evolution.

E. Conclusion

The correlation suggested by Trasatti between oxygen evolution overpotential and the enthalpy of the oxide transition as shown in the so-called "volcano shaped plot" was qualitatively in agreement with observations for oxygen overpotential of the mixed oxides as compared to lead dioxide. However, this correlation did not predict the fact that whereas the addition of bismuth to lead dioxide enhance a large increase in catalytic activity, the addition of

Table VII-4. Standard values of the enthalpy of transition of oxides from a lower to the higher oxidation state

Oxides of lower valence state	Oxides of higher valence state	Heat of transition ΔH_t (Kj mol^{-1})
Tl_2O	Tl_2O_3	66.8
As_2O_3	As_2O_5	129.5
Sb_2O_3	Sb_2O_5	138.6
Bi_2O_3	Bi_2O_5	193.2
BiO	Bi_2O_3	160.4

Figure VII-6. Plots of values of transition enthalpy of some oxides on the "volcano shaped" curves

Enthalpy of transition was calculated from thermodynamic data

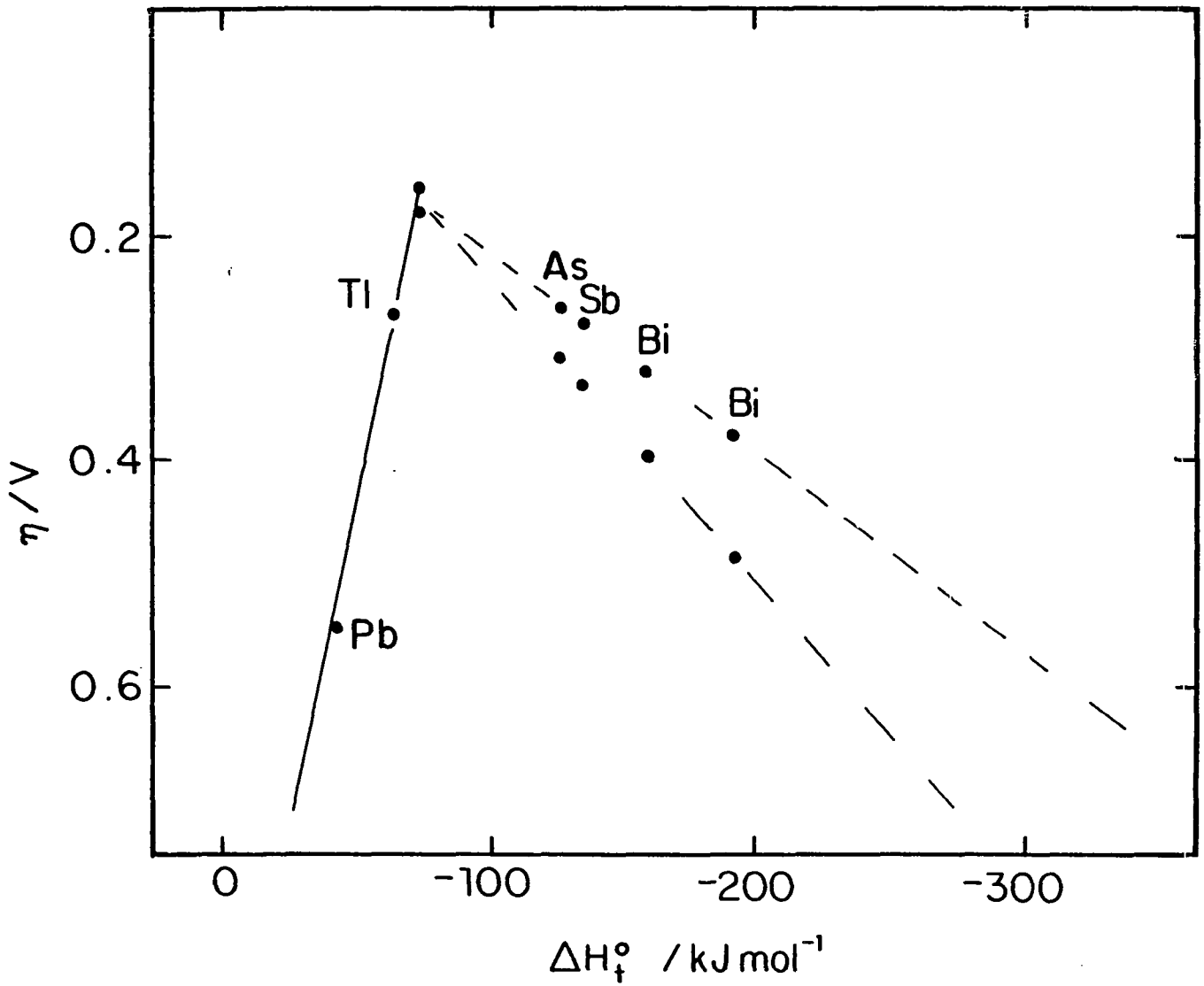
0.2
0.4
0.6
η / V
Tl
As
Sb
Bi
Bi
Pb
0
-100
-200
-300
ΔH°t / kJ mol⁻¹

Figure VII-7. Overpotential for oxygen evolution at constant current (50, 100 and 200μA) for electrodes of PbO_2 mixed with metal-oxide

Conditions for electrodeposition of mixed-oxide electrodes.
Deposition potential: 1.60 V vs. SCE
Rotation velocity of electrode (ω): 900 rev min^{-1}
Deposition time: 20.0 min
Solution: 1.0M $HClO_4$
A: 1.0mM Pb(II) + 0.1mM Tl(III)
B: 1.0mM Pb(II) + 0.1mM As(V)
C: 1.0mM Pb(II) + 0.1mM Bi(III)
D: 1.0mM Pb(II)
E: gold oxide

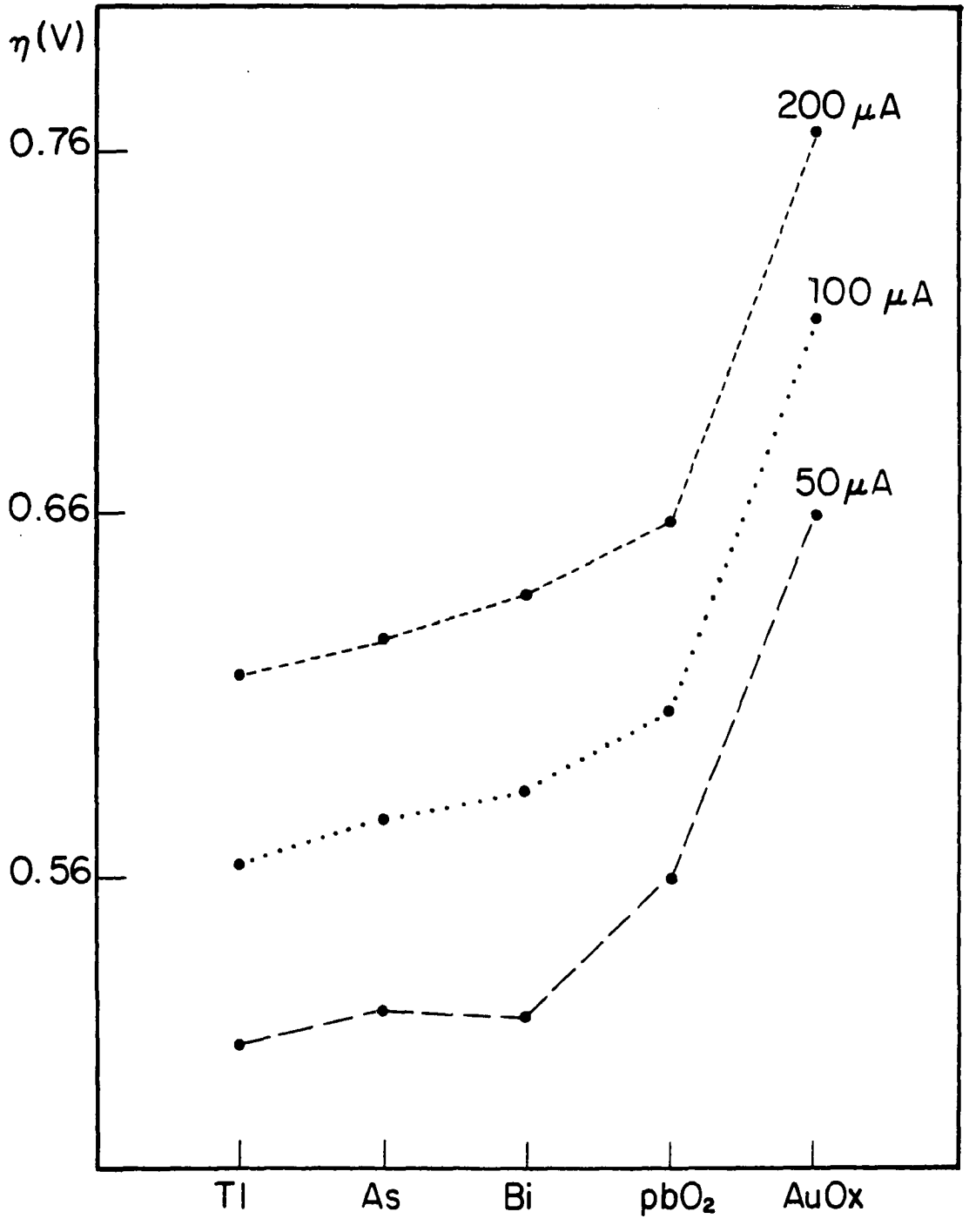
η(V)
0.76
0.66
0.56
200 μA
100 μA
50 μA
Tl
As
Bi
pbO2
AuOx

thalium caused a decrease of catalytic activity even though the two mixed oxides had very similar oxygen overpotentials.

It is concluded that the oxygen-transfer catalytic activity is controlled primarily by the surface density of active (or labile) oxygen and by local factors which influence the bond strength between the surface and the labile oxygen.

Without a truly convincing theoretical basis it is impossible to give a fully satisfactory explanation of the increase in electrocatalytic activity based on only either the number of oxygens or the metal-oxygen bond strength. In case of the mixed bismuth-lead oxide electrode, the number of oxygen is increased and the oxygen in the mixed oxide is more weakly bound to Bi, longer Bi-O bonds, than to Pb in pure β-PbO_2 as shown in many bismuth oxy-compounds [23].

The change of the strength of an individual metal-oxygen bond due to local factors of structure and environment is difficult to measure in situ. Unless the bond strength on the mixed oxide electrode is stronger than on pure PbO_2 the surface density of labile oxygen at the surface should be considered to explain the increase in the rate of oxygen evolution, i.e., lower oxygen overpotential. Likewise, the increased surface density of labile oxygen results in the increased rates of anodic oxygen-transfer. Hence, the increased rate for the oxidation of 2-TCA is concluded to be a result of high density of available oxygen at the surface of the mixed oxide electrode.

F. References

1. O'Grady, W. E.; Ross, P. N., Eds. In "Proceedings of the Symposium on Electrocatalysis"; Electrochem. Soc. Inc.: Pennington, New Jersey, 1982.

2. Weissermel, K.; Arpe, H. J. In "Industrial Organic Chemistry"; Verlag Chemie: New York, 1978.

3. Volta, J. C.; Desquesnes, W.; Moraweck, B. In "New Horizons in Catalysis"; Seiyama, T. et al., Eds.; Elsevier Scientific: New York, 1981; Page 1398.

4. Yoshida, S.; Ueda, A.; Tamura, K. In "New Horizons in Catalysis"; Seiyama, T. et al., Eds.; Elsevier Scientific: New York, 1981; Page 1377.

5. Voge, H. H.; Adams, C. R. Adv. Catalysis 1967, 17, 151.

6. Hucknall, D. J. In "Selective Oxidation of Hydrocarbons"; Academic: New York, 1974.

7. Ruetschi, P.; Delahay, P. J. Chem. Phys. 1955, 23, 556.

8. Carr, J. P.; Hampson, N. A. Chem. Rev. 1972, 72, 679.

9. Winter, E. R. S. J. Chem. Soc. 1968, A, 2889.

10. Trasatti, S. J. Electroanal. Chem. 1980, 111, 125.

11. Adzic, R. R.; O'Grady, W.; Srinivasan, S. Surf. Sci. 1980, 94, 1191.

12. Adzic, R. R.; Tripkovic, A. V.; O'Grady, W. E. In "Proceedings of the Symposium on Electrocatalysis"; O'Grady, W. E. et al., Eds.; Electrochem. Soc. Inc.: Pennington, New Jersey, 1982; Page 254.

13. Bard, A. J.; Faukner, L. R. In "Electrochemical Methods"; John Wiley: New York, 1980; Page 251.

14. Johnson, C. K. In "U.S. Atomic Energy Commission Report ORNL-3794"; Oak Ridge National Laboratory: Oak Ridge, 1970.

15. D'Antonio, P.; Santoro, A. Acta Cryst. 1980, B36, 2394.

16. Parsons, R.; Trans. Faraday Soc. 1958, 54, 1503.

17. Trasatti, S. In "Proceedings of the Symposium on Electrocatalysis"; O'Grady, W. E. et al., Eds.; Electrochem. Soc. Inc.: Pennington, New Jersey, 1982; Page 73.

18. Trasatti, S. Electrochim. Acta 1984, 29, 1503.

19. Samsonov, G. V. In "The Oxide Handbook"; 2nd Ed.; Plenum: New York, 1982.

20. Wicks, C. E.; Block, F. E. In "Thermodynamic Properties of 65 Elements"; U. S. Govt. Print Off.: Washington, 1963; U. S. Bureau of Mines, Bull. 605.

21. Rossini, F. D.; Wagman, D. D.; Evans, W. H.; Jaffe, I. In "Selected Values of Chemical Thermodynamic Properties"; Natl. Bur. Std. U. S. Circ. 500, 1952.

22. Yeo, I-H.; Johnson, D. C. J. Electrochem. Soc. to be submitted for publication.

23. Well, A. F. In "Structural Inorganic Chemistry"; 5th Ed.; Clarenden Press: Oxford, 1984.

VIII. SUMMARY

The goal of this research was to increase the electrocatalytic reactivity of electrodeposited lead dioxide electrodes for anodic oxygen-transfer reactions. The modification of catalytic activity was attempted by addition of foreign metal ions to the solutions of Pb(II) used for the electrodeposition of the oxide materials.

Of more than 33 elements tested as dopants, bismuth was found to be the most effective for increasing the electrocatalytic reactivity in the oxidation of Mn(II) and various organic compounds. Oxidation rates of some organic and inorganic compounds on the mixed bismuth-lead dioxide electrodes were determined to be increased up to 100X or more compared to the pure electrodeposited PbO_2. Very large changes in electrocatalytic activity were found for oxidations of phenol, citric acid, and 2-thiophene carboxylic acid. These compounds are inactive at the pure PbO_2 electrode, but are oxidized at mass transport-limited rates at the mixed bismuth-lead dioxide electrodes. Values of heterogeneous rate constant for many oxygen-transfer reactions at the mixed oxide electrode increase as the amount of bismuth in the oxide increases. It was observed also that arsenic, also a Group VA element, is effective for electrocatalysis: however, its effectiveness is less than for bismuth.

An added benefit found for the mixed bismuth-lead dioxide was a significant increase in cathodic stability of the mixed oxide.

From the analysis of X-ray diffraction profiles, the mixed bismuth-lead dioxide was determined to be electrodeposited in such a way that the (020) plane of the rutile structure is preferentially oriented parallel to the electrode surface. The highest degree of preferred orientation was found to occur for the mixed oxide electrodeposited from a solution of $C^b_{Bi(III)}/C^b_{Pb(II)}$ = 0.7/1.0. The density of oxygens per metal site calculated from pictures drawn by ORTEP has the highest value for the (020) face. Maximum rate constant for oxidation of 2-thiophene caboxylic acid was obtained on the mixed electrode whose surface has the highest oxygen-metal ratio.

The overpotential for the anodic evolution of O_2 ($\eta\ O_2\uparrow$) decreases as the level of bismuth in the mixed oxide increases, up to $C^b_{Bi(III)}/C^b_{Pb(II)}$ = 0.7. This mixed oxide electrode has the highest degree of preferred orientation of the (020) plane parallel with the substrate. The (020) face has the highest density of surface oxygen per metal site. Therefore, the decrease in oxygen overpotential is concluded to be the result of the preferential growth of the mixed bismuth-lead dioxide. The fact that oxygen overpotential is decreased at mixed oxide electrodes containing Tl, As, Sb and Bi, compared to pure PbO_2, is consistent with predictions

based on the volcano-shaped curves plotted from thermodynamic data.

From the comparison with the results of calculated density of surface oxygen and the values of heterogeneous rate constant for oxidation of 2-TCA, it is concluded that the increase in electrocatalytic activity for oxygen-transfer reactions at the mixed bismuth-lead dioxide electrode is due to the increase in the number of surface oxygen at the mixed oxide electrodes.

IX. FUTURE RESEARCH

Characteristics of electrodeposited pure lead dioxide, such as reactivity and stability, were improved by the incorporation of foreign metal oxides into the β-lead dioxide rutile structure. This shows a bright future for the developments and design of metal-oxide mixed lead dioxide electrode as a new analytical transducer. The mixed bismuth-lead dioxides tested were not useful for oxidation of various alcohols which are predicted from thermodynamics to be easily oxidized. This indicates that the function of a doping agent may be specific for oxidation of a certain class of compounds. By the appropriate choice of the doping metal oxide, selective oxidation of certain compounds may be possible on modified lead dioxide electrode. The design and development of a selective anodes could be very important for analytical applications as well as for electrochemical incineration where it is desired for the sake of efficiency to incinerate only the chemical functionality responsible for the toxicity of a molecule.

The electrodeposition of mixed oxides from solutions of Pb(II) containing other metal ions is not the only method for preparation of conducting metal oxides. Another method for the preparation of mixed oxide electrodes is the thermal decomposition. This method always involves high temperature calcination. The method consists in mixing of the solutions

of nitrates of the corresponding metal, metal oxides, or in coprecipitation of hydroxides and oxalates of the corresponding metals and then decomposing the mixture at high temperature in an oxygen environment. The calcination temperature and procedure of preparation can be varied to modify the characteristics of the mixed oxides produced. Advantage of this method compared to electrodeposition is that any difficulty from the chemical interactions, such as chemical stripping of lead dioxide and metal hydroxide formation in the deposition solution, can be removed. The thermally prepared electrodes might have significantly different surface morphology, electrical conductivity, and chemical properties so that the electrocatalytic reactivity could be much different from that of the electrodeposited metal oxides. Therefore, other methods for the preparation of the oxides should be tested.

For the study of mechanism of anodic oxygen-transfer, spectroscopic measurement should continue to obtain the informations of metal-oxygen bond strength and bond length at the oxide surface. This information is hard to get from in situ measurements. Electrochemical data combined with spectro-scopic information may be greatly helpful for further elucidation of the oxygen-transfer mechanism.

X. ACKNOWLEDGEMENT

I would like to express gratitude to my major professor, Dr. Dennis C. Johnson. His encouragement, guidance, and friendship throughout my graduate studies cannot be stated within a few lines. He certainly made my stay in Ames more comfortable and enjoyable, and led me to a new way of life.

I would also like to thank the faculty members of Sogang University and, especially, Dr. Woon-kie Paik who initially guided me to the beautiful world of electrochemistry.

The financial support from Iowa State University, Ames Laboratory (USDOE), and The Electrochemical Society, through The Energy Research Summer Fellowship of 1986 are gratefully acknowledged. Also, the spiritual guidance of Dr. Winston Malmquist will never be forgotten.

Special thanks go to the many people who helped me with my experiments: Sangsoo Kim and Professor Robert Jacobson are to be thanked for X-ray diffraction analysis and scientific communications and John Bauer and Brian Wels for exhaustive coulometry.

I would like to thank the members of the electrochemistry group. Special thanks to Glen Neuburger for his friendship and his scientific discussions.

Finally, I would like to thank my parents, my brother, and my sisters for their constant support.

XI. APPENDIX

A. Heterogeneous Rate Constants

As discussed in Chapter III, this Appendix contains the kinetic results for oxidation of organic and inorganic compounds on pure and doped β-PbO_2 anodes.

Table XI-1. Heterogeneous rate constants for oxidation of various analytes at the electrodeposited pure β-PbO_2 and mixed β-PbO_2 electrodes

Analyte (mM)	Dopants	Concentration of dopants (μM) in 1000μM Pb(II)	Rate constants $k \times 10^3$ (cm sec^{-1})
5-sulfosalicylic acid (1.0)	-	-	4.5
	Bi(III)	1000	110
	Ca(II)	10	7.05
	Cd(II)	10	6.96
	Mg(II)	10	7.05
	Na(I)	20	5.35
	$SO_4^=$	10	6.51
	Ti(IV)	2	5.26
	Ti(IV)	10	6.08

Table XI-1. (continued)

Analyte (mM)	Dopants	Concentration of dopants (μM) in 1000μM Pb(II)	Rate constants $k \times 10^3$ (cm sec^{-1})
manganese(II)	-	-	4.04
(1.0)	Ag(I)	10	4.43
	Ag(I)	50	3.52
	Ag(II)	10	6.25
	Ag(II)	58.6	8.05
	As(III)	10	6.87
	As(III)	40	30.0
	As(V)	20	5.20
	As(V)	100	90.6
	As(V)	200	22.0
	As(V)	1000	56.5
	Bi(III)	5	4.35
	Bi(III)	10	5.74
	Bi(III)	50	11.8
	Bi(III)	100	69.3
	Bi(III)	1000	463
	Ca(II)	10	4.53
	Cd(II)	10	4.79
	Cd(II)	1000	3.08
	Cr(III)	10	4.74
	Cu(II)	10	4.02
	Fe(III)	50	3.65
	Ga(III)	1000	3.5
	Ge(IV)	50	4.83
	In(III)	1000	3.4
	Ir(IV)	0.8	16.2
	K(I)	20	2.97
	Mg(II)	10	3.98

Table XI-1. (continued)

Analyte (mM)	Dopants	Concentration of dopants (μM) in 1000μM Pb(II)	Rate constants $k \times 10^3$ (cm sec^{-1})
manganese(II)	Mg(II)	100	3.56
(1.0)	Mn(II)	10	3.71
	Mn(II)	1000	2.41
	Mo(VI)	10	4.19
	Mo(VI)	50	4.72
	Mo(VI)	1000	2.91
	Na(I)	20	6.40
	Ni(II)	100	4.11
	Ni(II)	1000	2.69
	Pd(II)	0.04	6.17
	Pt(IV)	2	6.54
	Rh(III)	0.8	7.59
	Ru(IV)	1.6	4.37
	$SO_4^=$	10	3.14
	Ti(IV)	2	4.23
	Ti(IV)	10	2.73
	Tl(I)	40	3.09
	Tl(III)	100	2.3
	V(IV)	100	4.90
	V(IV)	1000	4.84
	Zn(II)	10	3.84
	Zn(II)	1000	4.60

Table XI-1. (continued)

Analyte (mM)	Dopants	Concentration of dopants (μM) in 1000μM Pb(II)	Rate constants $k \times 10^3$ (cm sec^{-1})
dimethyl sulfoxide (1.0)	-	-	*
	Bi(III)	1000	693
phenol (1.0)	-	-	*[a]
	Bi(III)	100	mst[b]
	Bi(III)	500	mst
	Bi(III)	1000	mst
cystine (0.1)	-	-	9.0
	Bi(III)	100	9.45
	Bi(III)	500	25.2
	Bi(III)	1000	15
2-thiophen carboxylic acid (0.1)	-	-	0.45
	Bi(III)	300	7.74
	Bi(III)	500	8.58
	Bi(III)	700	9.45
	Bi(III)	1000	4.34

[a] * represents that the oxidation reaction is very slow at the electrode so that the rate constant can not be calculated.

[b] mst represents mass-transport limited reactions.

Table XI-1. (continued)

Analyte (mM)	Dopants	Concentration of dopants (μM) in 1000μM Pb(II)	Rate constants $k \times 10^3$ (cm sec^{-1})
2-thiophen acetic acid (0.1)	-	-	84.4
	Bi(III)	100	131
3-thiophen malonic acid (0.05)	-	-	28.7
	Bi(III)	300	40.6
	Bi(III)	500	51.9
	Bi(III)	700	57.5
	Bi(III)	1000	52.5
hydroxyquinone (1.0)	-	-	10.2
	Bi(III)	100	249
	Bi(III)	500	92.9
	Bi(III)	1000	52.5
vanadium(IV) (1.0)	-	-	88.7
	Bi(III)	1000	186
	Ti(IV)	2	35.2
citric acid (1.0)	-	-	*
	Bi(III)	1000	0.93
$S_2O_3^{=}$ (1.0)	-	-	51.3
	Bi(III)	1000	mst

B. Procedure for X-ray Diffraction

The following procedure was used to obtain the X-ray diffraction pattern with a PICKER Powder Diffractometer in the laboratories of Professor Robert Jacobson, Ames Laboratory USDOE.

1. Mount sample (electrodeposited PbO_2 oxide on disc substrate)on the sample holder.

2. Adjust the position of the sample to make sure X-ray beam is centered on the sample.

3. Turn on a strip chart recorder connected to the PICKER to record peak intensities as a function of 2θ.

4. Login XRAVAX with the commands
   user name: USER
   password : HELP

5. Type POW at "$" prompt and hit RETURN key then, the following will be printed out.

   "Two theta is now at nnnn if you agree type Y" : nnnn is a 2θ value of computer reading which indicates the position of the X-ray beam.

6. If the nnnn value is not the same as your reading appeared on the digital meter (this meter is attached on the one of the arms of the PICKER), then type N otherwise type Y and hit RETURN key. The following will be printed out:

   "type in two theta position"

7. Type your reading with four digit if you answered N in the first print out and hit RETURN key.

8. Answer a file name if you want to save the data on the disk.

9. Type three kind of input (two-theta minimum, two-theta maximum, and stepsize) and hit RETURN key at each step; when you type the inputs remember that 1 degree of 2θ corresponds 100. That is, if you want to scan from 10° to 30° then type 1000 for the two-theta minimum, 3000 for the two-theta maximum.

10. With preset time = 1.0 sec, scan over large 2θ range with a large stepsize.

11. Observe the strip chart profile to find a peak that shows maximum intensity.

12. Once you find a peak of maximum intensity, then, use this peak for the fine tuning of the sample/X-ray position.

13. To increase the intensity of the peak, adjust the horizontal height of the sample with control knobs. The control knobs (two allen wrenches) are attached to the holder.

14. Once the intensity of the peak is maximized, the fine adjustment is finished.

15. Scan over a whole range of 2θ with a small stepsize.

    Typical inputs to obtain X-ray diffraction pattern of mixed bismuth-lead dioxide electrode are followings:

    two theta minimum = 4° (type 400 for the input).
    two theta maximum = 50° (type 5000 for the input).
    step size = 0.04° (type 4 for the input).
    preset time = 10 sec (type 10. for the input).

16. If you finish scanning the whole range close the shutter for X-ray beam.

17. Login VAXLB or VAXLA.

18. Type following commands to transfer data profile from the XRAVAX to your directory and hit RETURN key.

    "$ copy XRAVAX::DQA1:[USER]Chemistry *.*/LOG"

    Here, XRAVAX is VAX node name which PICKER is attached to, DQA1 is the name of disk containg the data file of PICKER, [USER] is directory, and Chemistry is the file name given in the input of the scan procedure.

19. Run this file for the plot.